The Sampling Variability and the Validation of High Frequency Radar Measurements of the Sea Surface

Markus Gintas Šova

School of Mathematics and Statistics
University of Sheffield

Submitted for the degree of Doctor of Philosophy

February 1995

The Sampling Variability and the Validation of High Frequency Radar Measurements of the Sea Surface

Markus Gintas Šova

Abstract

Remote sensing is becoming an increasingly important tool for ocean wave measurement, and over the past decade much progress has been made in the development of the wave measuring capabilities of HF (*H*igh *F*requency) radar. This system is able to make detailed and near continuous observations of the sea surface over a wide area. However, because the mathematics of the data extraction process is rather difficult, the statistical properties of the observed data have to date been poorly understood.

In this study, the approximate sampling distributions of a variety of measurements from HF radar (including significant waveheight, mean wave period, wind direction, and various spectral parameters) are derived in terms of quantities that are either known or estimable. The resulting confidence intervals are, in the case of significant waveheight and mean wave period, of comparable width to those obtained from the corresponding NURWEC2 (*N*etherlands *UK* *R*adar *W*ave buoy *E*xperimental *C*omparison) wave buoy measurements, and in the case of spectral power, they are narrower.

Furthermore, methods are derived by which such radar measurements may be compared with their corresponding wave buoy measurements in a statistically valid manner, and their relative biases estimated. These methods are then applied to data taken during the NURWEC2 field trial, which suggest that the radars and the wave buoy show good correspondence for measurements of significant waveheight and of spectral power (over $85 - 125mHz$ — the frequencies with most wave power, and hence those of most importance). There is also a fair correspondence for mean period measurements in the range $6.8 - 11.0secs$. Spectral mean direction shows good correspondence over $85 - 155mHz$ over the somewhat limited directional range (*i.e.* as observed during the NURWEC2 storm) of the data.

Acknowledgements

I would like to express my gratitude to the following :

to Dr L R Wyatt and Prof R M Loynes (both of the University of Sheffield) for their supervision, help, advice and encouragement throughout this study.

to those fellow research students with whom I shared the Applied Mathematics postgraduate room — mutual encouragement, academic discussion and friendship were an important part of those years.

To all of the above, I offer my sincere thanks.

Markus Šova, February 1995

Contents

1 Introduction **6**

1.1 Summary 6

1.2 Overview 7

1.3 Background Ocean Wave Theory 8

1.3.1 Formation and Classification 8

1.3.2 Measurement and Stationarity 8

1.4 The NURWEC2 Field Trial 10

1.5 Normal Approximations and Confidence Intervals 10

2 Background Spectral Theory **13**

2.1 Introduction 13

2.2 Functions of Continuous Time 13

2.2.1 The Fourier Transform 13

2.2.2 Random Functions and Stationarity 14

2.2.3 The Power Spectrum and Auto-Covariance Function . 15

2.3 Discrete Time Series 18

2.3.1 The Discrete Fourier Transform and the Power and Energy Spectra 18

2.3.2 The Distribution of an Energy Spectrum of Normal White Noise 19

2.3.3 Linear Filters 21

2.3.4 The Distribution of the Energy Spectrum of a Stationary Process 22

2.3.5 Spectral Leakage and Tapers 23

2.3.6 Averaging of Sequential and Time-Overlapped Spectra 27

2.4 Multivariate Time Series 31

2.4.1 The Cross- Co- and Quadrature Spectra 31

3 Spectral Integrals and Moments **33**

3.1 Introduction 33

3.2 The Definition of a Spectral Moment 33

3.3 The Distribution of the Total Energy in a Set of Frequency Bins of a Periodogram 34

3.4 Extension for a Tapered Time Series 35

3.5 The Distribution of a Weighted Sum of Periodogram Energy . 41

3.6 The Covariance of Two Weighted Sums of Periodogram Energy 42

3.7 Extension for a Tapered Time Series 42

3.8 Extension for the Covariance of Two Weighted Sums of Spectral Energy of a Tapered Time Series 46

3.9 Comment 46

4 Wave Buoy Theory **47**

4.1 Introduction 47

4.2 The Non-Directional Ocean Wave Spectrum 47

4.3 Directional Parameters 49

4.3.1 Truncated Estimation of the Directional Wave Spectrum 49

4.3.2 Model and Parameter Estimation of the Directional Wave Spectrum 54

4.4 Equipment Problems 55

5 HF Radar Theory **56**

5.1 Introduction 56

5.2 Pulse and FMICW Radars 56

5.3 The Effect of Ocean Waves on a Radar Signal 57

5.3.1 The First Order Effect 57

5.3.2 Second Order Effects 58

5.3.3 Statistical Properties of the Doppler Spectrum 61

5.4 Parameters derived from the Doppler Spectra 63

5.4.1 Wind Direction 63

5.4.2 Significant Waveheight 67

5.4.3 Mean Wave Period 72

5.4.4 Wind Speed 73

5.4.5 The Wind-Driven Spectrum 77

5.5 The Inversion Problem 80

5.5.1 Introduction 80

5.5.2 Analysis Overview and the Inversion Procedure 80

5.5.3 Estimating the Statistical Properties of the Parameters Derived from the Inversion 83

5.5.4 Results from the Simulation Study 86

6 System Intercomparisons **97**

6.1 Introduction 97

6.2 Required Assumptions 98

6.3 Existing Approaches to System Intercomparison 98

6.4 The Basic Principles of Maximum Likelihood Estimation . . . 99

6.5 Application to Wave Measurement System Intercomparison . . 100

6.5.1 Linear Relationship Case 100

6.5.2 Linear Relationship of Logarithms Case 104

6.5.3 Directional Difference Case 106

7 Results from NURWEC2 **110**

7.1 Introduction 110

7.2 Significant Waveheight 111

7.3 Mean Wave Period 111

7.4 Spectral Power 116

7.4.1 Spectral Power at 30-45mHz 116

7.4.2 Spectral Power at 45-60mHz 116

7.4.3 Spectral Power at 60-85mHz 119

7.4.4 Spectral Power at 85-100mHz 119

7.4.5 Spectral Power at 100-125mHz 119

7.4.6 Spectral Power at 125-155mHz 124

7.4.7 Spectral Power at 160-200mHz 128

7.4.8 Comment on Radar Performance 129
7.5 Spectral Mean direction 129
7.5.1 Spectral Mean Direction at 30-45mHz 129
7.5.2 Spectral Mean Direction at 45-60mHz 129
7.5.3 Spectral Mean Direction at 60-85mHz 131
7.5.4 Spectral Mean Direction at 85-100mHz 133
7.5.5 Spectral Mean Direction at 100-125mHz 133
7.5.6 Spectral Mean Direction at 125-155mHz 134
7.5.7 Spectral Mean Direction at 160-200mHz 136
7.5.8 Comment on Radar Performance 137
7.6 Spectral Directional Spread 137
7.7 Intercomparison Summary 137

8 Conclusions **139**

8.1 Theoretical Developments 139
8.2 HF Radar Performance during the NURWEC2 Field Trial . . 140
8.3 Possibilities for Further Research 141

Chapter 1

Introduction

1.1 Summary

Remote sensing is becoming an increasingly important tool for ocean wave measurement with the advent of such systems as HF (*H*igh *F*requency) radar, SAR (*S*ynthetic *A*perture *R*adar), satellite altimeters and others. The ocean wave measuring potential of radar was discovered virtually by accident. Radar was first used at sea to monitor ship movements during the second world war, each vessel being represented by a "blip" on the radar screen. However, under certain conditions wave motion would generate a cluster of blips (known as *sea clutter*) which during periods of rougher weather could obscure the trace of a ship. Much effort went into the removal of this sea clutter, but it was later realised that much oceanographic information is contained therein (see Shearman (1983) for further historical details).

Over the past decade, much progress has been made in the development of the wave measuring capabilities of HF radar. HF radar has the advantage of being able to make near continuous and detailed observations of the sea surface (including the full directional power spectrum) over a wide area. The disadvantage is that the mathematics of the data extraction process is rather difficult, and hence the statistical properties of the observed data were poorly understood. Because such use of radars is a recent innovation, in early 1987 the NURWEC2 (*N*etherlands *UK* *R*adar *W*ave buoy *E*xperimental *C*omparison, see section 1.4) field trial was conducted in order to compare the performance of an HF radar wave measuring system with that

of a wave buoy, and hence to validate the radar measurements. The bulk of the analyses performed to date on the NURWEC2 data have involved such techniques as simple least squares regression, (see section 6.3), which do not allow for the fact that there is sampling variability in the measurements from both systems.

The purpose of this study has been to derive the statistical properties of HF radar ocean wave measurements, to use this information to compare the performances of the wave buoy and HF radar systems used in NURWEC2 in a statistically valid manner, and hence to gain some insight into the behaviour of the radar system. New intercomparison techniques have been developed for this purpose.

1.2 Overview

In order to understand the theory behind the use of HF radars and wave buoys to measure ocean waves, it is first necessary to be familiar with the theory of spectral analysis. This is introduced in chapter 2, and expanded upon in chapter 3 to include spectral integrals which are used in both wave buoy and HF radar analysis. The theory behind wave buoy measurements is covered in chapter 4. This information is necessary for any intercomparison with HF radar to be meaningful. In chapter 5 the theory of HF radar wave measurement is described together with the analysis technique which has been used on the NURWEC2 data. The statistical properties of data so analysed are derived. In particular, section 5.5 deals with the non-linear integral inversion problem which is the main difficulty in the radar analysis. Intercomparison methods suitable for use with the NURWEC2 data are derived in chapter 6, and in chapter 7 these are applied to data from the trial and the results are discussed.

Throughout this study, graphical examples are presented of real data whose variabilities have been displayed in terms of their confidence intervals. Because the derivation of these intervals involves the same type of approximations for both radar and wave buoy observations, the basic theory is presented in this chapter (in section 1.5).

Firstly, however, we shall briefly introduce the subjects of ocean waves (section 1.3), and the NURWEC2 field trial (section 1.4).

1.3 Background Ocean Wave Theory

1.3.1 Formation and Classification

When wind starts to blow across the sea surface, short capillary waves are formed travelling in the same direction as the wind. If the wind ceases, these waves quickly die away. However, if it continues to blow, the waves grow in both length and height. Once these waves exceed a wavelength of about $1.73cm$ they become gravity waves which will continue to propagate even if the wind ceases (fully developed waves typically have wavelengths in the order of tens of metres). For further details the reader is referred to Kinsman (1965). Waves may also be generated by other means (such as the motion of the moon, earthquakes, the wake produced by a ship, *etc*) but the waves of interest to this study are wind-generated and fall broadly into three categories :

1. **Wind waves** are the waves generated by the action of the local wind (*i.e.* at the place at which the waves are observed).

2. **Old waves** (or old sea) are those waves generated by *previous* wind action at the site of observation, the wind field having since changed to produce wind waves with different properties (*e.g.* travelling in a different direction).

3. **Swell waves** are waves generated by some distant wind field which have propagated to the observation site. Swell waves tend to be of longer wavelength than old and wind waves.

1.3.2 Measurement and Stationarity

Wind action and wave interaction generate waves travelling in a range of directions and frequencies. Because of this, ocean waves may be represented by a directional wave spectrum (see section 2.2.3). The directional spectrum however is not very straightforward to estimate — the problems associated with this estimation are described in the chapters on the respective wave measurement systems (chapters 4 and 5 for wave buoys and HF radars, respectively).

Since HF radars measure the ocean wave spectrum as a function of directional wavenumber, as opposed to directional frequency, it is necessary to relate these two domains. The deep water dispersion relationship gives the angular frequency (ω) of ocean waves in the following form :

$$\omega^2 = g|\mathbf{k}|$$

where $\mathbf{k}$ is ocean wavenumber and g is acceleration due to gravity. Strictly, this formula is only valid for infinitesimal waves on an infinitely deep sea, but is usually considered a good approximation for all but the longest waves (see Wyatt and Holden (1991)) if the sea depth is at least $50m$.

One commonly used parameter for summarising ocean wave activity is significant waveheight (H_s) which is defined as follows :

$$H_s = 4\sqrt{m_0}$$

where m_0 is the zeroth spectral moment (see section 3.2) of sea surface elevation. This quantity is supposed to approximate the wave height that a seafarer on a ship would estimate by eye.

It is typically assumed that the sea surface displacement caused by wave motion is approximately Normally distributed. This is justified by considering such displacement as a sum of many contributions caused by relatively unrelated forces acting at different times. Treating these contributions as random then allows the application of the central limit theorem. This is discussed by Kinsman (1965), who goes on to use observed data to demonstrate that the departure from Normality is "very small".

In the context of ocean waves, stationarity (spatial or temporal) can be thought of in terms of a wave field having the same (or approximately the same) underlying directional wave spectrum over the area and time duration of interest (see section 2.2.2 for a more formal mathematical definition). Stationarity is an important concept in ocean wave measurement, since most systems need to measure over a period of time (typically about 30 minutes) and many measure over an area (in the case of HF radar, typically about $50km^2$). If the wave field is non-stationary then any such measurements would be difficult to interpret. Scales of temporal and spatial stationarity have been examined by Šova and Wyatt (1994), and their results are summarised in section 6.2.

1.4 The NURWEC2 Field Trial

The NURWEC2 (*N*etherlands *U*K *R*adar *W*ave buoy *E*xperimental *C*omparison) was conducted during the first four months of 1987 by the Department of Electronic and Electrical Engineering at the University of Birmingham (UK) and Neptune Radar Ltd with assistance from the Netherlands Rijkswaterstaat, SERC, the Wolfson Foundation, Wimpol Ltd, Institute of Oceanographic Sciences, Rutherford & Appleton Laboratory, the Department of Energy, BP plc, the Meteorological Office and ARE. It was set up in order to gather ocean wave measurements from a pair of HF radars and a directional wave buoy for the purpose of comparing the performance of the radars with that of the wave buoy. The radar system used was of the PISCES type, under development by Neptune Radar Ltd from a prototype of the University of Birmingham (UK). The wave buoy was a Wavec directional buoy manufactured by Datawell bv (of the Netherlands). The radar installations were at East Blockhouse (south Dyfed) and Nabor Point (north Devon), the beams crossing over the Celtic Sea (see figure 1.1 for details). Unfortunately, most of the data were available only in frequency domain form (as opposed to the original time series), thus restricting the types of analysis possible. This "pre-processing", along with the statistical properties of data thus derived, is discussed in chapters 4 and 5 (for the wave buoy data and radar data, respectively). The data of particular interest to this study were collected during a storm (March 25^{th} to March 29^{th}) — it was during this period that the greatest variation of sea conditions was experienced and that the radar data was of the best quality (see Wyatt (1988a), Wyatt (1988b) and Wyatt (1991) for further details of NURWEC2). Except where otherwise specified, the radar data used in this study has been taken from an area of sea which includes the position of the Wavec buoy.

1.5 Normal Approximations and Confidence Intervals

The distributions of a number of wave parameters as measured by wave buoys and HF radars are given in terms of a Normal approximation (see chapters 4 and 5 respectively). Each such measurement is a function of other measurements with known distribution properties, and its variance may be

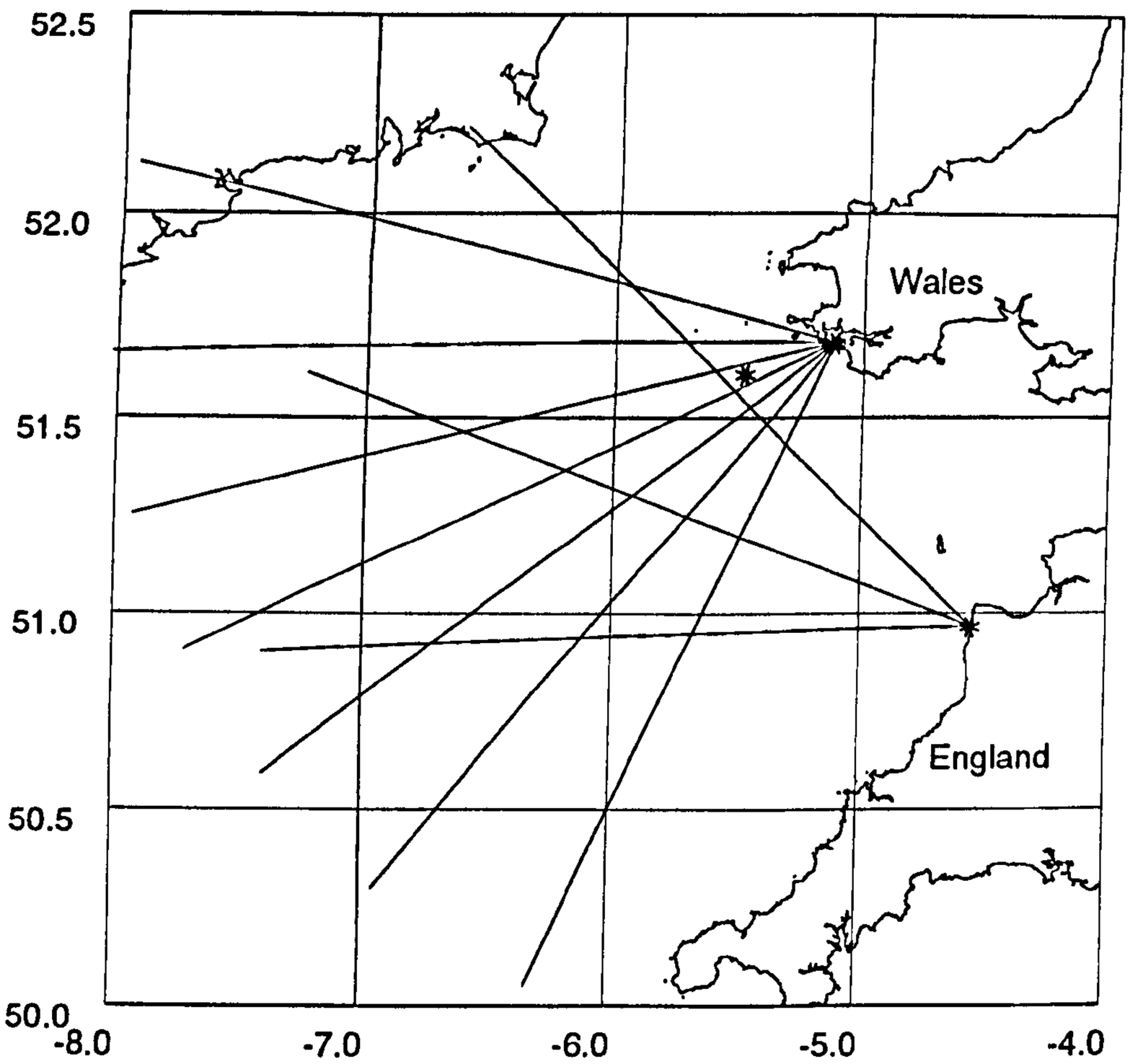

Figure 1.1: A map showing the NURWEC2 measurement site of the Celtic Sea. The horizontal lines measure degrees latitude north of the Equator, and the vertical lines measure degrees longitude relative to the Greenwich Meridian. The other straight lines (which converge at the radar sites) represent the paths of the radar beams (showing $200km$ range) and the asterisk to the west of the Welsh radar site marks the position of the wave buoy.

estimated using a Taylor series expansion. Suppose we have a measurement Y (*e.g.* mean wave period as measured by HF radar, see section 5.4.3) which is some function of a measurement vector $\mathbf{x}$ (*e.g.* a Doppler spectrum). Then :

$$\mathrm{Var}(Y) = \mathbf{d}\mathbf{V}_{\mathbf{x}}\mathbf{d}^T$$

where $\mathbf{V}_{\mathbf{x}}$ is the variance-covariance matrix of $\mathbf{x}$, and

$$\mathbf{d} = \{d_j\}, d_j = \left.\frac{\partial Y}{\partial x_j}\right|_{\mathrm{E}(\mathbf{x})}$$

(see Krogstad *et al.* (1988) for details). This is easily extended to the case where Y is a multivariate random variable (such as is used in section 5.4.4).

If we have an approximately Normally distributed random variable with estimated mean $\hat{\mu}$ (*e.g.* observed mean wave period) and estimated variance $\hat{\sigma}^2$ (as approximated above), then the following limits define an approximate $100(1-\alpha)\%$ confidence interval for the true (*i.e.* underlying) mean :

$$\hat{\mu} \pm z_{1-\frac{\alpha}{2}}\sqrt{\hat{\sigma}^2}$$

where z_β is the β-th quantile of the N(0, 1) distribution. Such a confidence interval should be interpreted as follows :

Under repeated sampling, $100(1-\alpha)\%$ *of such intervals will contain the true mean.*

This emphasises that it is the true mean that is fixed, and the interval which is a random variable. 90% confidence intervals are commonly used in oceanographic texts, whereas statistical texts tend to favour 95% confidence intervals. A larger percentage produces a wider interval, but reduces the chance of error (*i.e.* of the interval *not* containing the true mean), and so some balance between these conflicting factors needs to be struck. We will keep to convention by using 90% confidence intervals for wave parameters and 95% confidence intervals for relative bias estimates. The z-values for 90% and 95% confidence intervals are 1.65 and 1.96 respectively. Other z-values have been tabulated (such as by Neave (1978)).

Chapter 2

Background Spectral Theory

2.1 Introduction

Wave measurements from both HF radar and wave buoys are derived from information in the frequency domain. This chapter introduces spectral (*i.e.* frequency domain) analysis. The distribution of the observed spectrum of a Normal white noise process is derived and linear filters used to extend this result to the distribution of the observed spectrum of a stationary process with an arbitrary underlying spectrum (as may be used to model ocean waves). The effect of applying a taper is also examined, and finally multivariate spectral analysis is introduced.

2.2 Functions of Continuous Time

2.2.1 The Fourier Transform

A (complex or purely real) function of continuous time $f(t)$ may be expressed as the limit of a linear combination of sinusoids of different frequencies. Mathematically, this transition from the time domain to the frequency domain is performed by the Fourier transform :

$$F(\omega) = \int_{-\infty}^{\infty} f(t)e^{-i\omega t}dt$$

$F(\omega)$ is a complex function of angular frequency (ω) which contains the amplitude and phase information of the sinusoids. The Fourier transform is sometimes denoted thus :

$$F(\omega) = \mathcal{F}(f(t))$$

The inverse Fourier transform performs the reverse procedure :

$$f(t) = \frac{1}{2\pi} \int_{-\infty}^{\infty} F(\omega) e^{i\omega t} d\omega$$

Together, $f(t)$ and $F(\omega)$ are known as a Fourier transform pair, and denoted thus :

$$f(t) \longleftrightarrow F(\omega)$$

2.2.2 Random Functions and Stationarity

As the functions of time of interest to this study are random (as opposed to deterministic), it is necessary to introduce the concept of stationarity.

Strong Stationarity

A process $X(t)$ is said to be strongly stationary if all finite joint distributions of $X(t)$ are the same as the corresponding joint distributions of $X(t+\tau)$ for all values of τ. This is also known as *strict stationarity.*

Intuitively, this is roughly the same as saying that the underlying process is in some stable equilibrium.

Weak Stationarity

A process $X(t)$ is said to be weakly stationary if the first and second order moments (*i.e.* mean vector and covariance matrix) of all finite joint distributions of $X(t)$ are the same as those of the joint distributions of $X(t+\tau)$ for all values of τ. This is also known as *second order stationarity.*

An important special type of random function is one in which all finite joint distributions are multivariate Normal; such a function is called *Normal*, or *Gaussian.* Because a multivariate Normal distribution is completely defined

by its first and second order moments, a weakly stationary Normal process must also be strongly stationary.

2.2.3 The Power Spectrum and Auto-Covariance Function

The power spectrum (or more correctly *the power spectral density*) $\hat{S}(\omega)$ of a function of time is the square of the modulus of its Fourier transform, and (roughly speaking) gives the power density as a function of frequency :

$$\hat{S}(\omega) = |F(\omega)|^2$$

There exist various proofs of the relationship between the power spectrum and auto-covariance function, but the one the author has found most useful and straightforward is that of Cox and Miller (1965), which is summarised below.

Consider the following process :

$$X(t) = \int_{-\infty}^{\infty} e^{i\omega t} dR(\omega)$$

where each $dR(\omega)$ is some complex random variable, independent for each ω (hence R is non-differentiable).

If $X(t)$ has first order stationarity :

$$\mathrm{E}(dR(\omega)) = 0 \; \forall \omega \neq 0$$

and if $X(t)$ has second order stationarity :

$$\mathrm{E}(dR(\omega)dR^*(\omega')) = 0 \; \forall \omega \neq \omega'$$

(where * denotes the complex conjugate).

Consider now the auto-covariance function of this process $\gamma(h)$:

$$\begin{aligned} \gamma(h) &= \mathrm{E}(X(t+h)X^*(t)) \\ &= \mathrm{E}\left(\int_{-\infty}^{\infty} e^{i\omega(t+h)} dR(\omega) \int_{-\infty}^{\infty} e^{-i\omega' t} dR^*(\omega')\right) \end{aligned}$$

$$= \int_{-\infty}^{\infty}\int_{-\infty}^{\infty} e^{i\omega h}e^{it(\omega-\omega')}\underbrace{\mathrm{E}(dR(\omega)dR^*(\omega'))}_{=0 \text{ if } \omega \neq \omega'}$$

This integration is over the diagonal $\omega = \omega'$ and hence may be written as :

$$\gamma(h) = \int_{-\infty}^{\infty} e^{i\omega h}dG(\omega)$$

where $dG(\omega) = \mathrm{E}(dR(\omega)dR^*(\omega))$, and provided that $\mathrm{E}(X(t)) = 0$.

Consider now the variance of this process :

$$\mathrm{Var}(X(t)) = \gamma(0) = \int_{-\infty}^{\infty} dG(\omega)$$

Hence, $dG(\omega)$ gives the contribution to the variance (or power) of the process at frequency ω — *i.e.* $G(\omega)$ is the cumulative power spectrum of $X(t)$.

Usually it will be true that G is differentiable (though occasionally there is a jump at some fixed frequencies, such as 0), in which case :

$$\frac{dG(\omega)}{d\omega} = \mathrm{E}(\hat{S}(\omega))$$

. .

giving

$$\gamma(h) = \int_{-\infty}^{\infty} \mathrm{E}(\hat{S}(\omega))e^{i\omega h}d\omega$$

and hence

$$\mathrm{Var}(X(t)) = \gamma(0) = \int_{-\infty}^{\infty} \mathrm{E}(\hat{S}(\omega))d\omega$$

Thus the underlying (*i.e.* expected) power spectrum of a random process is proportional to the Fourier transform of its auto-covariance function.

This proof can be easily extended to higher dimensions by allowing X to be a function of time and space. Consider the waveform in figure 2.1 travelling to the right, and then consider the elevation at point A as a function of time (figure 2.2). In the time dimension, the shape of the waveform has been reversed. Thus, going forwards in time is like going backwards in space. So the process may be expressed :

$$X(t, \mathbf{x}) = \int_{\omega,\mathbf{k}} e^{i(\omega t - \mathbf{k}.\mathbf{x})}dR(\omega, \mathrm{k})$$

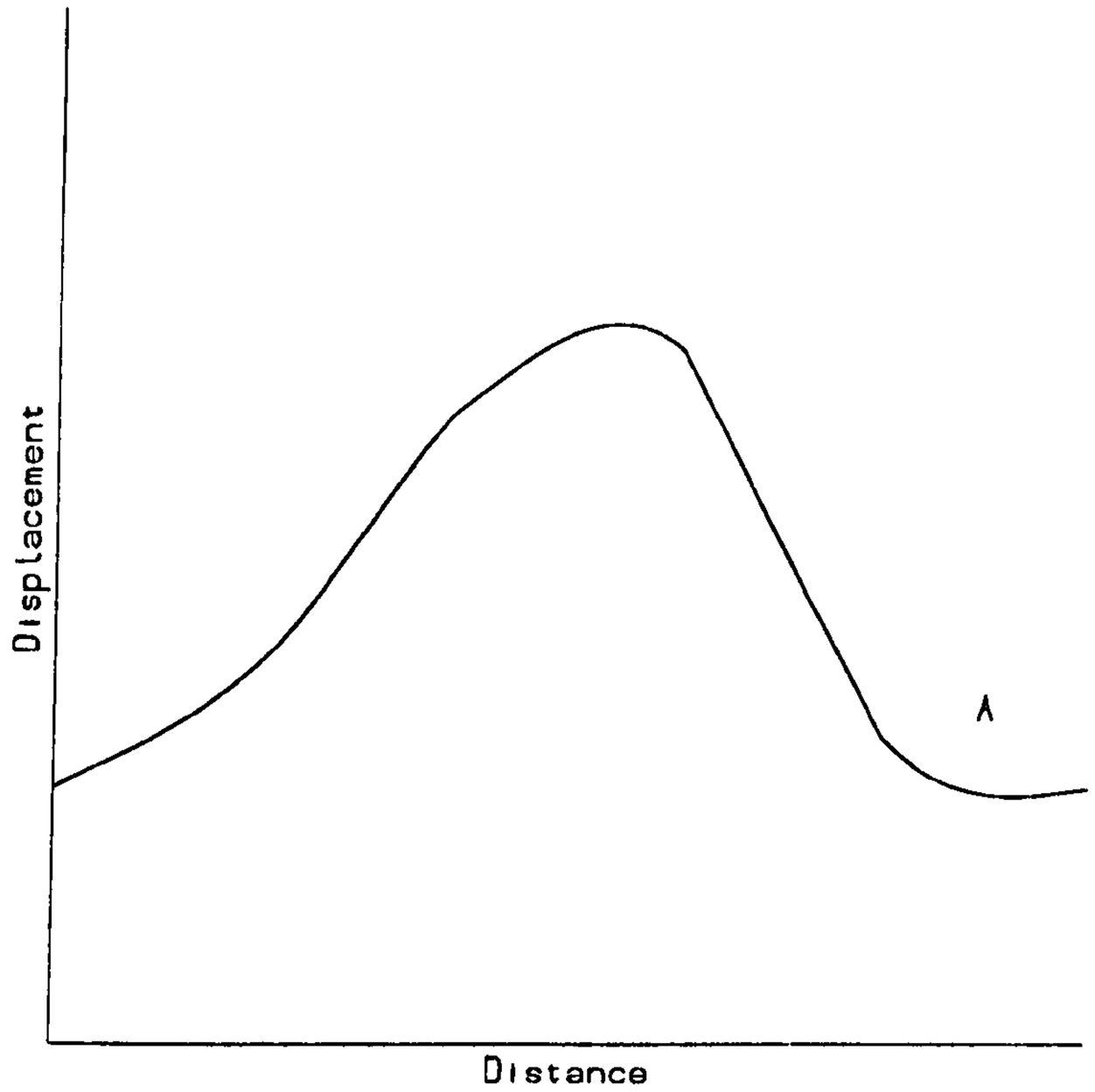

Figure 2.1: An arbitrary waveform moving past some point A.

Figure 2.2: Elevation at point A as a function of time.

This gives the autocovariance :

$$\gamma(h, \mathbf{r}) = \int_{\omega,\mathbf{k}} e^{i(\omega h - \mathbf{k}.\mathbf{r})} dG(\omega, \mathbf{k})$$

and hence,

$$\mathrm{Var}(X(t, \mathbf{x})) = \gamma(0, \mathbf{0}) = \int_{\omega,\mathbf{k}} dG(\omega, \mathbf{k})$$

So, as in the one dimensional case, the underlying power spectrum of a random process in space and time is proportional to the Fourier transform of its auto-covariance function.

2.3 Discrete Time Series

2.3.1 The Discrete Fourier Transform and the Power and Energy Spectra

Section 2.2 introduced the theory of stationary processes in continuous time. The observed time series in this study each consist of a finite set of equally spaced observations of the process in question. As this is an incomplete picture of the full process, Fourier analysis produces only an estimate of the underlying power spectrum (the distribution theory associated with this estimate is given in sections 2.3.2 and 2.3.4). The discrete equivalent of the Fourier transform is the DFT (*D*iscrete *F*ourier *T*ransform). The DFT fits sinusoids of a finite set of equally spaced frequencies to the time series $X(t_j)$, $j = -\frac{n}{2} \ldots \frac{n}{2} - 1$:

$$\hat{F}(\omega_l) = \frac{1}{n} \sum_{j=-\frac{n}{2}}^{\frac{n}{2}-1} X(t_j) e^{-i\omega_l t_j} \qquad l = -\tfrac{n}{2} \ldots \tfrac{n}{2} - 1 \tag{2.1}$$

where $\begin{cases} n \text{ is the number of observations in the time series} \\ \omega_l = l\Delta_\omega \\ \Delta_\omega = \frac{2\pi}{T} \text{ is the frequency step} \\ T \text{ is the duration of the time series} \end{cases}$

The interval $(\omega_l - \frac{\Delta_\omega}{2}, \omega_l + \frac{\Delta_\omega}{2})$ is known as a *frequency bin.*

Equation 2.1 may also be written :

$$X(t_j) \overset{\mathcal{D}}{\longleftrightarrow} \hat{F}(\omega_l)$$

$\hat{F}(\omega_l)$ is a complex function containing amplitude and phase information. Also, because $\hat{F}$ is defined only for frequencies which are integer multiples of Δ_ω, $\hat{F}$ describes a process which is periodic in T.

The basic discrete equivalent of the power spectrum is the periodogram (this name is somewhat misleading, because it is a function of frequency and not of period) :

$$\hat{S}(\omega_l) = |\hat{F}(\omega_l)|^2$$

Alternatively, we may think in terms of the *energy spectrum* $\hat{c}_{XX}(\omega_l)$ ($energy = power \times time$, with the subscripts identifying the original process) :

$$\hat{c}_{XX}(\omega_l) = T\hat{S}(\omega_l) = n\Delta_t\hat{S}(\omega_l) \tag{2.2}$$

where Δ_t is the sampling interval. In the continuous case, this becomes :

$$c_{XX}(\omega) = TS(\omega)$$

In this context, the usual units for the "energy" spectrum are m^2/Hz.

2.3.2 The Distribution of an Energy Spectrum of Normal White Noise

Consider a real process $W(t_j)$ of normally distributed white noise :

$$W(t_j) \sim \mathrm{N}(0, \sigma^2) \;\; i.i.d. \;\; \forall t_j = -\tfrac{n}{2} \ldots \tfrac{n}{2} - 1$$

(*i.i.d.* means *i*ndependent and *i*dentically *d*istributed). From equations 2.1 and 2.2 we get :

$$\hat{c}_{WW}(\omega_l) = \frac{\Delta_t}{n}\left(\left(\sum_{j=-\frac{n}{2}}^{\frac{n}{2}-1} W(t_j)\cos(\omega_l t_j)\right)^2 + \left(\sum_{j=-\frac{n}{2}}^{\frac{n}{2}-1} W(t_j)\sin(\omega_l t_j)\right)^2\right), \quad l = -\tfrac{n}{2} \ldots \tfrac{n}{2} - 1 \tag{2.3}$$

$$\left.\begin{array}{rcl} \text{Let } A(\omega_l) & = & \sum_{j=-\frac{n}{2}}^{\frac{n}{2}-1} W(t_j)\cos(\omega_l t_j) \\ B(\omega_l) & = & \sum_{j=-\frac{n}{2}}^{\frac{n}{2}-1} W(t_j)\sin(\omega_l t_j) \end{array}\right\} \; l = -\tfrac{n}{2}\ldots\tfrac{n}{2}-1$$

We have :

$$\mathrm{E}(W(t_j)) = 0 \;\forall t_j$$

Therefore,

$$\mathrm{E}(A(\omega_l)) = \mathrm{E}(B(\omega_l)) = 0 \;\forall \omega_l$$

and hence,

$$\mathrm{Var}(A(\omega_l)) = \mathrm{E}(A^2(\omega_l)) = \sigma^2 \sum_{j=-\frac{n}{2}}^{\frac{n}{2}-1} \cos^2(\omega_l t_j) = \begin{cases} \frac{n\sigma^2}{2} & l = \pm 1 \ldots \pm(\frac{n}{2}-1) \\ n\sigma^2 & l = 0, -\frac{n}{2} \end{cases}$$

Similarly,

$$\mathrm{Var}(B(\omega_l)) = \begin{cases} \frac{n\sigma^2}{2} & l = \pm 1 \ldots \pm(\frac{n}{2}-1) \\ 0 & l = 0, -\frac{n}{2} \end{cases}$$

For $l \neq m$:

$$\mathrm{Cov}(A(\omega_l), A(\omega_m)) = \sigma^2 \sum_{j=-\frac{n}{2}}^{\frac{n}{2}-1} \cos(\omega_l t_j)\cos(\omega_m t_j) = 0$$

and similarly,

$$\mathrm{Cov}(B(\omega_l), B(\omega_m)) = 0$$

Also, $\forall l, m$:

$$\mathrm{Cov}(A(\omega_l), B(\omega_m)) = 0$$

As A and B are linear combinations of independent normal variables, A and B are also normally distributed. Hence :

$$\frac{A^2(\omega_l)}{\mathrm{Var}(A(\omega_l))} = \left\{ \begin{array}{ll} \frac{2A^2(\omega_l)}{n\sigma^2} & l = \pm 1 \ldots \pm(\frac{n}{2}-1) \\ \frac{A^2(\omega_l)}{n\sigma^2} & l = 0, -\frac{n}{2} \end{array} \right\} \sim \chi_1^2$$

and similarly :

$$\frac{B^2(\omega_l)}{\mathrm{Var}(B(\omega_l))} = \frac{2B^2(\omega_l)}{n\sigma^2} \sim \chi_1^2, \quad l = \pm 1 \ldots \pm(\tfrac{n}{2}-1)$$

Because the distinct As and Bs are uncorrelated and jointly normally distributed, they are also independent. So, using equation 2.3 we get :

$$\frac{2}{n\sigma^2}(A^2(\omega_l) + B^2(\omega_l)) = \frac{2\hat{c}_{WW}(\omega_l)}{\Delta_t \sigma^2} = \frac{2\hat{c}_{WW}(\omega_l)}{c_{WW}(\omega_l)} \sim \chi^2_2, \quad l = \pm 1 \ldots \pm\left(\tfrac{n}{2} - 1\right)$$

$$\frac{1}{n\sigma^2}A^2(\omega_l) = \frac{\hat{c}_{WW}(\omega_l)}{\Delta_t \sigma^2} = \frac{\hat{c}_{WW}(\omega_l)}{c_{WW}(\omega_l)} \sim \chi^2_1, \quad l = 0, -\tfrac{n}{2}$$

i.e. :

$$\frac{\hat{c}_{WW}(\omega_l)}{c_{WW}(\omega_l)} \sim \frac{\chi^2_\nu}{\nu} \tag{2.4}$$

where ν =1 or 2, according to the value of l. Equation 2.4 also holds when W is a complex process. In such cases however, B will be non-zero when $l = 0, -\frac{n}{2}$ and hence $\nu = 2 \ \forall l$.

Hence, a $100(1-\alpha)\%$ confidence interval for each $c_{WW}(\omega_l)$ may be constructed :

$$\left(\frac{\nu\hat{c}_{WW}(\omega_l)}{\chi^2_{\nu,1-\frac{\alpha}{2}}}, \frac{\nu\hat{c}_{WW}(\omega_l)}{\chi^2_{\nu,\frac{\alpha}{2}}}\right) \tag{2.5}$$

where $\chi^2_{\nu,\beta}$ is the β-*th* quantile of the χ^2_ν distribution.

Since equation 2.4 deals with *ratios* of energy, power may be substituted for energy using equation 2.2 leading to a $100(1-\alpha)\%$ confidence interval for power $S(\omega_l)$:

$$\left(\frac{\nu\hat{S}(\omega_l)}{\chi^2_{\nu,1-\frac{\alpha}{2}}}, \frac{\nu\hat{S}(\omega_l)}{\chi^2_{\nu,\frac{\alpha}{2}}}\right) \tag{2.6}$$

2.3.3 Linear Filters

A linear filter is a transformation which when applied to a time series will affect the component at each frequency independently. This effect on frequency is called the *frequency response function.* Consider a function of time $Y(t)$ produced by passing a time series $X(t)$ with Fourier transform $\hat{F}(\omega)$ through a linear filter with frequency response function $\eta(\omega)$:

$$Y(t) \longleftrightarrow \hat{F}(\omega)\eta(\omega)$$

Consider now $H(t)$, the inverse Fourier transform of $\eta(\omega)$:

$$H(t) \longleftrightarrow \eta(\omega)$$

Hence :

$$Y(t) = X(t) * H(t)$$

where $*$ denotes convolution. $H(t)$ is called the *impulse response function* of the linear filter.

Also,

$$c_{YY}(\omega) = |\eta(\omega)|^2 c_{XX}(\omega)$$

We may thus model a stationary process with arbitrary energy spectrum as a white noise process passed through a linear filter.

2.3.4 The Distribution of the Energy Spectrum of a Stationary Process

Consider a process $W(t_j)$ of normally distributed white noise, passed through a linear filter with impulse response function $H(t_j)$, producing a stationary linear process $X(t_j)$:

$$\begin{aligned} &W(t_j) \sim \mathrm{N}(0,1) \;\; i.i.d. \; \forall t_j \\ &X(t_j) = W(t_j) * H(t_j) \\ &H(t_j) \overset{\mathcal{D}}{\longleftrightarrow} \eta(\omega_l) \end{aligned}$$

This gives us the following estimated energy spectrum of X :

$$\begin{aligned} \hat{c}_{XX}(\omega_l) &= \frac{\Delta_t}{n}\left(\left(\sum_{j=-\frac{n}{2}}^{\frac{n}{2}-1} X(t_j)\cos(\omega_l t_j)\right)^2 + \left(\sum_{j=-\frac{n}{2}}^{\frac{n}{2}-1} X(t_j)\sin(\omega_l t_j)\right)^2\right), \\ &= \underline{\Delta_t |\eta(\omega_l)|^2} \\ &\quad \left(\left(\sum_{j=-\frac{n}{2}}^{\frac{n}{2}-1} W(t_j)\cos(\omega_l t_j)\right)^2 + \left(\sum_{j=-\frac{n}{2}}^{\frac{n}{2}-1} W(t_j)\sin(\omega_l t_j)\right)^2\right), \\ &\quad n \\ &l = -\tfrac{n}{2} \ldots \tfrac{n}{2} - 1 \end{aligned}$$

and substituting from equation 2.3 we get :

$$\hat{c}_{XX}(\omega_l) = |\eta(\omega_l)|^2 \hat{c}_{WW}(\omega_l)$$

Hence using equations 2.4 we get :

$$\frac{|\eta(\omega_l)|^2 \hat{c}_{WW}(\omega_l)}{|\eta(\omega_l)|^2 c_{WW}(\omega_l)} = \frac{\hat{c}_{XX}(\omega_l)}{c_{XX}(\omega_l)} \sim \chi^2_1$$

for $l = 0, n$ if the process is purely real, and

$$\frac{2|\eta(\omega_l)|^2 \hat{c}_{WW}(\omega_l)}{|\eta(\omega_l)|^2 c_{WW}(\omega_l)} = \frac{2\hat{c}_{XX}(\omega_l)}{c_{XX}(\omega_l)} \sim \chi^2_2$$

otherwise.

This yields the following $100(1-\alpha)\%$ confidence interval for $c_{XX}(\omega_l)$:

$$\left(\frac{\nu \hat{c}_{XX}(\omega_l)}{\chi^2_{\nu,1-\frac{\alpha}{2}}}, \frac{\nu \hat{c}_{XX}(\omega_l)}{\chi^2_{\nu,\frac{\alpha}{2}}} \right) \tag{2.7}$$

and the confidence interval for the power $S_X(\omega_l)$ takes the same form as in equation 2.6.

The theory in this section is derived under the assumption that the process X exhibits energy only at a finite set of frequencies $\{\omega_l\}$. Since the time domain processes of interest to this study have energy over a continuum of frequencies, an effect known as spectral leakage occurs (see section 2.3.5) and as a result, the theory presented above is only approximate.

2.3.5 Spectral Leakage and Tapers

In section 2.3.1 it was mentioned that $\hat{F}$ describes a periodic process. If the underlying process $X(t)$ includes a component at some frequency which does not exactly match any observed frequency bin ω_l, an effect known as spectral leakage occurs. The Fourier transform assigns the power at this non-matching component to a range of frequency bins, with most of the power being assigned to those bins whose frequencies are closest to that of the component (such as in figure 2.3). Thus, it appears as though power from the non-matching component has "leaked" into neighbouring frequencies.

If the underlying power spectrum is smooth, the effects of spectral leakage are not too serious, if however it contains spikes, spectral leakage can swamp lower powered frequencies.

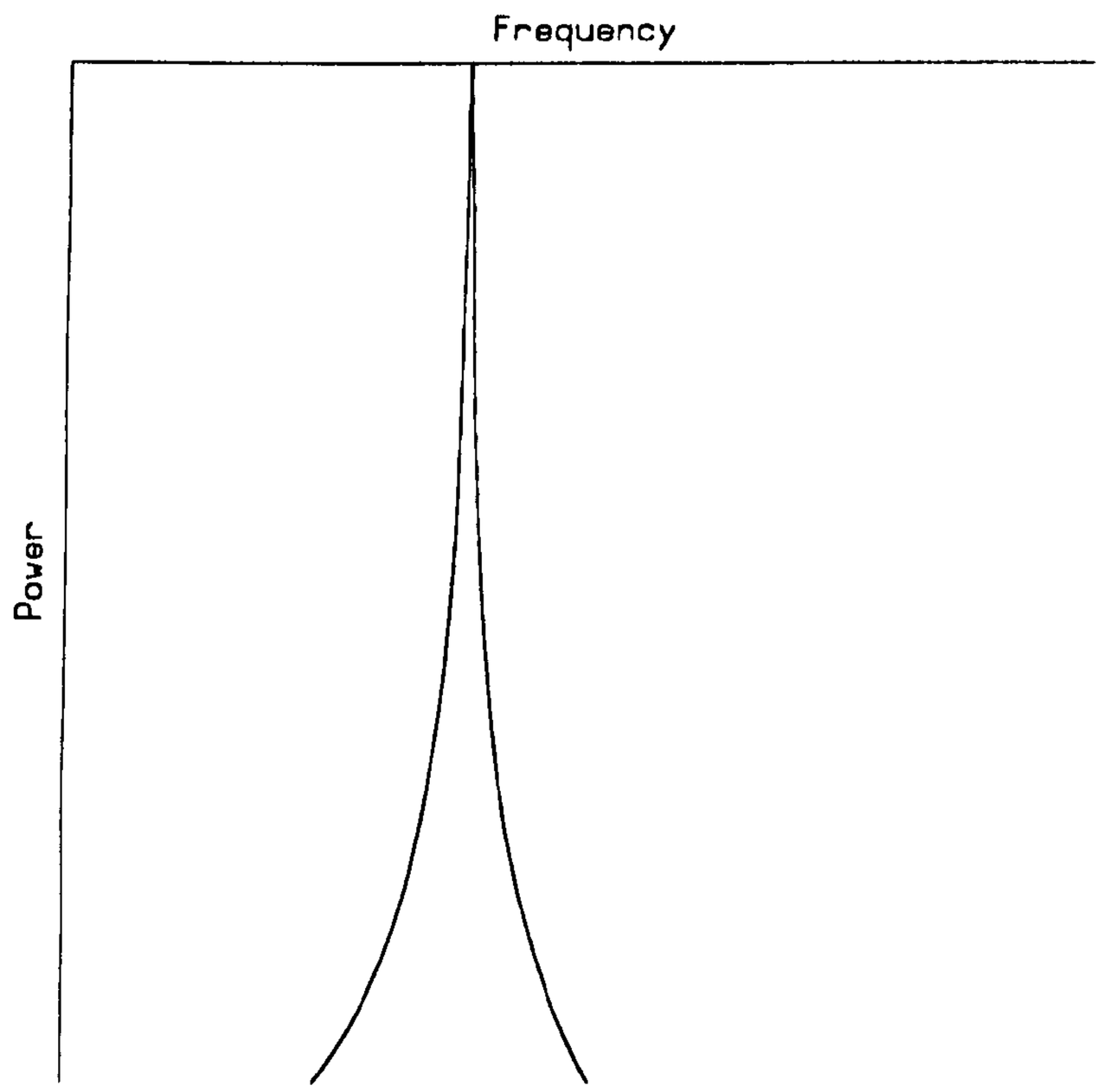

Figure 2.3: A spectrum showing leakage, obtained from a sinusoid whose frequency does not *exactly* correspond to any frequency bin. The power peaks at the frequency bin closest to the frequency of the signal, but some power has "leaked" into neighbouring frequencies.

Consider the function $z(t_j),\ j = -\infty \ldots \infty$

$$z(t_j) = \begin{cases} 1 & \text{if } j = -\frac{n}{2} \ldots \frac{n}{2} - 1 \\ 0 & \text{otherwise} \end{cases}$$

and let $Y(t_j),\ j = -\infty \ldots \infty$ be the process $X(t_j)$ measured over infinite time.

$$i.e.\ X(t_j) = Y(t_j)z(t_j)$$

Thus,

$$X(t_j) \overset{\mathcal{D}}{\longleftrightarrow} \mathcal{F}(Y(t_j)) * \mathcal{F}(z(t_j))$$

Since $\mathcal{F}(z(t_j))$ is a sinc function (*i.e.* of the form $\frac{\sin(t)}{t}$), the effect of convolution is to cause some of the power to spread into neighbouring frequencies (this is a more mathematical explanation of leakage). Because of this, tapers (also known as *data windows*) are sometimes applied to the data. A taper is a function $z(t_j)$ whose properties in the frequency domain are more desirable than those of the sinc function (because of the shape of $z(t_j)$ defined above, an untapered time series is sometimes referred to as having a *square taper* or *rectangular taper*).

Harris (1978) has examined various properties of a wide range of tapers. Perhaps the best known of these is the Hanning taper (the process of applying this taper is ofter referred to as *Hanning*) which has the following form :

$$z(t_j) = \begin{cases} 0.5\left(1 + \cos\left(\frac{2\pi j}{n}\right)\right) & \text{if } j = -\frac{n}{2} \ldots \frac{n}{2} - 1 \\ 0 & \text{otherwise} \end{cases}$$

Whilst such a taper will go some way towards counteracting spectral leakage (as shown below), it does have the disadvantage of broadening any spikes. Consider $z'(t_j)$, the finite subset of $z(t_j)$ corresponding to the observed data $X(t_j)$:

$$i.e.\ z'(t_j) = z(t_j),\quad j = -\frac{n}{2} \ldots \frac{n}{2} - 1$$

Now consider its DFT :

$$\mathcal{F}(z'(t_j)) = \begin{cases} 0 & \text{if } m = -\frac{n}{2} \ldots -2 \\ 0.25 & \text{if } m = -1 \\ 0.5 & \text{if } m = 0 \\ 0.25 & \text{if } m = 1 \\ 0 & \text{if } m = 2 \ldots \frac{n}{2} - 1 \end{cases}$$

Since it is this DFT with which the observed periodogram is convolved, it

can be seen how a peak (corresponding to $m = 0$) is broadened — compare this with the DFT of a square taper :

$$\mathcal{F}(z'(t_j)) = \begin{cases} 0 & \text{if } m = -\frac{n}{2} \ldots -1 \\ 1 & \text{if } m = 0 \\ 0 & \text{if } m = 1 \ldots \frac{n}{2} - 1 \end{cases}$$

The Hanning taper is an example of the Blackman-Harris family of tapers, defined by :

$$z'(t_j) = a_0 + a_1 \cos\left(\frac{2\pi j}{n}\right) + a_2 \cos\left(\frac{4\pi j}{n}\right) + a_3 \cos\left(\frac{6\pi j}{n}\right), \; j = -\frac{n}{2} \ldots \frac{n}{2} - 1$$

where $a_0 \ldots a_3$ are constants satisfying :

$$\sum_{m=0}^{3} a_m = 1$$

The *minimum 4-sample Blackman Harris taper* (hereafter referred to as the *4-point Blackman-Harris taper*) is particularly effective at reducing spectral leakage (see figure 2.4 which shown the effect of this taper applied to the same signal as in figure 2.3) and has the following coefficients :

$$\begin{aligned} a_0 &= 0.35875 \\ a_1 &= 0.48829 \\ a_2 &= 0.14128 \\ a_3 &= 0.01168 \end{aligned}$$

The DFT of the Blackman-Harris family of tapers is :

$$\mathcal{F}(z'(t_j)) = \begin{cases} 0 & \text{if } m = -\frac{n}{2} \ldots -4 \\ \frac{a_{|m|}}{2} & \text{if } m = -3, -2, -1, 1, 2, 3 \\ a_0 & \text{if } m = 0 \\ 0 & \text{if } m = 4 \ldots \frac{n}{2} - 1 \end{cases}$$

hence their use can considerably broaden any spikes in the spectrum.

We define the *order* of a taper as its highest order non-zero harmonic. Thus the Hanning taper has order 1, and the 4-point Blackman-Harris taper has order 3.

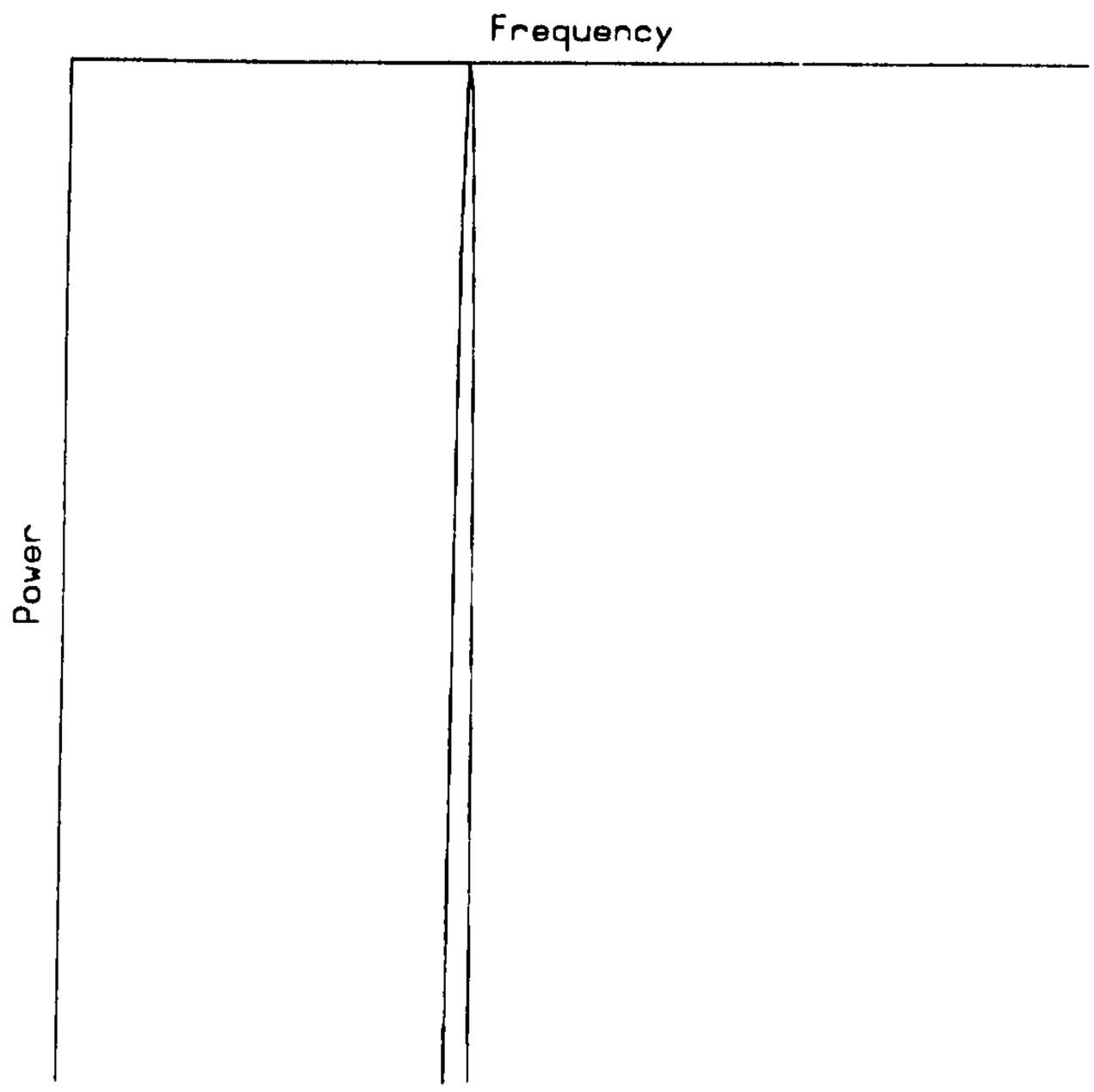

Figure 2.4: The spectrum of a "leaky" signal, calculated after the application of a 4-Point Blackman-Harris taper.

2.3.6 Averaging of Sequential and Time-Overlapped Spectra

The main problem with the confidence intervals for energy and power given by equations 2.6 and 2.7 is that they are independent of n, the number of observations in the time series (*i.e.* they are not consistent estimators). One way to overcome this is to partition the observations into N shorter sequential time series, each of length n' (*i.e.* $n = Nn'$), calculate the energy spectra and take the average. Because these sequential spectra are asymptotically independent, $N\nu$ is substituted for ν in equation 2.7, thus reducing the width of the confidence interval (*i.e.* decreasing the variance of the estimated energy). However, if a taper is being used, variance may be further reduced by overlapping the individual time series.

Consider a linear process $Y(t_j),\ \ j = 0 \ldots n-1$ partitioned into a sequence of N time series of length T', each with n' (possibly tapered) observations such that each series overlaps with the preceeding and succeeding series by

50% (*i.e.* by $\frac{n'}{2}$ observations).

$$\begin{aligned}
\text{Let } A_m(\omega_l) &= \sum_{j=\frac{n'm}{2}}^{\frac{n'(m+2)}{2}-1} Y(t_j) z'(t_{j-\frac{n'(m+1)}{2}}) \cos(\omega_l t_{j-\frac{n'(m+1)}{2}}) \\
B_m(\omega_l) &= \sum_{j=\frac{n'm}{2}}^{\frac{n'(m+2)}{2}-1} Y(t_j) z'(t_{j-\frac{n'(m+1)}{2}}) \sin(\omega_l t_{j-\frac{n'(m+1)}{2}}) \\
& \qquad m = 0 \ldots N-1 \\
& \qquad l = -\tfrac{n}{2} \ldots \tfrac{n}{2} - 1
\end{aligned} \tag{2.8}$$

Hence we estimate $c_{YY}(\omega_l)$ with :

$$\hat{c}_{YY} = \frac{\Delta_t}{Nn'} \sum_{m=0}^{N-1} (A_m^2(\omega_l) + B_m^2(\omega_l))$$

This involves a sum of correlated χ_1^2 variables which may be approximated by a single χ_ν^2 variable whose degrees of freedom are given below. We get :

$$\mathrm{E}\left(\frac{\sum_{m=0}^{N-1} A_m^2(\omega_l)}{N} \right) = \frac{\sum_{m=0}^{N-1} \mathrm{E}(A_m^2(\omega_l))}{N} = \frac{n'|\eta(\omega_l)|^2}{2}, \quad l \neq 0, -\tfrac{n'}{2}$$

and similarly,

$$\mathrm{E}\left(\frac{\sum_{m=0}^{N-1} B_m^2(\omega_l)}{N} \right) = \frac{n'|\eta(\omega_l)|^2}{2} \quad l \neq 0, -\tfrac{n'}{2}$$

Also,

$$\mathrm{Var}\left(\sum_{m=0}^{N-1} A_m^2(\omega_l) \right) = \sum_{m=0}^{N-1} \mathrm{Var}(A_m^2) + \sum_{m' \neq m} \sum_{m=0}^{N-1} \mathrm{Cov}(A_m^2, A_{m'}^2)$$

But since the spectra of non-overlapping series are (approximately) independent,

$$\begin{aligned}
\mathrm{Var}\left(\sum_{m=0}^{N-1} A_m^2(\omega_l) \right) &= \sum_{m=0}^{N-1} \mathrm{Var}(A_m^2) + \sum_{m=0}^{N-2} \mathrm{Cov}(A_m^2, A_{m+1}^2) \\
&\quad + \sum_{m=1}^{N-1} \mathrm{Cov}(A_m^2, A_{m-1}^2) \\
&= \frac{n'^2 |\eta(\omega_l)|^4}{4} (N + 4(N-1)\rho^2(50\%))
\end{aligned} \tag{2.9}$$

where $\rho(50\%)$ is the correlation between each pair of successive As. Similarly,

$$\text{Var}\left(\sum_{m=0}^{N-1} B_m^2(\omega_l)\right) = \frac{n'^2|\eta(\omega_l)|^4}{4}(N + 4(N-1)\rho^2(50\%)) \qquad (2.10)$$

Consider now a pair of successive As. Each is a sum of the product of three components — the observations, the taper (if any) and the sinusoid (see equation 2.8).

The sets of observations for the two series are identical over the overlap region (and approximately independent elsewhere).

The sinusoid is periodic in T'. If the sinusoid is periodic in $\frac{T'}{2}$ (*i.e.* if l is even) then the sinusoidal components are identical over the overlap region. If the sinusoid is not periodic in $\frac{T'}{2}$ (*i.e.* if l is odd) then the sinusoidal components have a phase difference of π, and hence are identical in magnitude but with opposite signs (which can effectively be ignored since ρ appears in equations 2.9 and 2.10 as a square). Also, the sinusoidal components of the As and Bs of the same frequency all have a phase difference of $\frac{\pi}{2}$.

Thus, the important factor in calculating ρ is the effect of the taper. We get :

$$\begin{aligned}
&\text{Cov}(A_0(\omega_l), A_1(\omega_l)) \\
&= \text{Cov}\left(\sum_{j=0}^{n'-1} Y(t_j)z'(t_{j-\frac{n'}{2}})\cos(\omega_l t_{j-\frac{n'}{2}}), \sum_{j=\frac{n'}{2}}^{\frac{3n'}{2}-1} Y(t_j)z'(t_{j-n'})\cos(\omega_l t_{j-n'})\right) \\
&= \text{Cov}\left(\sum_{j=\frac{n'}{2}}^{n'-1} Y(t_j)z'(t_{j-\frac{n'}{2}})\cos(\omega_l t_{j-\frac{n'}{2}}), \sum_{j=\frac{n'}{2}}^{n'-1} Y(t_j)z'(t_{j-n'})\cos(\omega_l t_{j-n'})\right) \\
&= (-1)^l \frac{n'|\eta(\omega_l)|^2}{4} \sum_{j=\frac{n'}{2}}^{n'-1} z'(t_{j-\frac{n'}{2}})z'(t_{j-n'}) \\
&= (-1)^l \frac{n'|\eta(\omega_l)|^2}{4} \sum_{j=-\frac{n'}{2}}^{-1} z'(t_{j+\frac{n'}{2}})z'(t_j)
\end{aligned}$$

Hence :

$$\begin{aligned}
\rho(50\%) &= \text{Corr}(A_0(\omega_l), A_1(\omega_l)) \\
&= \frac{2}{n'|\eta(\omega_l)|^2}\text{Cov}(A_0(\omega_l), A_1(\omega_l)) \\
&= \frac{(-1)^l}{2} \sum_{j=-\frac{n'}{2}}^{-1} z'(t_{j+\frac{n'}{2}})z'(t_j)
\end{aligned}$$

Thus $\rho^2(50\%)$ is a function of the taper used (*i.e.* a known quantity), and

hence :

$$\begin{aligned}\nu &= \frac{2\mathrm{E}^2(\hat{c}_{YY})}{\mathrm{Var}(\hat{c}_{YY})} \\ &= \frac{\frac{\Delta_f^2}{n'^2} 2n'^2|\eta(\omega_l)|^4 N^2}{\frac{\Delta_f^2}{n'^2}\frac{n'^2|\eta(\omega_l)|^4}{2}(N+4(N-1)\rho^2(50\%))} \\ &= \frac{2N^2}{N+4(N-1)\rho^2(50\%)}\end{aligned}$$

Consider now the same process but with each series overlapping with the preceeding and succeeding series by 75% (*i.e.* by $\frac{3n'}{4}$ observations). Keeping for the moment A_m and B_m as defined in equations 2.8, the following table gives the phase differences of the sinusoidal components of the first 4 As and Bs with respect to A_0 :

	$\lvert l\rvert = 4, 8, 12\ldots$ (Periodic in $\frac{T'}{4}$)	$\lvert l\rvert = 2, 6, 10\ldots$ (Periodic in $\frac{T'}{2}$)	l odd (Periodic in T')
B_0	$\frac{\pi}{2}$	$\frac{\pi}{2}$	$\frac{\pi}{2}$
A_1	0	π	$\frac{\pi}{2}$
B_1	$\frac{\pi}{2}$	$\frac{\pi}{2}$	π
A_2	0	0	π
B_2	$\frac{\pi}{2}$	$\frac{\pi}{2}$	$\frac{\pi}{2}$
A_3	0	π	$\frac{\pi}{2}$
B_3	$\frac{\pi}{2}$	$\frac{\pi}{2}$	π

Thus if we swap the definitions of A_m and B_m where both m and l are odd, *i.e.* let

$$\left.\begin{aligned}A_m(\omega_l) &= \sum_{j=\frac{n'm}{2}}^{\frac{n'(m+2)}{2}-1} Y(t_j)z'(t_{j-\frac{n'(m+1)}{2}})\sin(\omega_l t_{j-\frac{n'(m+1)}{2}}) \\ B_m(\omega_l) &= \sum_{j=\frac{n'm}{2}}^{\frac{n'(m+2)}{2}-1} Y(t_j)z'(t_{j-\frac{n'(m+1)}{2}})\cos(\omega_l t_{j-\frac{n'(m+1)}{2}})\end{aligned}\right\} \begin{matrix} m \text{ odd} \\ l \text{ odd}\end{matrix}$$

then for each ω_l the sinusoidal components of all the As are identical in magnitude (though sometimes opposite in sign), and similarly for the sinusoidal components of all the Bs, and again the sinusoidal components of the As and Bs of the same frequency all have a phase difference of $\frac{\pi}{2}$. Hence we may proceed almost as before :

$$\mathrm{E}\left(\frac{\sum_{m=0}^{N-1} A_m^2(\omega_l)}{N}\right) = \frac{n'|\eta(\omega_l)|^2}{2} \quad l \neq 0, -\tfrac{n'}{2}$$

$$\mathrm{E}\left(\frac{\sum_{m=0}^{N-1} B_m^2(\omega_l)}{N}\right) = \frac{n'|\eta(\omega_l)|^2}{2} \quad l \neq 0, -\tfrac{n'}{2}$$

$$\begin{aligned}
\mathrm{Var}\left(\sum_{m=0}^{N-1} A_m^2(\omega_l)\right) &= \sum_{m=0}^{N-1} \mathrm{Var}(A_m^2) + \sum_{m' \neq m} \sum_{m=0}^{N-1} \mathrm{Cov}(A_m^2, A_{m'}^2) \\
&= \sum_{m=0}^{N-1} \mathrm{Var}(A_m^2) \\
&\quad + \sum_{m=0}^{N-2} \mathrm{Cov}(A_m^2, A_{m+1}^2) + \sum_{m=1}^{N-1} \mathrm{Cov}(A_m^2, A_{m-1}^2) \\
&\quad + \sum_{m=0}^{N-3} \mathrm{Cov}(A_m^2, A_{m+2}^2) + \sum_{m=2}^{N-1} \mathrm{Cov}(A_m^2, A_{m-2}^2) \\
&\quad + \sum_{m=0}^{N-4} \mathrm{Cov}(A_m^2, A_{m+3}^2) + \sum_{m=3}^{N-1} \mathrm{Cov}(A_m^2, A_{m-3}^2)
\end{aligned}$$

giving :

$$\nu = \frac{2N^2}{N + 4(N-1)\rho^2(75\%) + 4(N-2)\rho^2(50\%) + 4(N-3)\rho^2(25\%)} \quad (N \geq 3)$$

where
$$\begin{cases}
\rho(25\%) = \frac{(-1)^l}{2} \sum_{j=-\frac{n'}{2}}^{-\frac{n'}{4}-1} z'(t_{j+\frac{3n'}{4}}) z'(t_j) \\
\rho(75\%) = \frac{(-1)^l}{2} \sum_{j=-\frac{n'}{2}}^{\frac{n'}{4}-1} z'(t_{j+\frac{n'}{4}}) z'(t_j)
\end{cases}$$

Alternative forms of the formulae for the approximate numbers of degrees of freedom (describing the same relationships) are given by Welch (1967) and Harris (1978).

2.4 Multivariate Time Series

2.4.1 The Cross- Co- and Quadrature Spectra

The basic tool for examining the relationship between two time series (X and Y, say) in the frequency domain is the (energy) cross-spectrum $\hat{\xi}_{XY}$:

$$\hat{\xi}_{XY}(\omega_l) = \frac{\Delta_t}{n} \left(\sum_{j=-\frac{n}{2}}^{\frac{n}{2}-1} X(t_j) e^{-i\omega_l t_j}\right) \left(\sum_{j=-\frac{n}{2}}^{\frac{n}{2}-1} Y^*(t_j) e^{i\omega_l t_j}\right)$$

Because it is a complex function, the cross-spectrum is often split into its co-spectrum $\hat{c}_{XY}$ and quadrature spectrum $\hat{q}_{XY}$:

$$\begin{aligned} \hat{c}_{XY} &= \mathrm{Re}(\hat{\xi}_{XY}) \\ \hat{q}_{XY} &= -\mathrm{Im}(\hat{\xi}_{XY}) \\ i.e.\ \hat{\xi}_{XY} &= \hat{c}_{XY} - i\hat{q}_{XY} \end{aligned}$$

If X and Y are identical then the cross-spectrum takes the values of the energy spectrum of the process, and since this is purely real, so does the co-spectrum (this explains the double subscript in the notation $\hat{c}_{XX}$ of the energy spectrum). The statistical properties of these spectra have been summarised by Long (1980) :

$$\begin{aligned} \mathrm{Cov}(\hat{c}_{AB}, \hat{c}_{CD}) &= \frac{c_{AC}c_{BD} + q_{AC}q_{BD} + c_{AD}c_{BC} + q_{AD}q_{BC}}{\nu} \\ \mathrm{Cov}(\hat{c}_{AB}, \hat{q}_{CD}) &= \frac{c_{AC}q_{BD} - q_{AC}c_{BD} - c_{AD}q_{BC} + q_{AD}c_{BC}}{\nu} \\ \mathrm{Cov}(\hat{q}_{AB}, \hat{q}_{CD}) &= \frac{c_{AC}c_{BD} + q_{AC}q_{BD} - c_{AD}c_{BC} - q_{AD}q_{BC}}{\nu} \end{aligned}$$

where A, B, C and D represent 4 *not necessarily distinct* time series, ν is the number of degrees of freedom in the spectral estimates, and c and q represent the expectations of $\hat{c}$ and $\hat{q}$ respectively. Furthermore, Long (1980) states that for large ν (> 25) the $\hat{c}$s and $\hat{q}$s are approximately Normally distributed.

Chapter 3

Spectral Integrals and Moments

3.1 Introduction

Many of the formulae relating to HF radar analysis (and to a lesser extent wave buoy analysis) considered in this study involve integrals over the whole or a part of an energy spectrum. Such integrals are estimated by a summation of the observed energy spectrum (possibly with weights) over the appropriate range of frequencies. This chapter deals with the statistical properties of such estimators, and derives some new expressions for the variances and covariances of such integrals calculated from tapered data.

Since for most practical applications it is more convenient to consider functions of frequency f rather than angular frequency ω ($\omega = 2\pi f$), we shall now adopt this convention.

3.2 The Definition of a Spectral Moment

The j-th spectral moment m_j of a spectrum $c_{XX}(f)$ is defined as :

$$m_j = \int_{-\infty}^{\infty} f^j c_{XX}(f) df$$

This is estimated by :

$$\hat{m}_j = \sum_f f^j \hat{c}_{XX}(f)\Delta_f$$

3.3 The Distribution of the Total Energy in a Set of Frequency Bins of a Periodogram

For an observed untapered energy spectrum, we have from section 2.3.4 :

$$\hat{c}_{XX}(f) \sim \frac{c_{XX}(f)\chi^2_2}{2} \quad \text{approx.}$$

Suppose we are interested in the total energy in a set Ω, of frequencies (for convenience, f will now refer to the frequency bin index number, and we will drop the frequency step term Δ_f).

$$\begin{aligned}
\mathrm{E}\left(\sum_{f\in\Omega} \hat{c}_{XX}(f)\right) &= \mathrm{E}\left(\sum_{f\in\Omega} \frac{c_{XX}(f)\chi^2_{2,f}}{2}\right) \\
&= \sum_{f\in\Omega} \frac{c_{XX}(f)}{2}\mathrm{E}(\chi^2_{2,f}) \\
&= \sum_{f\in\Omega} c_{XX}(f) \qquad (3.1) \\
\mathrm{Var}\left(\sum_{f\in\Omega} \hat{c}_{XX}(f)\right) &= \mathrm{Var}\left(\sum_{f\in\Omega} \frac{c_{XX}(f)\chi^2_{2,f}}{2}\right) \\
&= \sum_{f\in\Omega} \frac{c^2_{XX}(f)}{4}\mathrm{Var}(\chi^2_{2,f}) \\
&= \sum_{f\in\Omega} c^2_{XX}(f) \quad \text{asymptotically}
\end{aligned}$$

The distribution of this sum over frequency bins may be approximated by $h\chi^2_\nu$, (by equating the means and variances) where :

$$h = \frac{\sum_{f\in\Omega} c^2_{XX}(f)}{2\sum_{f\in\Omega} c_{XX}(f)} \qquad (3.2)$$

$$\nu = \frac{2\left(\sum_{f\in\Omega} c_{Xx}(f)\right)^2}{\sum_{f\in\Omega} c^2_{Xx}(f)} \tag{3.3}$$

3.4 Extension for a Tapered Time Series

We will now consider the distribution of the total energy in a set of consecutive frequency bins derived from a tapered time series. In addition to the assumptions in section 3.3, we define :

$$X(t) \overset{\mathcal{D}}{\longleftrightarrow} \zeta(f)$$

$$\begin{pmatrix} \mathrm{Re}(\zeta(f)) \\ \mathrm{Im}(\zeta(f)) \end{pmatrix} \sim \mathrm{MN}_2\left(\begin{pmatrix} 0 \\ 0 \end{pmatrix}, \begin{pmatrix} \frac{c_{Xx}(f)}{2} & 0 \\ 0 & \frac{c_{Xx}(f)}{2} \end{pmatrix}\right)$$

where $\mathrm{MN}_p(\mu, \Sigma)$ refers to the p-dimensional multivariate Normal distribution with mean vector μ and variance-covariance matix Σ.

Suppose we now apply a taper $z'(t)$ of order λ (*i.e.* with $2\lambda + 1$ coefficients) :

$$z'(t) \overset{\mathcal{D}}{\longleftrightarrow} a_f$$

Since in practice tapers are even functions, a_f is purely real.

Let

$$Y(t) = X(t)z'(t)$$

Hence,

$$\hat{c}_{YY}(f) = \mathrm{Re}^2\left(\sum_{j=-\lambda}^{\lambda} a_j\zeta(f-j)\right) + \mathrm{Im}^2\left(\sum_{j=-\lambda}^{\lambda} a_j\zeta(f-j)\right)$$

Assuming that the summation is over a series of *consecutive* frequency bins, f_L to f_U, we have :

$$\sum_{f=f_L}^{f_U} \hat{c}_{YY}(f) = \sum_{f=f_L}^{f_U} \mathrm{Re}^2\left(\sum_{j=-\lambda}^{\lambda} a_j\zeta(f-j)\right) + \sum_{f=f_L}^{f_U} \mathrm{Im}^2\left(\sum_{j=-\lambda}^{\lambda} a_j\zeta(f-j)\right)$$

and

$$\sum_{f=f_L}^{f_U} \mathrm{Re}^2\left(\sum_{j=-\lambda}^{\lambda} a_j \zeta(f-j)\right) = \sum_{f=f_L}^{f_U} \left(\mathrm{Re}\left(\sum_{j=-\lambda}^{\lambda} a_j \zeta(f-j)\right) \mathrm{Re}\left(\sum_{j=-\lambda}^{\lambda} a_j \zeta(f-j)\right)\right)$$

$$= \sum_{f=f_L}^{f_U} \left(\sum_{j=-\lambda}^{\lambda} a_j \mathrm{Re}(\zeta(f-j))\right)^2$$

$$= \sum_{f=f_L}^{f_U} \sum_{j=-\lambda}^{\lambda} \sum_{l=-\lambda}^{\lambda} a_j a_l \mathrm{Re}(\zeta(f-j))\mathrm{Re}(\zeta(f-l))$$

and similarly for the imaginary part, giving :

$$\sum_{f=f_L}^{f_U} \hat{c}_{YY}(f) = \sum_{f=f_L}^{f_U} \sum_{j=-\lambda}^{\lambda} \sum_{l=-\lambda}^{\lambda} a_j a_l (\mathrm{Re}(\zeta(f-j)\mathrm{Re}(\zeta(f-l)) + \mathrm{Im}(\zeta(f-j)\mathrm{Im}(\zeta(f-l)))$$

Now,

$$\mathrm{E}(\zeta(f)) = 0 \ \ \forall f$$

and

$$\mathrm{E}(\zeta(f_1)\zeta(f_2)) = \mathrm{E}(\zeta(f_1))\mathrm{E}(\zeta(f_2)) = 0 \ \ \forall f_1 \neq f_2$$

due to independence. Hence

$$\mathrm{E}\left(\sum_{f=f_L}^{f_U} \hat{c}_{YY}(f)\right) = \sum_{f=f_L}^{f_U} \sum_{j=-\lambda}^{\lambda} a_j^2 \mathrm{E}(\mathrm{Re}^2(\zeta(f-j)) + \mathrm{Im}^2(\zeta(f-j)))$$

$$= \sum_{j=-\lambda}^{\lambda} a_j^2 \sum_{f=f_L}^{f_U} c_{XX}(f-j) \tag{3.4}$$

We now turn our attention to the variance of our sum over frequency bins. Consider

$$\mathrm{E}\left(\left(\sum_{f=f_L}^{f_U} \hat{c}_{YY}(f)\right)^2\right) = \mathrm{E}\left(\sum_{f=f_L}^{f_U} \sum_{g=f_L}^{f_U} \hat{c}_{YY}(f)\hat{c}_{YY}(g)\right)$$

$$= \sum_{f=f_L}^{f_U} \sum_{g=f_L}^{f_U} \mathrm{E}(\hat{c}_{YY}(f)\hat{c}_{YY}(g))$$

$$
\begin{aligned}
= & \sum_{f=f_L}^{f_U}\sum_{g=f_L}^{f_U} \mathrm{E}\Bigg(\sum_{j=-\lambda}^{\lambda}\sum_{l=-\lambda}^{\lambda} a_j a_l (\mathrm{Re}(\zeta(f-j))\mathrm{Re}(\zeta(f-l)) \\
& \qquad +\mathrm{Im}(\zeta(f-j))\mathrm{Im}(\zeta(f-l))) \\
& \qquad \times \sum_{j'=-\lambda}^{\lambda}\sum_{l'=-\lambda}^{\lambda} a_{j'} a_{l'} (\mathrm{Re}(\zeta(g-j'))\mathrm{Re}(\zeta(g-l')) \\
& \qquad +\mathrm{Im}(\zeta(g-j'))\mathrm{Im}(\zeta(g-l'))))
\end{aligned}
$$

$$
= \sum_{f=f_L}^{f_U}\sum_{g=f_L}^{f_U}\sum_{j=-\lambda}^{\lambda}\sum_{l=-\lambda}^{\lambda}\sum_{j'=-\lambda}^{\lambda}\sum_{l'=-\lambda}^{\lambda} a_j a_l a_{j'} a_{l'} (J+K+L+M)
$$

$$
\text{where} \begin{cases}
J = \mathrm{E}(\mathrm{Re}(\zeta(f-j))\mathrm{Re}(\zeta(f-l))\mathrm{Re}(\zeta(g-j'))\mathrm{Re}(\zeta(g-l'))) \\
K = \mathrm{E}(\mathrm{Re}(\zeta(f-j))\mathrm{Re}(\zeta(f-l))\mathrm{Im}(\zeta(g-j'))\mathrm{Im}(\zeta(g-l'))) \\
L = \mathrm{E}(\mathrm{Im}(\zeta(f-j))\mathrm{Im}(\zeta(f-l))\mathrm{Re}(\zeta(g-j'))\mathrm{Re}(\zeta(g-l'))) \\
M = \mathrm{E}(\mathrm{Im}(\zeta(f-j))\mathrm{Im}(\zeta(f-l))\mathrm{Im}(\zeta(g-j'))\mathrm{Im}(\zeta(g-l')))
\end{cases}
$$

As the real and imaginary components of each ζ are independent with zero means, J, K, L, and M will be zero if *any* ζ-term appears only once in the relevant expression. Thus, K and L are only non-zero if $j = l$ and $j' = l'$. Hence both become

$$
\sum_{f=f_L}^{f_U}\sum_{g=f_L}^{f_U}\sum_{j=-\lambda}^{\lambda}\sum_{j'=-\lambda}^{\lambda} a_j^2 a_{j'}^2 \frac{c_{xx}(f-j)}{2}\frac{c_{xx}(g-j')}{2}
$$

$$
= \left(\sum_{j=-\lambda}^{\lambda} a_j^2 \sum_{f=f_L}^{f_U} \frac{c_{xx}(f-j)}{2}\right)^2 \tag{3.5}
$$

At least one of three conditions needs to be satisfied for J and M to be non-zero :

$\mathcal{A}$: $j = l$ and $j' = l'$,

$\mathcal{B}$: $f - j = g - j'$ and $f - l = g - l'$,

$\mathcal{C}$: $f - j = g - l'$ and $f - l = g - j'$.

The expressions for J and M will be quartic (in terms of a single ζ-term) if all the arguments are equal, *i.e.* if $j = l$ and $j' = l'$ (condition $\mathcal{A}$) and $f - j = g - j'$ (and hence $f - l = g - l'$, condition $\mathcal{B}$). Thus, using set notation :

$\mathcal{A} \cap \mathcal{B} \Leftrightarrow$ quartic

Consider $\mathcal{A} \cap \mathcal{C} : j = l, j' = l', f - j = g - l', f - l = g - j'$

$\Rightarrow f - j = g - j', f - l = g - l'$

i.e. $\mathcal{A} \cap \mathcal{C} \subseteq \mathcal{B}$

Hence $\mathcal{A} \cap \mathcal{C} = \mathcal{A} \cap \mathcal{B} \cap \mathcal{C}$

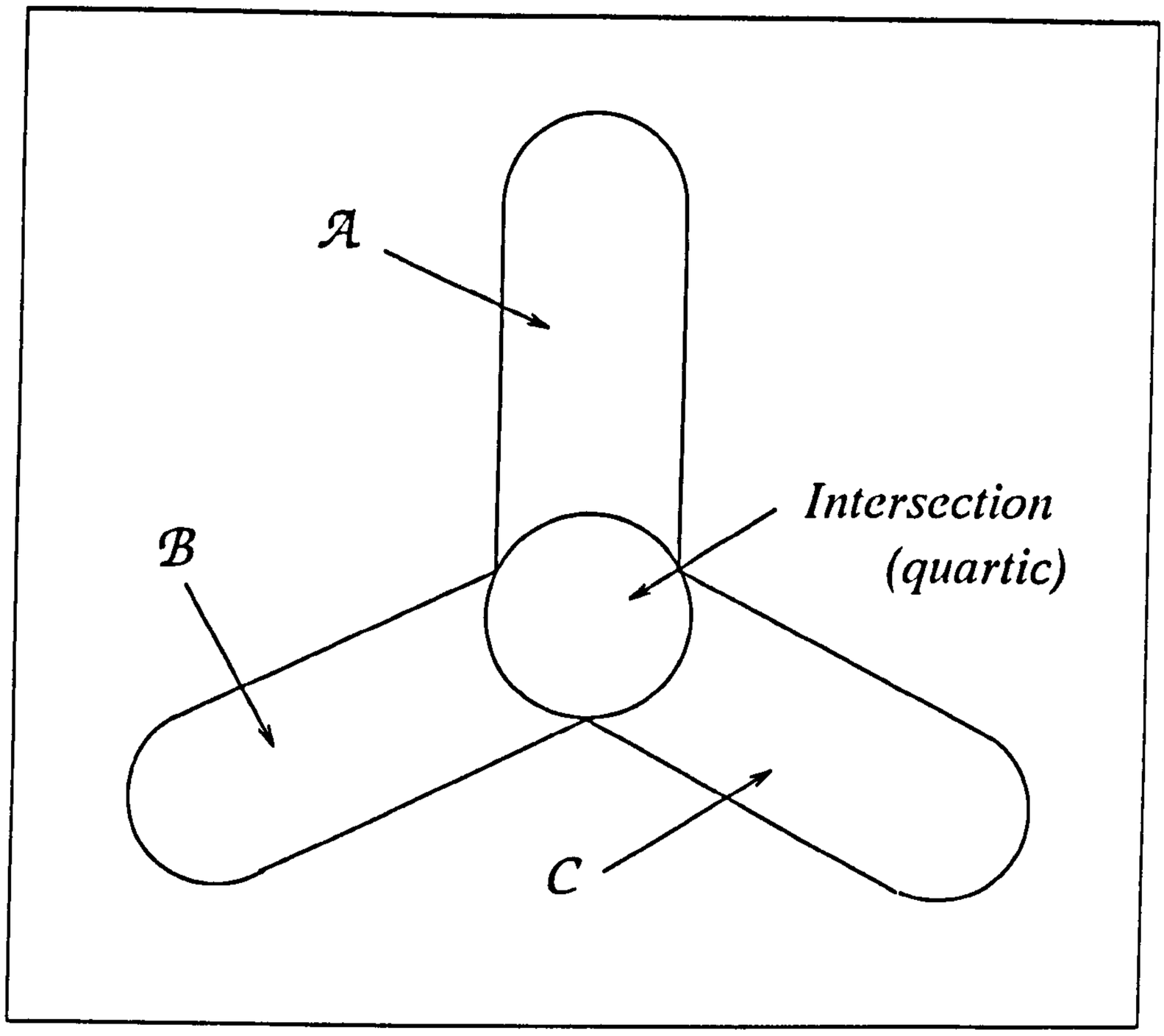

Figure 3.1: A graphical representation of conditions $\mathcal{A}$, $\mathcal{B}$ and $\mathcal{C}$.

Consider $\mathcal{A} \cap \mathcal{B} : j = l, j' = l', f - j = g - j', f - l = g - l'$
$\Rightarrow f - j = g - l', f - l = g - j'$
i.e. $\mathcal{A} \cap \mathcal{B} \subseteq \mathcal{C}$
Hence $\mathcal{A} \cap \mathcal{B} = \mathcal{A} \cap \mathcal{B} \cap \mathcal{C} = \mathcal{A} \cap \mathcal{C}$

Consider $\mathcal{B} \cap \mathcal{C} : f - j = g - j', f - l = g - l', f - j = g - l', f - l = g - j'$
$\Rightarrow f - j = f - l, g - j' = g - l'$
$\Rightarrow j = l, j' = l'$
i.e. $\mathcal{B} \cap \mathcal{C} \subseteq \mathcal{A}$
Hence $\mathcal{B} \cap \mathcal{C} = \mathcal{A} \cap \mathcal{B} \cap \mathcal{C} = \mathcal{A} \cap \mathcal{B} = \mathcal{A} \cap \mathcal{C}$

This gives the Venn diagram in figure 3.1, which we will now use to evaluate J and M.

Evaluating the contribution of condition $\mathcal{A}$ to J and M as a double quadratic (*i.e.* as a product of two quadratic expressions in ζ-terms) : $j = l, j' = l'$ gives

$$\sum_{f=f_L}^{f_U} \sum_{g=f_L}^{f_U} \sum_{j=-\lambda}^{\lambda} \sum_{j'=-\lambda}^{\lambda} a_j^2 a_{j'}^2 \frac{cxx(f-j)}{2} \frac{cxx(g-j')}{2}$$

$$= \frac{1}{4}\left(\sum_{j=-\lambda}^{\lambda} a_j^2 \sum_{f=f_L}^{f_U} c_{XX}(f-j)\right)^2 \tag{3.6}$$

Evaluating the contribution of condition $\mathcal{B}$ to J and M as a double quadratic :
$f-j=g-j'$,
$f-l=g-l'$ gives

$$\frac{1}{4}\sum_{f=f_L}^{f_U}\sum_{g=f_L}^{f_U}\sum_{j=-\lambda}^{\lambda}\sum_{l=-\lambda}^{\lambda} a_j a_l a_{g+j-f} a_{g+l-f} c_{XX}(f-j) c_{XX}(f-l) \tag{3.7}$$

Evaluating the contribution of condition $\mathcal{C}$ to J and M as a double quadratic :
$f-j=g-l'$,
$f-l=g-j'$ gives

$$\frac{1}{4}\sum_{f=f_L}^{f_U}\sum_{g=f_L}^{f_U}\sum_{j=-\lambda}^{\lambda}\sum_{l=-\lambda}^{\lambda} a_j a_l a_{g+l-f} a_{g+j-f} c_{XX}(f-j) c_{XX}(f-l) \tag{3.8}$$

We note that this is the same as equation 3.7.

Evaluating the contribution of condition $\mathcal{A}\cap\mathcal{B}$ to J and M as a double quadratic : $j=l$, $j'=l'$, $f-j=g-j'$, $(f-l=g-l')$ gives

$$\frac{1}{4}\sum_{f=f_L}^{f_U}\sum_{g=f_L}^{f_U}\sum_{j=-\lambda}^{\lambda} a_j^2 a_{g+j-f}^2 c_{XX}^2(f-j) \tag{3.9}$$

To consider the quartic case, it is first necessary to derive the expectation of the fourth power of a Normally distributed variable with zero mean. Let :

$$Z \sim \mathrm{N}(0,h) \Rightarrow Z^2 \sim h\chi_1^2$$

Now,

$$\begin{aligned}
\mathrm{E}\left((h\chi_\nu^2)^2\right) &= \mathrm{Var}(h\chi_\nu^2) + \mathrm{E}^2(h\chi_\nu^2) \\
&= 2h^2\nu + h^2\nu^2 \\
&= h^2\nu(\nu+2)
\end{aligned}$$

Hence :

$$\mathrm{E}(Z^4) = 3h^2$$

Hence, evaluating the contribution of condition $\mathcal{A}\cap\mathcal{B}$ to J and M as a quartic

(in ζ-terms) gives

$$\frac{3}{4}\sum_{f=f_L}^{f_U}\sum_{g=f_L}^{f_U}\sum_{j=-\lambda}^{\lambda} a_j^2 a_{g+j-f}^2 c_{XX}^2(f-j) \tag{3.10}$$

We may now use set theory to evaluate $\mathrm{E}\left(\left(\sum_{f=f_L}^{f_U}\hat{c}_{YY}(f)\right)^2\right)$ by evaluating the following expression :

$$\mathcal{A}\cup\mathcal{B}\cup\mathcal{C} = \mathcal{A}+\mathcal{B}+\mathcal{C}-3\times(\mathcal{A}\cap\mathcal{B}_{\text{double quadratic}})+\mathcal{A}\cap\mathcal{B}_{\text{quartic}}$$

Hence equations 3.5 and 3.6 to 3.10 combine to give

$$\begin{aligned}
&\mathrm{E}\left(\left(\sum_{f=f_L}^{f_U}\hat{c}_{YY}(f)\right)^2\right)\\
&\quad= 2\left(\tfrac{1}{4}\left(\sum_{j=-\lambda}^{\lambda}a_j^2\sum_{f=f_L}^{f_U}c_{XX}(f-j)\right)^2\right.\\
&\qquad+\tfrac{1}{2}\sum_{f=f_L}^{f_U}\sum_{g=f_L}^{f_U}\sum_{j=-\lambda}^{\lambda}\sum_{l=-\lambda}^{\lambda}a_j a_l a_{g+j-f}a_{g+l-f}c_{XX}(f-j)c_{XX}(f-l)\\
&\qquad-\tfrac{3}{4}\sum_{f=f_L}^{f_U}\sum_{g=f_L}^{f_U}\sum_{j=-\lambda}^{\lambda}a_j^2a_{g+j-f}^2c_{XX}^2(f-j)\\
&\qquad+\tfrac{3}{4}\sum_{f=f_L}^{f_U}\sum_{g=f_L}^{f_U}\sum_{j=-\lambda}^{\lambda}a_j^2a_{g+j-f}^2c_{XX}^2(f-j)\\
&\qquad\left.+\tfrac{1}{4}\left(\sum_{j=-\lambda}^{\lambda}a_j^2\sum_{f=f_L}^{f_U}c_{XX}(f-j)\right)^2\right)\\
&\quad=\left(\sum_{j=-\lambda}^{\lambda}a_j^2\sum_{f=f_L}^{f_U}c_{XX}(f-j)\right)^2\\
&\qquad+\sum_{f=f_L}^{f_U}\sum_{g=f_L}^{f_U}\sum_{j=-\lambda}^{\lambda}\sum_{l=-\lambda}^{\lambda}a_j a_l a_{g+j-f}a_{g+l-f}c_{XX}(f-j)c_{XX}(f-l)
\end{aligned}$$

Hence (using equation 3.4)

$$\mathrm{Var}\left(\sum_{f=f_L}^{f_U}\hat{c}_{YY}(f)\right)=\sum_{f=f_L}^{f_U}\sum_{g=f_L}^{f_U}\sum_{j=-\lambda}^{\lambda}\sum_{l=-\lambda}^{\lambda}a_j a_l a_{g+j-f}a_{g+l-f}c_{XX}(f-j)c_{XX}(f-l) \tag{3.11}$$

Once more approximating using $h\chi_\nu^2$, equations 3.4 and 3.11 may be com-

bined to give

$$\nu = \frac{2\left(\sum_{j=-\lambda}^{\lambda} a_j^2 \sum_{f=f_L}^{f_U} c_{XX}(f-j)\right)^2}{\sum_{f=f_L}^{f_U}\sum_{g=f_L}^{f_U}\sum_{j=-\lambda}^{\lambda}\sum_{l=-\lambda}^{\lambda} a_j a_l a_{g+j-f} a_{g+l-f} c_{XX}(f-j) c_{XX}(f-l)} \tag{3.12}$$

and

$$h = \frac{\sum_{f=f_L}^{f_U}\sum_{g=f_L}^{f_U}\sum_{j=-\lambda}^{\lambda}\sum_{l=-\lambda}^{\lambda} a_j a_l a_{g+j-f} a_{g+l-f} c_{XX}(f-j) c_{XX}(f-l)}{2\sum_{j=-\lambda}^{\lambda} a_j^2 \sum_{f=f_L}^{f_U} c_{XX}(f-j)} \tag{3.13}$$

We note that under a square taper ($\lambda = 0, a_0 = 1$) equations 3.12 and 3.13 reduce to equations 3.3 and 3.2 respectively.

3.5 The Distribution of a Weighted Sum of Periodogram Energy

Consider now the sum over a set Ω of frequency bins of a periodogram where the energy in the bins has been weighted by some known function $w(f)$ (note that if Ω covers the entire periodogram and $w(f) = f^m$ then the sum is the m-th order moment).

$$\begin{aligned} \mathrm{E}\left(\sum_{f\in\Omega} w(f)\hat{c}_{XX}(f)\right) &= \mathrm{E}\left(\sum_{f\in\Omega} w(f)\frac{c_{XX}(f)\chi^2_{2,f}}{2}\right) \\ &= \sum_{f\in\Omega} w(f)c_{XX}(f) \\ \mathrm{Var}\left(\sum_{f\in\Omega} w(f)\hat{c}_{XX}(f)\right) &= \mathrm{Var}\left(\sum_{f\in\Omega} w(f)\frac{c_{XX}(f)\chi^2_{2,f}}{2}\right) \\ &= \sum_{f\in\Omega} w^2(f)c^2_{XX}(f) \quad \text{by independence} \end{aligned}$$

Approximating by $h\chi^2_\nu$ gives

$$h = \frac{\sum_{f\in\Omega} w^2(f)c^2_{XX}(f)}{2\sum_{f\in\Omega} w(f)c_{XX}(f)} \tag{3.14}$$

$$\nu = \frac{2\left(\sum_{f\in\Omega} w(f)c_{XX}(f)\right)^2}{\sum_{f\in\Omega} w^2(f)c^2_{XX}(f)} \tag{3.15}$$

We note that equations 3.14 and 3.15 reduce to equations 3.2 and 3.3 respectively if $w(f) = 1\ \forall f \in \Omega$.

3.6 The Covariance of Two Weighted Sums of Periodogram Energy

Consider now two known weighting functions, $w_1(f)$ and $w_2(f)$.

$$\mathrm{Cov}\left(\sum_{f\in\Omega} w_1(f)\hat{c}_{XX}(f), \sum_{f\in\Omega} w_2(f)\hat{c}_{XX}(f)\right)$$

$$\approx \mathrm{Cov}\left(\sum_{f\in\Omega} w_1(f)\frac{c_{XX}(f)\chi^2_{2,f}}{2}, \sum_{f\in\Omega} w_2(f)\frac{c_{XX}(f)\chi^2_{2,f}}{2}\right)$$

$$= \sum_{f\in\Omega} w_1(f)w_2(f)\frac{c^2_{XX}(f)}{4}\mathrm{Var}(\chi^2_{2,f}) \quad \text{by independence}$$

$$= \sum_{f\in\Omega} w_1(f)w_2(f)c^2_{XX}(f) \tag{3.16}$$

3.7 Extension for a Tapered Time Series

Again, let us now apply a taper $z'(t)$:

$$z'(t) \overset{\mathcal{D}}{\longleftrightarrow} a_f$$

Let

$$Y(t) = X(t)z'(t)$$

Summing over consecutive frequency bins, f_L to f_U, we have :

$$\sum_{f=f_L}^{f_U} w(f)\hat{c}_{YY}(f) = \sum_{f=f_L}^{f_U} w(f)\mathrm{Re}^2\left(\sum_{j=-\lambda}^{\lambda} a_j\zeta(f-j)\right) + \sum_{f=f_L}^{f_U} w(f)\mathrm{Im}^2\left(\sum_{j=-\lambda}^{\lambda} a_j\zeta(f-j)\right)$$

$$= \sum_{f=f_L}^{f_U} w(f) \sum_{j=-\lambda}^{\lambda}\sum_{l=-\lambda}^{\lambda} a_j a_l(\mathrm{Re}(\zeta(f-j)\mathrm{Re}(\zeta(f-l))+\mathrm{Im}(\zeta(f-j)\mathrm{Im}(\zeta(f-l)))$$

Thus

$$\mathrm{E}\left(\sum_{f=f_L}^{f_U} w(f)\hat{c}_{YY}(f)\right) = \sum_{f=f_L}^{f_U} w(f) \sum_{j=-\lambda}^{\lambda} a_j^2\mathrm{E}(\mathrm{Re}^2(\zeta(f-j)) + \mathrm{Im}(\zeta(f-j)))$$

$$= \sum_{f=f_L}^{f_U} w(f) \sum_{j=-\lambda}^{\lambda} a_j^2 c_{XX}(f-j) \tag{3.17}$$

Consider now :

$$\mathrm{E}\left(\left(\sum_{f=f_L}^{f_U} w(f)\hat{c}_{YY}(f)\right)^2\right) = \mathrm{E}\left(\sum_{f=f_L}^{f_U}\sum_{g=f_L}^{f_U} w(f)\hat{c}_{YY}(f)w(g)\hat{c}_{YY}(g)\right)$$

$$= \sum_{f=f_L}^{f_U} w(f) \sum_{g=f_L}^{f_U} w(g)\mathrm{E}(\hat{c}_{YY}(f)\hat{c}_{YY}(g))$$

$$= \sum_{f=f_L}^{f_U} w(f) \sum_{g=f_L}^{f_U} w(g) \sum_{j=-\lambda}^{\lambda}\sum_{l=-\lambda}^{\lambda}\sum_{j'=-\lambda}^{\lambda}\sum_{l'=-\lambda}^{\lambda} a_j a_l a_{j'} a_{l'}(J+K+L+M) \tag{3.18}$$

$$\text{where } \begin{cases} J = \mathrm{E}(\mathrm{Re}(\zeta(f-j))\mathrm{Re}(\zeta(f-l))\mathrm{Re}(\zeta(g-j'))\mathrm{Re}(\zeta(g-l'))) \\ K = \mathrm{E}(\mathrm{Re}(\zeta(f-j))\mathrm{Re}(\zeta(f-l))\mathrm{Im}(\zeta(g-j'))\mathrm{Im}(\zeta(g-l'))) \\ L = \mathrm{E}(\mathrm{Im}(\zeta(f-j))\mathrm{Im}(\zeta(f-l))\mathrm{Re}(\zeta(g-j'))\mathrm{Re}(\zeta(g-l'))) \\ M = \mathrm{E}(\mathrm{Im}(\zeta(f-j))\mathrm{Im}(\zeta(f-l))\mathrm{Im}(\zeta(g-j'))\mathrm{Im}(\zeta(g-l'))) \end{cases}$$

We now use the same arguments as in section 3.3. The contribution of each of K and L is

$$\sum_{f=f_L}^{f_U} w(f) \sum_{g=f_L}^{f_U} w(g) \sum_{j=-\lambda}^{\lambda}\sum_{j'=-\lambda}^{\lambda} a_j^2 a_{j'}^2 \frac{c_{XX}(f-j)}{2}\frac{c_{XX}(g-j')}{2}$$

$$= \left(\sum_{j=-\lambda}^{\lambda} a_j^2 \sum_{f=f_L}^{f_U} w(f) \frac{c_{XX}(f-j)}{2} \right)^2 \tag{3.19}$$

Turning our attention to J and M, we define our three conditions as before :
$\mathcal{A}$: $j = l$ and $j' = l'$,
$\mathcal{B}$: $f - j = g - j'$ and $f - l = g - l'$,
$\mathcal{C}$: $f - j = g - l'$ and $f - l = g - j'$.

Evaluating the contribution of $\mathcal{A}$ as a double quadratic : $j = l, j' = l'$ gives

$$\sum_{f=f_L}^{f_U} w(f) \sum_{g=f_L}^{f_U} w(g) \sum_{j=-\lambda}^{\lambda} \sum_{j'=-\lambda}^{\lambda} a_j^2 a_{j'}^2 \frac{c_{XX}(f-j)}{2} \frac{c_{XX}(g-j')}{2} \tag{3.20}$$

Evaluating the contribution of $\mathcal{B}$ as a double quadratic : $f - j = g - j'$, $f - l = g - l'$ gives

$$\frac{1}{4} \sum_{f=f_L}^{f_U} w(f) \sum_{g=f_L}^{f_U} w(g) \sum_{j=-\lambda}^{\lambda} \sum_{l=-\lambda}^{\lambda} a_j a_l a_{g+j-f} a_{g+l-f} c_{XX}(f-j) c_{XX}(f-l) \tag{3.21}$$

and the contribution of $\mathcal{C}$ as a double quadratic gives the same result.

Evaluating the contribution of $\mathcal{A} \cap \mathcal{B}$ as a double quadratic : $j = l$, $j' = l', f - j = g - j', (f - l = g - l')$ gives

$$\frac{1}{4} \sum_{f=f_L}^{f_U} w(f) \sum_{g=f_L}^{f_U} w(g) \sum_{j=-\lambda}^{\lambda} a_j^2 a_{g+j-f}^2 c_{XX}^2(f-j) \tag{3.22}$$

Evaluating the expectation of $\mathcal{A} \cap \mathcal{B}$ as a quartic gives

$$\frac{3}{4} \sum_{f=f_L}^{f_U} w(f) \sum_{g=f_L}^{f_U} w(g) \sum_{j=-\lambda}^{\lambda} a_j^2 a_{g+j-f}^2 c_{XX}^2(f-j) \tag{3.23}$$

Hence, using set theory as before, equations 3.19 and 3.20 to 3.23 combine to give

$$\mathrm{E}\left(\left(\sum_{f=f_L}^{f_U} w(f) \hat{c}_{YY}(f) \right)^2 \right)$$

$$
\begin{aligned}
= \; 2\Bigg(& \tfrac{1}{4}\sum_{f=f_L}^{f_U} w(f) \sum_{g=f_L}^{f_U} w(g) \sum_{j=-\lambda}^{\lambda} \sum_{j'=-\lambda}^{\lambda} a_j^2 a_{j'}^2 c_{XX}(f-j) c_{XX}(g-j') \\
& + \tfrac{1}{2}\sum_{f=f_L}^{f_U} w(f) \sum_{g=f_L}^{f_U} w(g) \sum_{j=-\lambda}^{\lambda} \sum_{l=-\lambda}^{\lambda} a_j a_l a_{g+j-f} a_{g+l-f} c_{XX}(f-j) c_{XX}(f-l) \\
& - \tfrac{3}{4}\sum_{f=f_L}^{f_U} w(f) \sum_{g=f_L}^{f_U} w(f) \sum_{j=-\lambda}^{\lambda} a_j^2 a_{g+j-f}^2 c_{XX}^2(f-j) \\
& + \tfrac{3}{4}\sum_{f=f_L}^{f_U} w(f) \sum_{g=f_L}^{f_U} w(g) \sum_{j=-\lambda}^{\lambda} a_j^2 a_{g+j-f}^2 c_{XX}^2(f-j) \\
& + \tfrac{1}{4}\sum_{f=f_L}^{f_U} w(f) \sum_{g=f_L}^{f_U} w(g) \sum_{j=-\lambda}^{\lambda} \sum_{j'=-\lambda}^{\lambda} a_j^2 a_{j'}^2 c_{XX}(f-j) c_{XX}(g-j') \Bigg)
\end{aligned}
$$

$$
\begin{aligned}
= \; & \sum_{f=f_L}^{f_U} w(f) \sum_{g=f_L}^{f_U} w(g) \sum_{j=-\lambda}^{\lambda} \sum_{j'=-\lambda}^{\lambda} a_j^2 a_{j'}^2 c_{XX}(f-j) c_{XX}(g-j') \\
& + \sum_{f=f_L}^{f_U} w(f) \sum_{g=f_L}^{f_U} w(g) \sum_{j=-\lambda}^{\lambda} \sum_{l=-\lambda}^{\lambda} a_j a_l a_{g+j-f} a_{g+l-f} c_{XX}(f-j) c_{XX}(f-l)
\end{aligned}
$$

Hence

$$
\operatorname{Var}\left(\sum_{f=f_L}^{f_U} w(f) \hat{c}_{YY}(f) \right)
$$

$$
= \sum_{f=f_L}^{f_U} w(f) \sum_{g=f_L}^{f_U} w(g) \sum_{j=-\lambda}^{\lambda} \sum_{l=-\lambda}^{\lambda} a_j a_l a_{g+j-f} a_{g+l-f} c_{XX}(f-j) c_{XX}(f-l) \tag{3.24}
$$

and approximating using $h\chi_\nu^2$, equations 3.17 and 3.24 combine to give

$$
\nu = \frac{2\left(\sum_{f=f_L}^{f_U} w(f) \sum_{j=-\lambda}^{\lambda} a_j^2 c_{XX}(f-j) \right)^2}{\sum_{f=f_L}^{f_U} w(f) \sum_{g=f_L}^{f_U} w(g) \sum_{j=-\lambda}^{\lambda} \sum_{l=-\lambda}^{\lambda} a_j a_l a_{g+j-f} a_{g+l-f} c_{XX}(f-j) c_{XX}(f-l)} \tag{3.25}
$$

and

$$
h = \frac{\sum_{f=f_L}^{f_U} w(f) \sum_{g=f_L}^{f_U} w(g) \sum_{j=-\lambda}^{\lambda} \sum_{l=-\lambda}^{\lambda} a_j a_l a_{g+j-f} a_{g+l-f} c_{XX}(f-j) c_{XX}(f-l)}{2 \sum_{f=f_L}^{f_U} w(f) \sum_{j=-\lambda}^{\lambda} a_j^2 c_{XX}(f-j)} \tag{3.26}
$$

We note that under a square taper ($\lambda = 0, a_0 = 1$) equations 3.25 and 3.26 reduce to equations 3.15 and 3.14 respectively, and that if $w(f) = 1 \; \forall f \in [f_L, f_U]$ then they reduce to equations 3.12 and 3.13 respectively.

3.8 Extension for the Covariance of Two Weighted Sums of Spectral Energy of a Tapered Time Series

Consider again two known weighting functions, $w_1(f)$ and $w_2(f)$.

$$\mathrm{E}\left(\left(\sum_{f=f_L}^{f_U} w_1(f)\hat{c}_{YY}(f)\right)\left(\sum_{f=f_L}^{f_U} w_2(f)\hat{c}_{YY}(f)\right)\right)$$

$$= \sum_{f=f_L}^{f_U} w_1(f) \sum_{g=f_L}^{f_U} w_2(g)\mathrm{E}(\hat{c}_{YY}(f)\hat{c}_{YY}(g))$$

$$= \sum_{f=f_L}^{f_U} w_1(f) \sum_{g=f_L}^{f_U} w_2(g) \sum_{j=-\lambda}^{\lambda} \sum_{l=-\lambda}^{\lambda} a_j a_l a_{g+j-f} a_{g+l-f} c_{XX}(f-j)c_{XX}(f-l)$$

Thus

$$\mathrm{Cov}\left(\sum_{f=f_L}^{f_U} w_1(f)\hat{c}_{YY}(f), \sum_{f=f_L}^{f_U} w_2(f)\hat{c}_{YY}(f)\right)$$

$$= \sum_{f=f_L}^{f_U} w_1(f) \sum_{g=f_L}^{f_U} w_2(g) \sum_{j=-\lambda}^{\lambda} \sum_{l=-\lambda}^{\lambda} a_j a_l a_{g+j-f} a_{g+l-f} c_{XX}(f-j)c_{XX}(f-l) \tag{3.27}$$

We note that under a square taper ($\lambda = 0, a_0 = 1$) equation 3.27 reduces to equation 3.16.

3.9 Comment

The formulae presented in this chapter give the statistical properties of estimated spectral integrals in terms of quantities which are either known (the taper used and the weighting function(s), if any) or estimable (the energy spectrum). It is thus possible to produce approximate confidence intervals for the measurement of interest from the observed spectrum.

Chapter 4

Wave Buoy Theory

4.1 Introduction

A frequently used method for measuring ocean waves *in situ* is with the use of a wave buoy. Such instruments are often used as a standard by which to evaluate the performance of other wave measuring systems. Older models (such as Datawell's original Waverider) measure vertical motion at a single point. Typical directional wave buoys (such as Datawell's Wavec) additionally measure the slope of the sea surface in two directions (such as north and east) at the same point. In this chapter we examine the statistical properties of a variety of wave parameters derived from wave buoy measurements.

4.2 The Non-Directional Ocean Wave Spectrum

The non-directional wave spectrum of the sea surface is the energy spectrum of its vertical motion at a fixed point. These spectral estimates have a χ^2 distribution as described in section 2.3.4 (Figure 4.1 shows an example of a non-directional wave spectrum as measured by a wave buoy, with its 90% confidence interval).

From this spectrum, significant waveheight (H_s) and mean wave period (T_m)

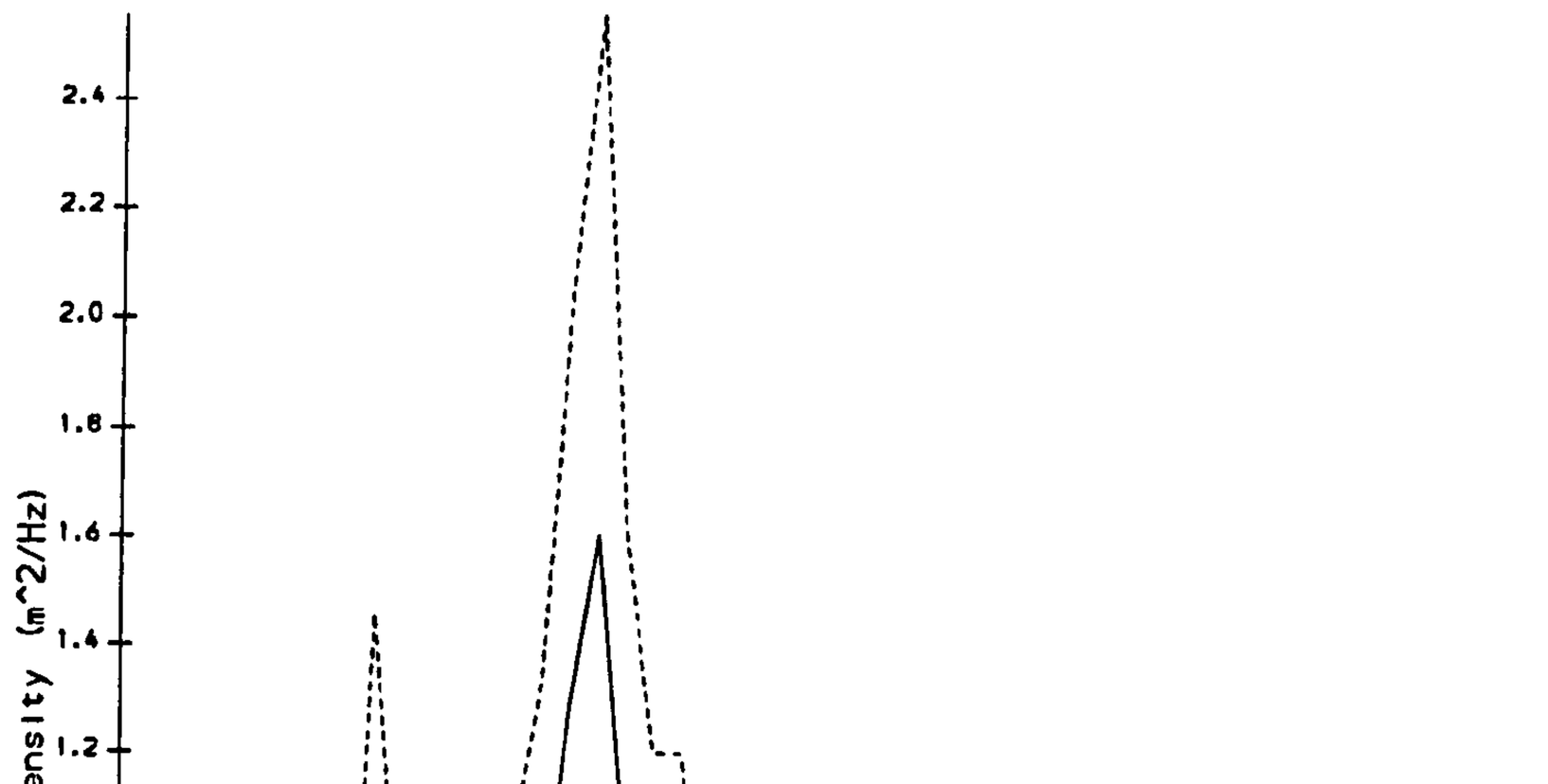

Figure 4.1: An example of a non-directional wave spectrum (with its 90% confidence interval) as measured by a Wavec directional wave buoy. The main mode represents waves generated by the local wind. The lower frequency mode (peaking at $90mHz$) represents a swell wave component.

may be estimated from the following formulae :

$$\begin{aligned} \hat{H}_s &= 4\sqrt{\hat{m}_0} \\ \hat{T}_m &= \frac{\hat{m}_0}{\hat{m}_1} \end{aligned}$$

where $\hat{m}_j$ is the observed j-th spectral moment (see section 3.2). As these are functions of weighted integrals of the wave spectrum, they behave as described in chapter 3. This allows us to produce approximate confidence intervals by using a Normal approximation (see Krogstad *et al.* (1988)) and estimating the variances with a Taylor expansion to first order :

$$\begin{aligned} \mathrm{Var}(\hat{H}_s) &\approx \frac{4\mathrm{Var}(\hat{m}_0)}{\hat{m}_0} \\ \mathrm{Var}(\hat{T}_m) &\approx \frac{\mathrm{Var}(\hat{m}_0)}{\hat{m}_1^2} - \frac{\hat{m}_0\mathrm{Cov}(\hat{m}_0,\hat{m}_1)}{\hat{m}_1^3} + \frac{\hat{m}_0^2\mathrm{Var}(\hat{m}_1)}{\hat{m}_1^4} \end{aligned}$$

Figures 4.2 and 4.3 respectively show significant waveheight and mean wave period estimates from a wave buoy, each with their 90% confidence intervals. At the time at which these measurements were taken, the sea state was rough but by no means stormy.

4.3 Directional Parameters

4.3.1 Truncated Estimation of the Directional Wave Spectrum

Let $X(t,\mathbf{x})$ describe the vertical displacement of the sea surface. From section 2.2.3 we have :

$$X(t,\mathbf{x}) = \int_{\omega,\mathbf{k}} e^{i(\omega t - \mathbf{k}.\mathbf{x})} dR(\omega,\mathbf{k})$$

Consider the northward slope of this process :

$$\frac{\partial X(t,\mathbf{x})}{\partial x_N} = -i \int_{\omega,\mathbf{k}} k\cos(\theta) e^{i(\omega t - \mathbf{k}.\mathbf{x})} dR(\omega,\mathbf{k})$$

where x_N is the northerly component of $\mathbf{x}$, $k = |\mathbf{k}|$ and θ is the direction of

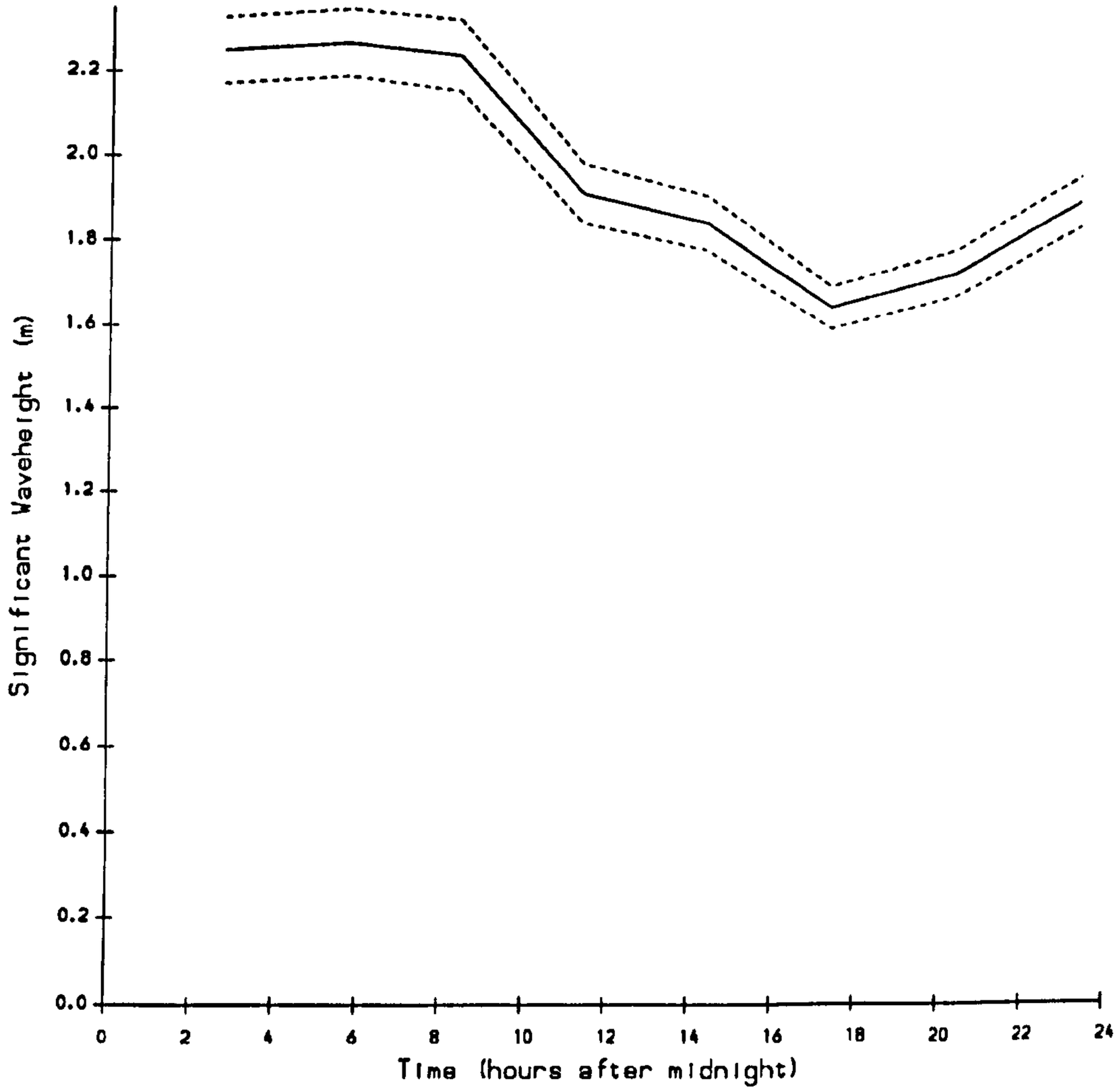

Figure 4.2: Significant waveheight measurements (with their 90% confidence intervals) as measured by a Wavec directional wave buoy on October 10^{th} 1985.

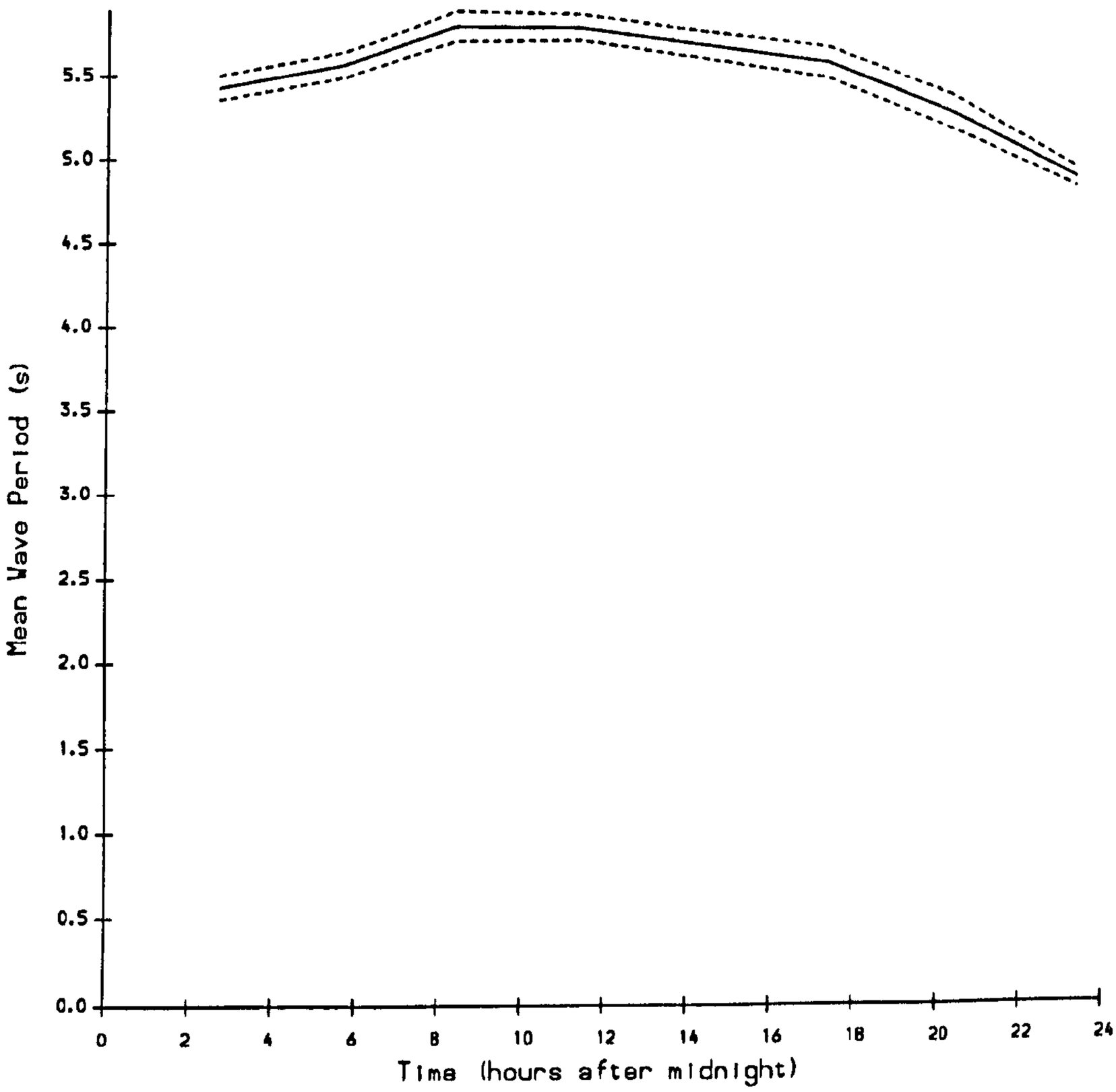

Figure 4.3: Mean wave period measurements (with their 90% confidence intervals) as measured by a Wavec directional wave buoy on October 10^{th} 1985.

$\mathbf{k}$ measured clockwise from the north.

Consider now the auto-covariance function of this process $\gamma_{NN}(h, \mathbf{r})$:

$$\begin{aligned}
\gamma_{NN}(h, \mathbf{r}) &= \mathrm{E}\left(\int_{\omega,\mathbf{k}} -ik\cos(\theta) e^{i(\omega(t+h)-\mathbf{k}.(\mathbf{x}+\mathbf{r}))} dR(\omega, \mathbf{k}) \right. \\
&\qquad \left. \int_{\omega',\mathbf{k}'} ik'\cos(\theta') e^{-i(\omega' t-\mathbf{k}'.\mathbf{x})} dR^*(\omega', \mathbf{k}') \right) \\
&= \int_{\omega,\mathbf{k},\omega',\mathbf{k}'} kk'\cos(\theta)\cos(\theta') e^{i(\omega h-\mathbf{k}.\mathbf{r})} e^{i(\omega-\omega')t} e^{i(\mathbf{k}'-\mathbf{k}).\mathbf{x}} \\
&\qquad \mathrm{E}(dR(\omega, \mathbf{k}) dR^*(\omega', \mathbf{k}')) \\
&= \int_{\omega,\mathbf{k}} k^2\cos^2(\theta) e^{i(\omega h-\mathbf{k}.\mathbf{r})} dG(\omega, \mathbf{k})
\end{aligned}$$

Hence, the energy spectrum of the northward slope equals that of the vertical displacement multiplied by $k^2\cos^2(\theta)$.

Similarly, the energy spectrum of the eastward slope equals that of the vertical displacement multiplied by $k^2\sin^2(\theta)$.

Also, we get the following multipliers for the various cross-spectra :

1^{st} Series	2^{nd} Series	Multiplier
Vertical	North Slope	$ik\cos(\theta)$
Vertical	East Slope	$ik\sin(\theta)$
North Slope	East Slope	$k^2\cos(\theta)\sin(\theta)$

It is worth noting that all the above are either purely real or purely imaginary. From Long (1980) we get :

$$\begin{aligned}
\mathrm{Var}(\hat{c}_{VV}(\omega)) &= c^2_{VV}(\omega) \\
\mathrm{Var}(\hat{c}_{NN}(\omega)) &= c^2_{NN}(\omega) \\
\mathrm{Var}(\hat{c}_{EE}(\omega)) &= c^2_{EE}(\omega) \\
\mathrm{Var}(\hat{q}_{VN}(\omega)) &= \frac{c_{VV}(\omega)c_{NN}(\omega) + q^2_{VN}(\omega)}{2} \\
\mathrm{Var}(\hat{q}_{VE}(\omega)) &= \frac{c_{VV}(\omega)c_{EE}(\omega) + q^2_{VE}(\omega)}{2} \\
\mathrm{Var}(\hat{c}_{NE}(\omega)) &= \frac{c_{NN}(\omega)c_{EE}(\omega) + q^2_{NE}(\omega)}{2} \\
\mathrm{Cov}(\hat{c}_{VV}(\omega), \hat{q}_{VN}(\omega)) &= c_{VV}(\omega)q_{VN}(\omega)
\end{aligned}$$

$$
\begin{aligned}
\mathrm{Cov}(\hat{c}_{VV}(\omega), \hat{q}_{VE}(\omega)) &= c_{VV}(\omega) q_{VE}(\omega) \\
\mathrm{Cov}(\hat{c}_{VV}(\omega), \hat{c}_{NE}(\omega)) &= q_{VN}(\omega) q_{VE}(\omega) \\
\mathrm{Cov}(\hat{q}_{VN}(\omega), \hat{q}_{VE}(\omega)) &= \frac{c_{VV}(\omega) c_{NE}(\omega) + q_{VN}(\omega) q_{VE}(\omega)}{2} \\
\mathrm{Cov}(\hat{q}_{VN}(\omega), \hat{c}_{NE}(\omega)) &= \frac{q_{VN}(\omega) c_{NE}(\omega) + c_{NN}(\omega) q_{VE}(\omega)}{2} \\
\mathrm{Cov}(\hat{q}_{VE}(\omega), \hat{c}_{NE}(\omega)) &= \frac{q_{VE}(\omega) c_{NE}(\omega) + c_{EE}(\omega) q_{VN}(\omega)}{2}
\end{aligned} \tag{4.1}
$$

These variances and covariances may be estimated by substituting the estimated spectra for the true spectra.

Using the deep water dispersion relationship (see section 1.3.2), let

$$
F(\omega, \theta) = \frac{g^2}{2\omega^3 T} \frac{\partial^2 \mathrm{E}\left(G\left(\omega, \begin{pmatrix} \frac{\omega^2}{g}\cos(\theta) \\ \frac{\omega^2}{g}\sin(\theta) \end{pmatrix} \right) \right)}{\partial\omega\partial\theta}
$$

(where F is the directional ocean wave spectrum, and assuming that this second derivative exists). At any fixed ω, F is periodic in θ :

$$
F(\omega, \theta) = \frac{a_0(\omega)}{2} + \sum_{j=1}^{\infty} a_j(\omega)\cos(\theta) + b_j(\omega)\sin(\theta)
$$

where the a_js and b_js are the Fourier coefficients of F, and hence :

$$
\begin{aligned}
a_0(\omega) &= \frac{1}{\pi}\int_0^{2\pi} F(\omega, \theta) d\theta \\
&= \frac{1}{\pi} c_{VV}(\omega) \\
a_1(\omega) &= \frac{1}{\pi}\int_0^{2\pi} F(\omega, \theta)\cos(\theta) d\theta \\
&= \frac{-1}{\pi k} q_{VN}(\omega) \\
b_1(\omega) &= \frac{1}{\pi}\int_0^{2\pi} F(\omega, \theta)\sin(\theta) d\theta \\
&= \frac{-1}{\pi k} q_{VE}(\omega) \\
a_2(\omega) &= \frac{1}{\pi}\int_0^{2\pi} F(\omega, \theta)\cos(2\theta) d\theta \\
&= \frac{1}{\pi}\int_0^{2\pi} F(\omega, \theta)(\cos^2(\theta) - \sin^2(\theta)) d\theta \\
&= \frac{1}{\pi k^2}(c_{NN}(\omega) - c_{EE}(\omega)) \\
b_2(\omega) &= \frac{1}{\pi}\int_0^{2\pi} F(\omega, \theta)\sin(2\theta) d\theta
\end{aligned}
$$

$$
\begin{aligned}
&= \frac{1}{\pi}\int_0^{2\pi} F(\omega,\theta)(2\sin(\theta)\cos(\theta))d\theta \\
&= \frac{2}{\pi k^2} c_{NE}(\omega) \qquad (4.2)
\end{aligned}
$$

Hence, a typical directional wave buoy measures the first five Fourier coefficients of the directional wave spectrum at each frequency. Summing these coefficients gives an approximation for $F(\omega,\theta)$ whose variance may be calculated by combining equations 4.1 and 4.2.

4.3.2 Model and Parameter Estimation of the Directional Wave Spectrum

The true directional wave spectrum is always positive, but the incomplete Fourier coefficient sum of equations 4.2 can lead to a negative estimate of this spectrum. An alternative approach is to fit some directional distribution (such as the *cosine-power distribution*, see Long (1980)) to these Fourier coefficients. This has the problem of having to make assumptions about the shape of the underlying directional distribution (for instance, the cosine-power distribution is unimodal and symmetrical).

A third approach is to estimate summary parameters of the directional distribution. This approach (described by Kuik and van Vledder (1984)) was chosen for NURWEC2. We can (for example) define mean direction (θ_0) and directional spread (σ_0) as measures of location and dispersion of the underlying directional distribution respectively (dropping the ω arguments for clarity) :

$$
\begin{aligned}
\theta_0 &= \tan^{-1}\left(\frac{b_1}{a_1}\right) \\
\sigma_0 &= \sqrt{2-2\sqrt{\frac{a_1^2+b_1^2}{a_0^2}}}
\end{aligned}
$$

Using a Taylor series expansion, the variances of the estimators of the above parameters are to first order :

$$
\begin{aligned}
\mathrm{Var}(\hat{\theta_0}) &= \left(\frac{\partial\theta_0}{\partial a_1}\right)^2 \mathrm{Var}(\hat{a_1}) + \left(\frac{\partial\theta_0}{\partial b_1}\right)^2 \mathrm{Var}(\hat{b_1}) + 2\frac{\partial\theta_0}{\partial a_1}\frac{\partial\theta_0}{\partial b_1}\mathrm{Cov}(\hat{a_1},\hat{b_1}) \\
\mathrm{Var}(\hat{\sigma_0}) &= \left(\frac{\partial\sigma_0}{\partial a_0}\right)^2 \mathrm{Var}(\hat{a_0}) + \left(\frac{\partial\sigma_0}{\partial a_1}\right)^2 \mathrm{Var}(\hat{a_1}) + \left(\frac{\partial\sigma_0}{\partial b_1}\right)^2 \mathrm{Var}(\hat{b_1})
\end{aligned}
$$

$$+2\frac{\partial\sigma_0}{\partial a_0}\frac{\partial\sigma_0}{\partial a_1}\mathrm{Cov}(\hat{a_0},\hat{a_1})+2\frac{\partial\sigma_0}{\partial a_0}\frac{\partial\sigma_0}{\partial b_1}\mathrm{Cov}(\hat{a_0},\hat{b_1})$$
$$+2\frac{\partial\sigma_0}{\partial a_1}\frac{\partial\sigma_0}{\partial b_1}\mathrm{Cov}(\hat{a_1},\hat{b_1})$$

4.4 Equipment Problems

Unfortunately, wave buoy technology has certain associated problems. These include :

- Wave buoys have a tendency to capsize in the stormier conditions of higher sea states, and are thus unreliable in the situations where the data is of most interest (Allender *et al.* (1989)).
- High amplitude waves may obstruct the radio transmission of data from the wave buoy to the data collection site (Wyatt *et al.* (1985)).
- There can be a tendency for the wave buoys to travel around (or even through) peaks in the sea surface, rather than over them (for instance Datawell's Waverider during WADIC, Allender *et al.* (1989)).
- Inevitably, there is the possibility of mechanical and instrumentation failures (for instance most wave buoy systems used during WADIC, Allender *et al.* (1989)).

Hence, although wave buoys are often used as a standard by which to evaluate other wave measuring systems, they have their own faults and any intercomparison should bear this in mind (see also Šova and Wyatt (1991)). An intercomparison of wave buoy and HF radar measurements using data from the NURWEC2 experiment is presented in chapter 7.

Chapter 5

HF Radar Theory

5.1 Introduction

Over the past decade HF (*H*igh *F*requency) radar has become an important tool for ocean wave (and wind) measurement. The main advantage of HF radar over other systems is the combination of wide area coverage and observation of the full directional wave spectrum. The main disadvantage is the mathematical complexity behind the theory which has only relatively recently been overcome. In this chapter this theory is introduced from the point of view of deriving the statistical properties of the wave parameters thus measured.

5.2 Pulse and FMICW Radars

When a radar signal is transmitted from a source, the beam typically "illuminates" a large area of sea (shaped like a wide circle segment, and in the case of the NURWEC2 radars, up to 200 kilometres in length). However, the antennae which receive the returning signal "observe" over a much narrower arc (such as 12°). In the NURWEC2 experiment, a selection of arcs was available at each radar site, and the operator would choose which to use. The returning signal from each arc contains information over a variety of distances. The process of separating the contribution from each distance is known as *range gating*. The method of range gating depends on whether

a pulse or FMICW (*F*requency *M*odulated *I*nterrupted *C*ontinuous *W*ave) radar is being used.

A pulse radar emits short equally spaced signals of a fixed frequency. Range is proportional to the time it takes for the signal to return, hence the range gating takes place in the time domain.

An FMICW radar emits continual "chirps" — a signal whose frequency gradually increases and then suddenly drops in a saw-tooth manner. As there is no waiting between chirps, signals are constantly arriving from all ranges. However, signals from further away will have a larger frequency difference from the emitted signal than signals from closer ranges. This is because the emitted signal will have had more time to increase its own frequency. Hence, range gating takes place in the frequency domain. As the radars used in NURWEC2 were FMICW, we shall restrict our attention to this system.

Each chirp of an FMICW signal produces a short (*e.g.* $0.4secs$) time series whose DFT gives a single complex number representing the radar backscatter at each range (or more correctly, for each *range cell* or *range bin*). Thus a series of such chirps will produce a complex time series for each range cell, spectral analysis of which produces the Doppler spectrum for that range cell.

5.3 The Effect of Ocean Waves on a Radar Signal

5.3.1 The First Order Effect

When a radar beam (radio wave) comes into "contact" with the ocean surface, it will generally scatter in many directions. However, if it meets waves travelling either *directly* towards or *directly* away from the radar site, *and* the wavelength of those waves is half the radar wavelength, then a first order effect known as *Bragg resonance* occurs (see figure 5.1) whereby those parts of the radar signal which are scattered back towards the radar source interfere constructively. Since the waves are moving (in this case either towards or away from the radar site) a frequency shift (the Doppler effect, see Shearman (1983)) occurs (in fact there are two separate shifts, one positive and one negative, for approaching and receding waves respectively). This may

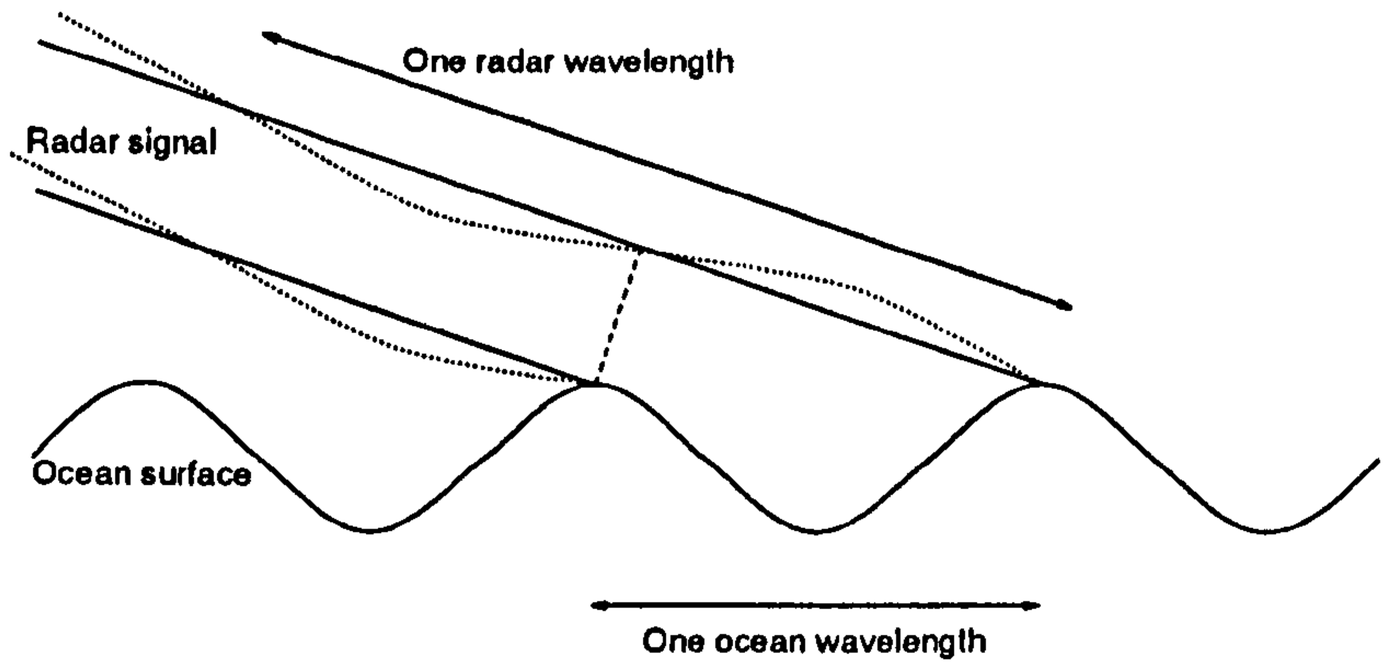

Figure 5.1: First order Bragg resonance.

be examined using a power spectrum (see section 2.3.1) of a time series of the returning radar signal. This power spectrum is referred to as a *Doppler spectrum.* Figure 5.2 shows an example of a Doppler spectrum. The prominent peak on each side of the graph (*i.e.* positive and negative frequency shift) shows the first order Bragg resonance effect (one peak each for the approaching and receding ocean waves).

5.3.2 Second Order Effects

As well as the first order effect, figure 5.2 also shows some power over the continua of frequencies to either side of the Bragg peaks. This is due to second order resonance which has three main sources (Shearman (1983)) :

The Trochoidal Effect

Since ocean waves are trochoidal in shape (as opposed to pure sinusoids), Bragg resonance is also caused by higher order harmonics of longer ocean waves. Since these longer waves move at faster speeds, the shift in frequency

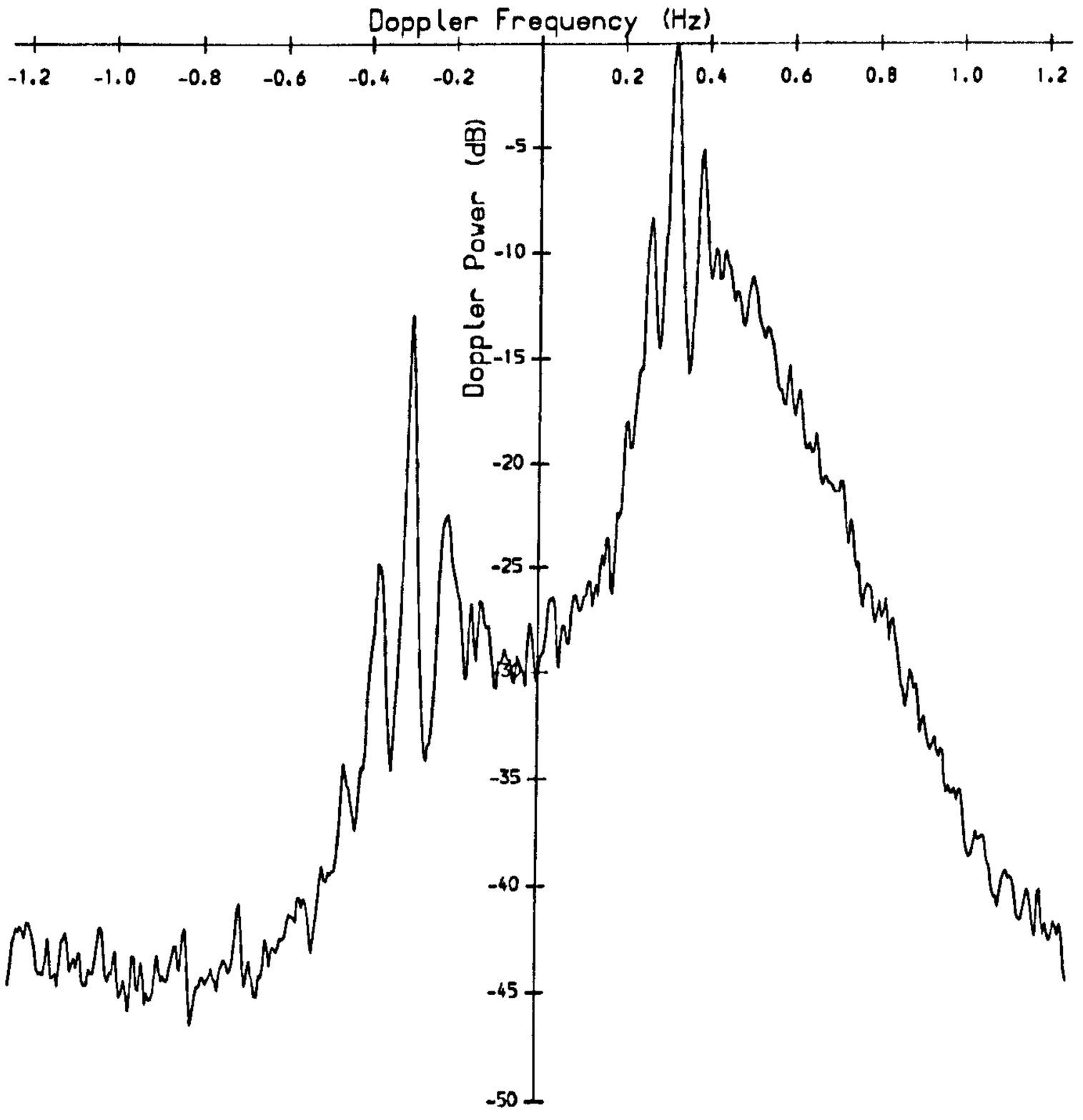

Figure 5.2: An observed Doppler spectrum (it is conventional to plot Doppler spectra on a decibel scale because the dynamic range is large).

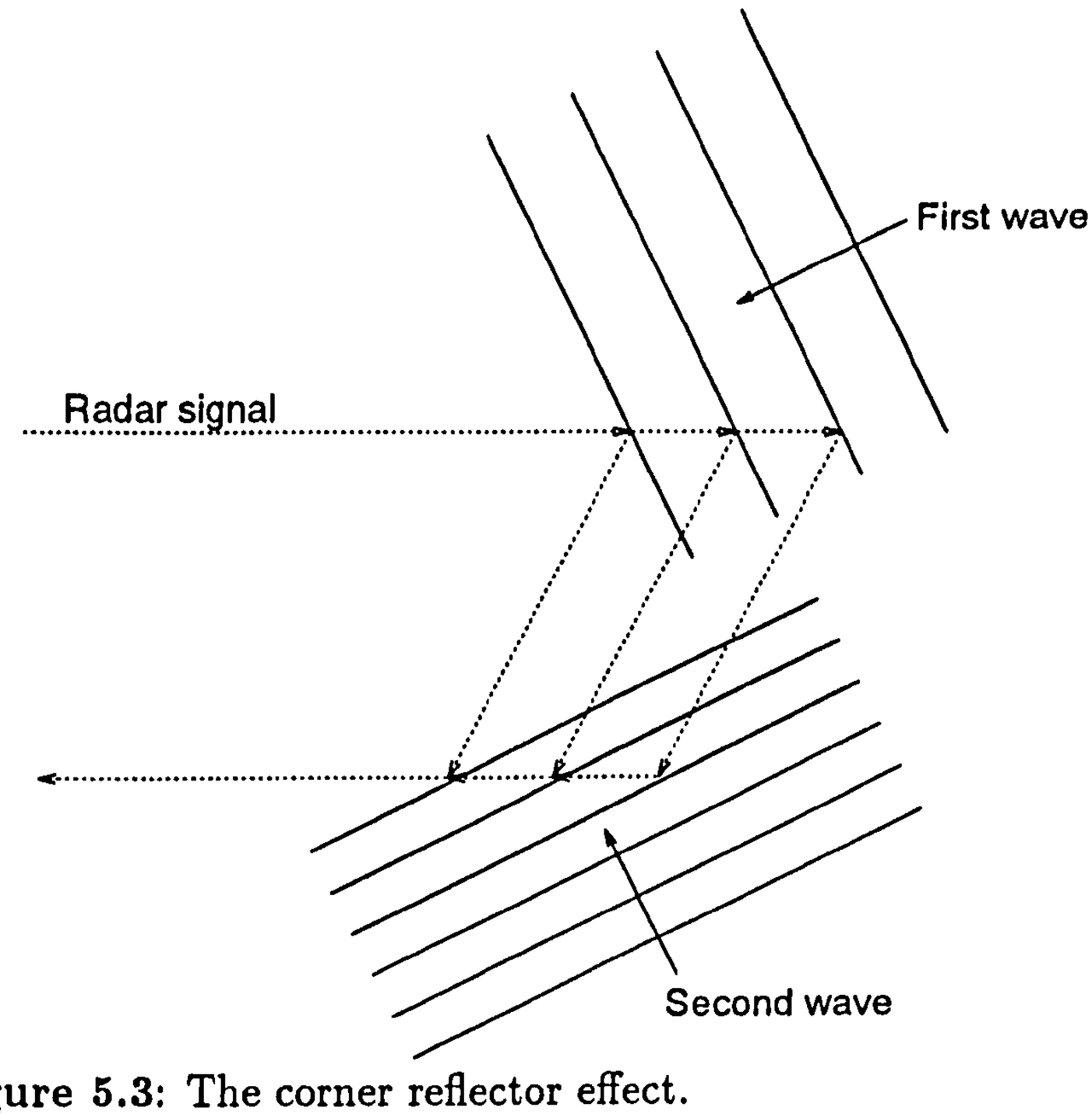

Figure 5.3: The corner reflector effect.

is greater than that for the first order effect.

The Corner Reflector Effect

If two ocean waves of suitable wavelength are travelling perpendicularly to each other, the radar beam will bounce off one and then the other and cause Bragg resonance at the radar site (see figure 5.3). The frequency shifts thus created depend on the velocities of both ocean waves.

The Interaction Wave Effect

Where two ocean waves cross, an interaction occurs. If the interaction has a wavelength half that of the radio wave and is moving either directly towards or directly away from the radar site, then Bragg resonance is again created (see figure 5.4). Again, the frequency shifts thus created depend on the velocities of both ocean waves.

Because first order power is of a much higher level than the surrounding

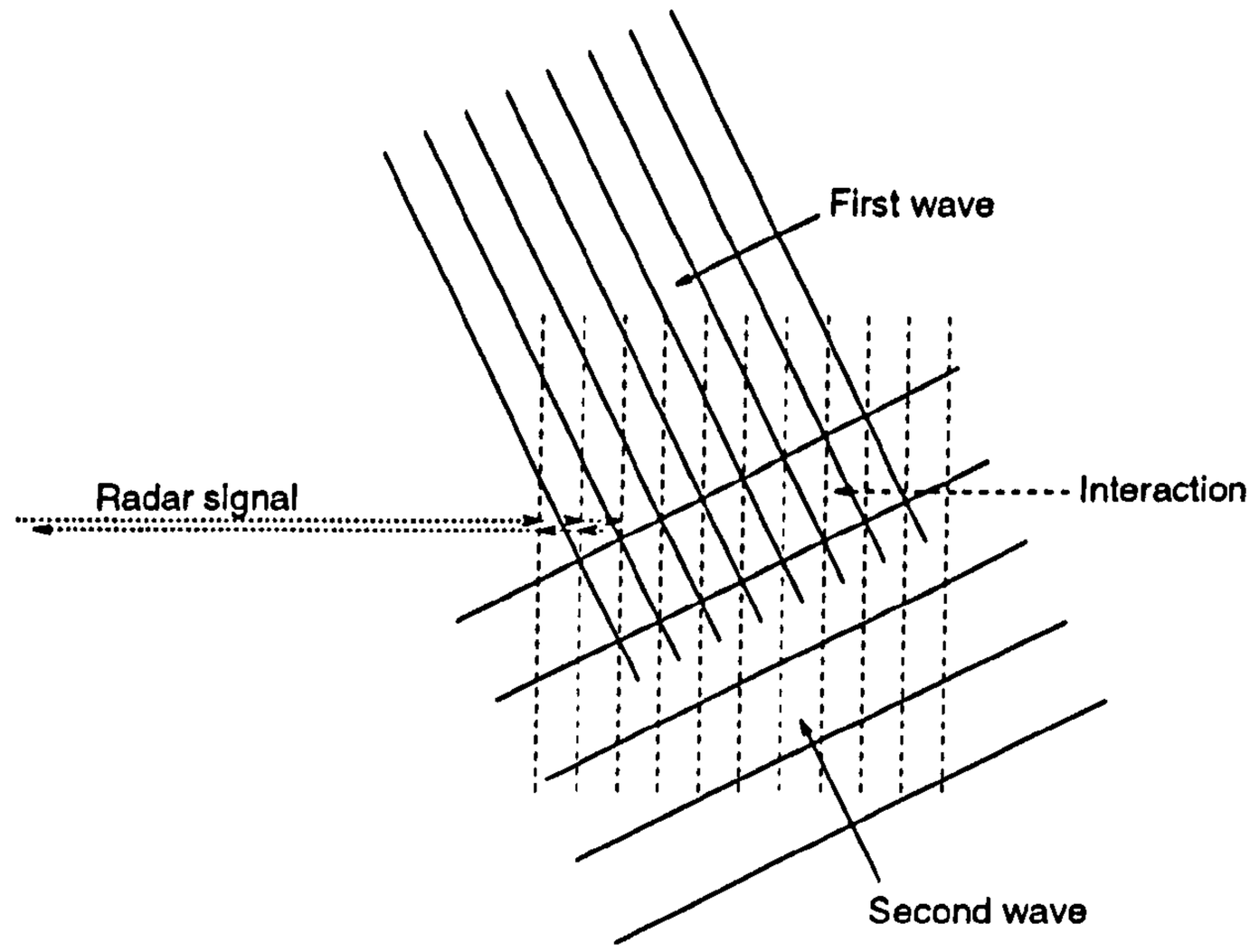

Figure 5.4: The interaction effect.

second order continuum, it can easily leak into neighbouring frequencies, thereby corrupting the spectrum. Consequently it is necessary to use a taper such as the four point Blackman-Harris taper (see section 2.3.5). Figure 5.5 shows part of a Doppler spectrum calculated with and without such a taper, and the following three features of using the taper are evident :

1. Frequencies with relatively low power are more clearly defined (*e.g.* around the first-order peak).

2. The first-order peak is broadened slightly.

3. The spectrum is "smoother".

5.3.3 Statistical Properties of the Doppler Spectrum

Barrick and Snider (1977) use central limit arguments to demonstrate the approximate Normality of HF radar backscatter based on the assumption of the approximate Normality of the ocean surface. Under this assumption we may use equation 2.7 from section 2.3.4 to obtain an approximate expression

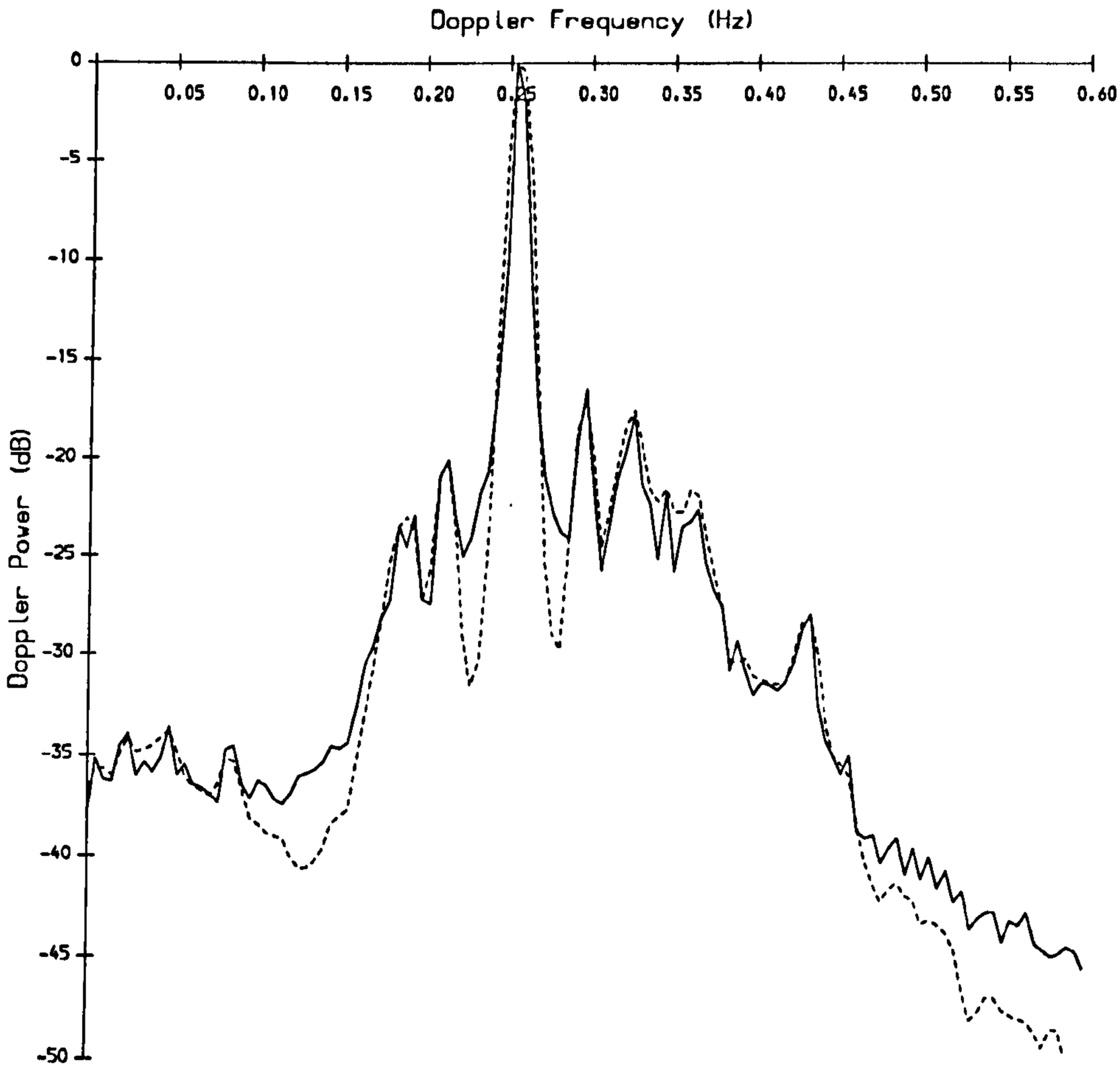

Figure 5.5: A Doppler spectrum calculated using (broken line) and without using (solid line) a taper.

for the distribution of an observed Doppler spectrum (this result is also given by Barrick and Snider (1977) and Barrick (1980)) :

$$\hat{S}_D(f) \sim \frac{\chi^2_\nu}{\nu} S_D(f) \tag{5.1}$$

where $\hat{S}_D(f)$ is the estimated Doppler spectrum, $S_D(f)$ is its expectation, and ν is the number of its degrees of freedom (see section 2.3.6 — to minimise leakage from the first order Bragg peaks, a 4-point Blackman-Harris taper (see section 2.3.5) is typically applied to the data). From equation 5.1, we derive the following $100(1-\alpha)\%$ confidence interval for the "underlying" (*i.e.* expected) Doppler spectrum :

$$\left(\frac{\nu \hat{S}_D(f)}{\chi^2_{\nu,1-\frac{\alpha}{2}}}, \frac{\nu \hat{S}_D(f)}{\chi^2_{\nu,\frac{\alpha}{2}}} \right)$$

Figure 5.6 shows an example Doppler spectrum with its (pointwise) 90% confidence interval. Because of the multiplicative nature of equation 5.1, the confidence interval has a uniform width on a logarithmic scale.

5.4 Parameters derived from the Doppler Spectra

There are certain wind and wave parameters which may be calculated directly from the Doppler spectra. This section describes the calculation (as used in the NURWEC2 experiment) of each such parameter, and the derivation of their confidence intervals.

5.4.1 Wind Direction

For radio frequencies in the HF range, first order Bragg resonance is caused by waves which have been generated by the local wind. Wind direction (relative to the direction of the radar signal) is calculated from the two first order peaks as described by Wyatt (1983) :

$$\cos(\theta_W) = \frac{-1 - r + 2\sqrt{r}}{1 - r} \tag{5.2}$$

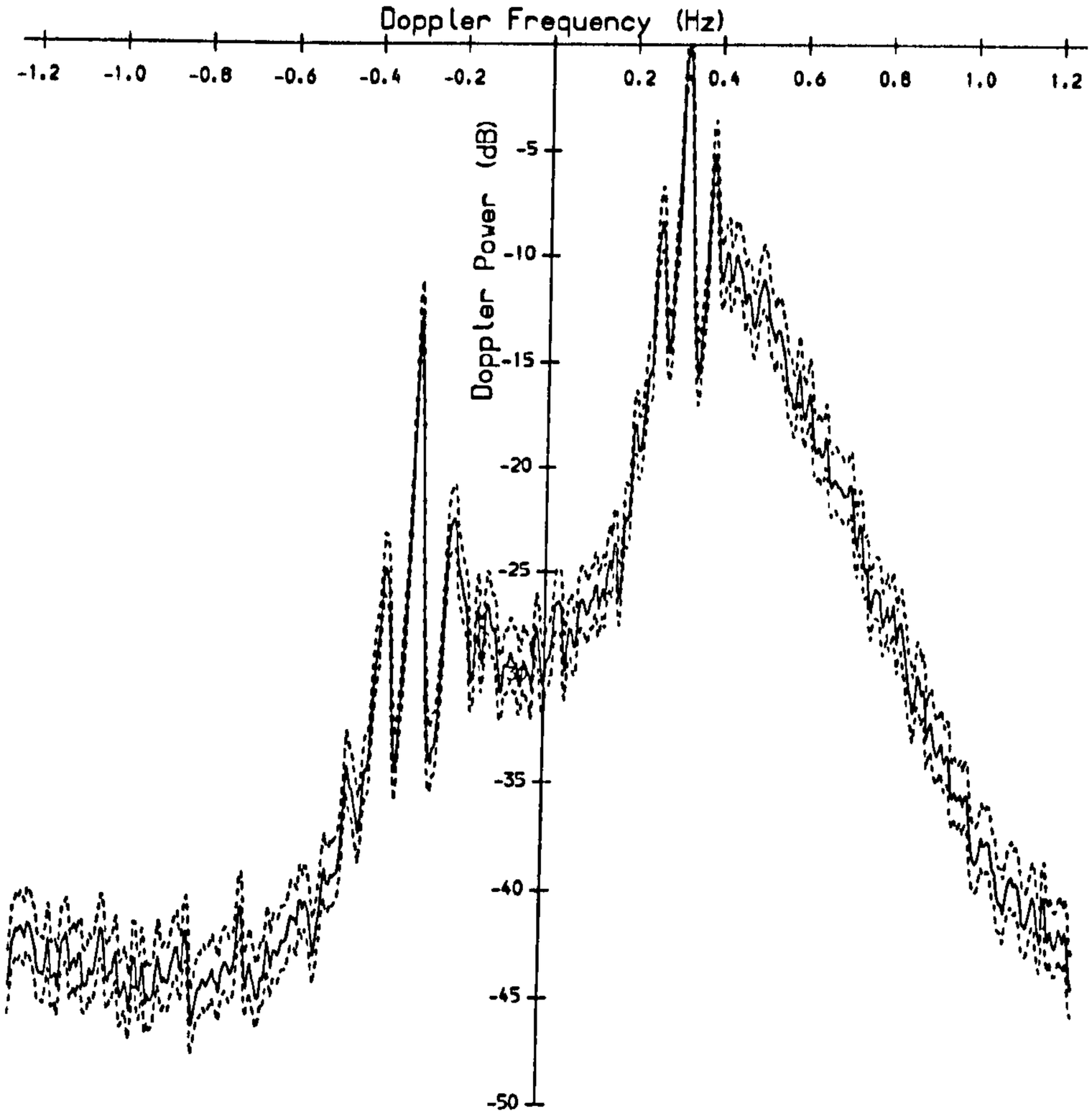

Figure 5.6: A Doppler spectrum (solid line) with its 90% confidence interval (broken lines).

$$\text{where} \begin{cases} \theta_W = \text{wind direction with respect to radar beam} \\ r = \frac{\sigma_{1-}}{\sigma_{1+}} \\ \sigma_{1+} = \text{power in positive first order peak} \\ \sigma_{1-} = \text{power in negative first order peak} \end{cases}$$

We get from equation 5.1 :

$$\begin{aligned} \hat{r} &= \frac{\hat{\sigma}_{1-}}{\hat{\sigma}_{1+}} \\ &\sim \frac{\sigma_{1-} \times \chi^2_\nu/\nu}{\sigma_{1+} \times \chi^2_\nu/\nu} \quad \text{with both } \chi^2 \text{ variables independent} \\ &\sim r\mathrm{F}_{\nu,\nu} \quad \text{approx.} \end{aligned}$$

where $\hat{r}$, $\hat{\sigma}_{1-}$ and $\hat{\sigma}_{1+}$ are the estimates of r, σ_{1-} and σ_{1+} respectively.

We may now estimate the variance of $\hat{\theta}_W$ by using a Taylor series expansion :

$$\begin{aligned} \frac{\partial \cos(\theta_W)}{\partial r} &= \frac{(1-r)(-1+\frac{1}{\sqrt{r}}) + (-1-r-2\sqrt{r})}{(1-r)^2} \\ &= \frac{1-\sqrt{r}}{\sqrt{r}(1-r)} - \frac{(\sqrt{r}-1)^2}{(1-r)^2} \end{aligned}$$

Hence,

$$\begin{aligned} \frac{\partial \theta_W}{\partial r} &= \frac{-1}{\sqrt{1-\cos^2(\theta_W)}} \left(\frac{1-\sqrt{r}}{\sqrt{r}(1-r)} - \frac{(\sqrt{r}-1)^2}{(1-r)^2} \right) \\ &= -\sqrt{\frac{1-r}{-2\sqrt{r}+2}} \left(\frac{1-\sqrt{r}}{\sqrt{r}(1-r)} - \frac{(\sqrt{r}-1)^2}{(1-r)^2} \right) \end{aligned}$$

We may thus estimate $\mathrm{Var}(\hat{\theta}_W)$ by substituting $\hat{r}$ for r in the following approximation :

$$\mathrm{Var}(\hat{\theta}_W) = \left(\frac{\partial \theta_W}{\partial r} \right)^2 \mathrm{Var}(\hat{r}) \quad \text{approx. to first order}$$

where $\mathrm{Var}(\hat{r}) = r^2 \frac{2\nu^2(2\nu-2)}{\nu(\nu-2)^2(\nu-4)}$ (*i.e.* the variance of the $F_{\nu,\nu}$ distribution). Using a Normal approximation, we may construct approximate confidence intervals for wind direction. Figure 5.7 shows a plot of wind direction (with respect to the radar beam) with its 90% confidence interval.

Formula 5.2 gives wind direction (relative to the radar beam) only in terms of its cosine. This results in a directional ambiguity since each possible value of the cosine function (except for ± 1) is associated with *two* directions. Thus,

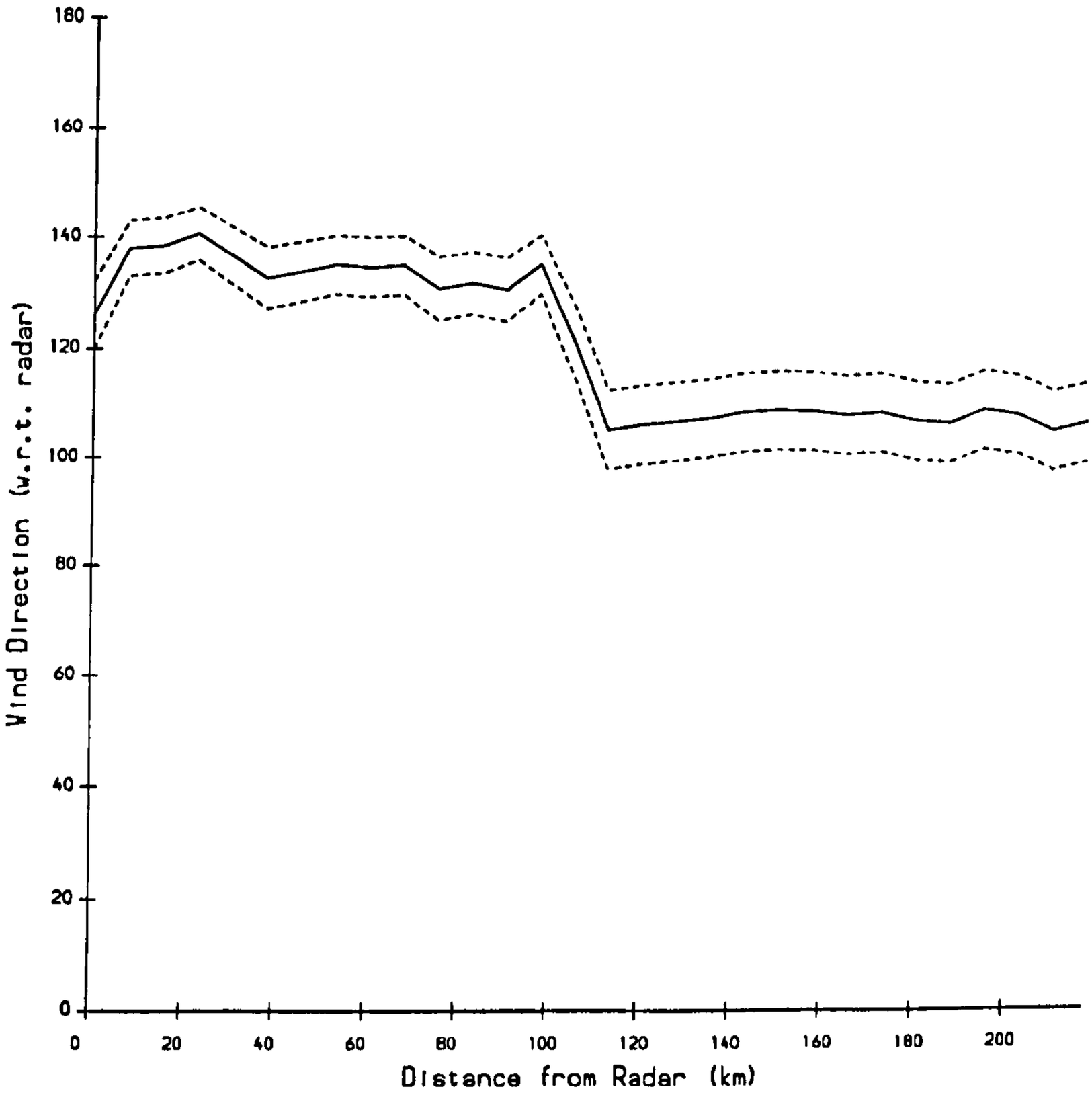

Figure 5.7: A plot of wind direction (with respect to the radar beam) with its 90% confidence interval, as a function of distance from the radar site, taken on March 27^{th} 1987.

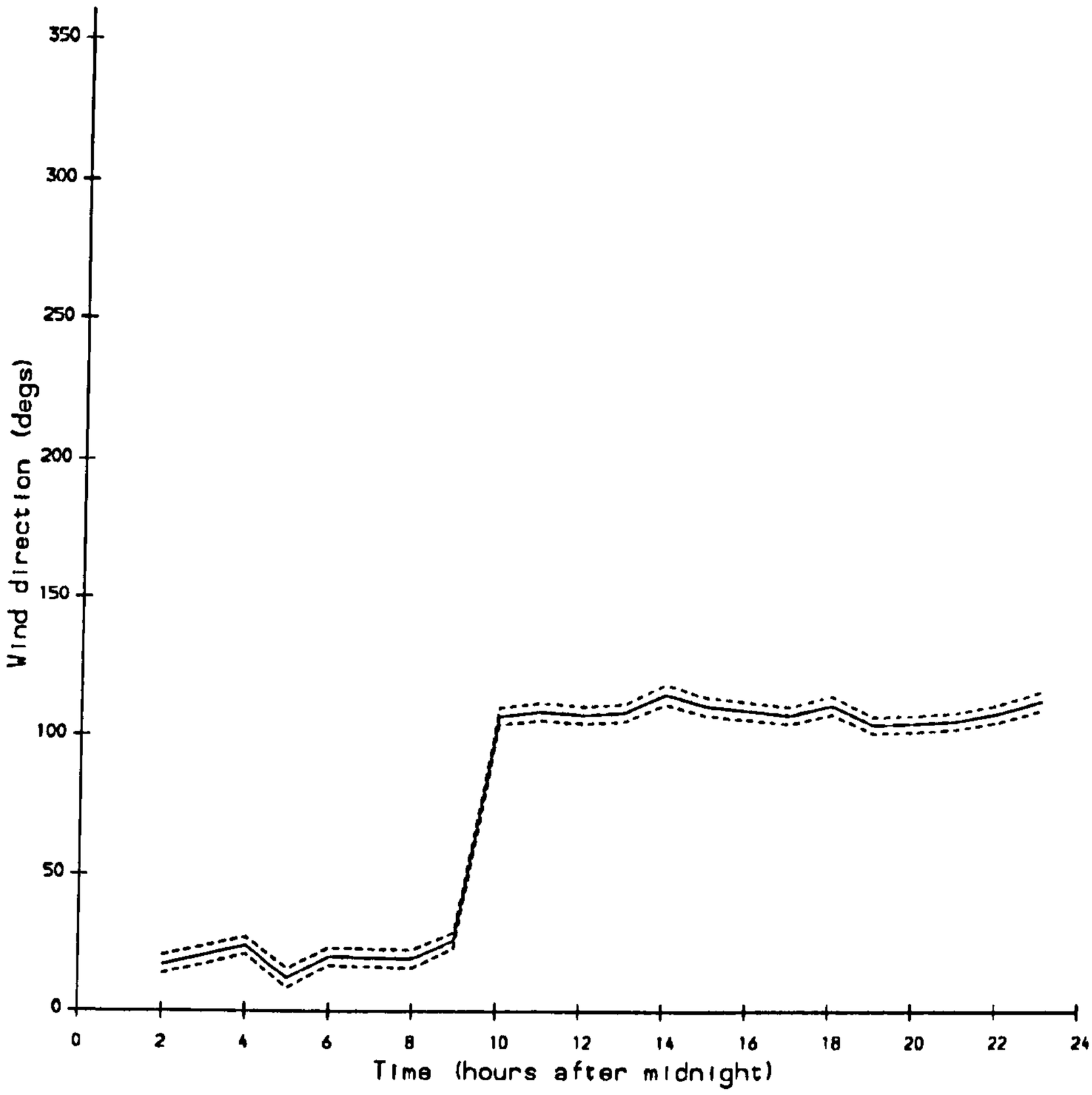

Figure 5.8: A plot of (absolute) wind direction with its 90% confidence interval during March 27^{th} 1987.

absolute wind direction (*i.e.* relative to True North) needs to be be estimated by comparing estimates from two radar sites (which by necessity will be operating either at different radio frequencies or non-simultaneously) and combining those estimates which most closely match. The NURWEC2 wind direction data have been calculated using data from the Dyfed site. Data from the Devon site have only been used to resolve the directional ambiguity — they have not been averaged with the Dyfed site data. Figure 5.8 shows a plot of absolute wind direction with its 90% confidence interval as a function of time.

5.4.2 Significant Waveheight

There are two formulae (each valid under different conditions — see below) describing the relationship between significant waveheight (H_s, defined as

four times the standard deviation of the sea surface, see section 1.3.2) and the Doppler spectrum (see Wyatt *et al.* (1986) and Wyatt (1988c)) :

$$H_s = \frac{\sqrt{\sum_{H_L} \sigma_2(\eta)} + \sqrt{\sum_{H_U} \sigma_2(\eta)}}{\psi k_0} \tag{5.3}$$

$$H_s = \left(\frac{\sqrt{\sum_{H_L} \sigma_2(\eta)} + \sqrt{\sum_{H_U} \sigma_2(\eta)}}{2} \right)^{\alpha} \times \frac{\beta}{k_0} \tag{5.4}$$

where
- η is the normalised Doppler frequency
- $\sigma_2(\eta)$ is the Doppler spectrum divided by the first order Bragg power
- H_U, H_L define the upper and lower side lobes of the second order continuum
- k_0 is the radar wavenumber
- α, β, ψ are known engineering parameters

The normalised frequency, η, is a linear function of frequency such that the negative Bragg peak occurs at $\eta = -1$, and the positive Bragg peak occurs at $\eta = +1$. These formulae refer only to the half of the Doppler spectrum which contains the Bragg peak with the most power, and it is the power of this Bragg peak by which the second order power is divided to give $\sigma_2(\eta)$. H_L and H_U are the sets of frequency bins corresponding to $\eta \in [0.4\eta_P, \eta_P]$ and $\eta \in [\eta_P, 1.6\eta_P]$ respectively, excluding those bins which contain first order power (η_P is the normalised frequency of the Bragg peak with most energy, hence $|\eta_P| = 1$).

Formula 5.3 is appropriate if the mode wave direction is (approximately) perpendicular to the radar beam, otherwise formula 5.4 is used (although at this stage of the analysis, such directional information is unavailable). The different formulae result from the very different form that the Doppler spectrum takes when the mode wave direction is perpendicular to the radar beam (see Wyatt (1988c)). Both of these formulae are functions of sums of spectral power (initially dividing by first order power). Thus, estimating ν_L and ν_U (the number of degrees in the spectral integrals over H_L and H_U respectively) using equation 3.12 we get :

$$\sum_{H_L} \hat{\sigma}_2(\eta) \sim \mathrm{F}_{\nu_L,\nu} \mathrm{E}\left(\sum_{H_L} \sigma_2(\eta)\right)$$
$$\sum_{H_U} \hat{\sigma}_2(\eta) \sim \mathrm{F}_{\nu_U,\nu} \mathrm{E}\left(\sum_{H_U} \sigma_2(\eta)\right)$$

where ν is the number of degrees of freedom in the Doppler spectral estimates. This allows us to estimate the variance of $\hat{H}_s$ (the estimate of H_s) using a Taylor series expansion. Hence, when using formula 5.3 :

$$\mathrm{Var}(\hat{H}_s) = \frac{\frac{1}{4\sum_{H_L}\sigma_2(\eta)}\mathrm{Var}(\mathrm{F}_{\nu_L,\nu})\mathrm{E}^2(\sum_{H_L}\sigma_2(\eta)) + \frac{1}{4\sum_{H_U}\sigma_2(\eta)}\mathrm{Var}(\mathrm{F}_{\nu_U,\nu})\mathrm{E}^2(\sum_{H_U}\sigma_2(\eta))}{\psi^2 k_0^2}$$

approx. to first order (5.5)

and when using formula 5.4 :

$$\mathrm{Var}(\hat{H}_s) = \frac{\frac{1}{4\sum_{H_L}\sigma_2(\eta)}\mathrm{Var}(\mathrm{F}_{\nu_L,\nu})\mathrm{E}^2(\sum_{H_L}\sigma_2(\eta)) + \frac{1}{4\sum_{H_U}\sigma_2(\eta)}\mathrm{Var}(\mathrm{F}_{\nu_U,\nu})\mathrm{E}^2(\sum_{H_U}\sigma_2(\eta))}{4} \times \left(\frac{\sqrt{\mathrm{E}\left(\sum_{H_L}\sigma_2(\eta)\right)} + \sqrt{\mathrm{E}\left(\sum_{H_U}\sigma_2(\eta)\right)}}{2}\right)^{2\alpha-2} \frac{\alpha^2\beta^2}{k_0^2}$$

approx. to first order (5.6)

Using a Normal approximation, formulae 5.5 and 5.6 may be used to construct approximate confidence intervals for significant waveheight. Figure 5.9 shows a plot of significant waveheight (using both formulae — the higher and lower lines represent formula 5.3 and 5.4, respectively) with 90% confidence intervals. Barrick (1980) gives an alternative expression for the standard deviation of the significant waveheight estimate which is based on the assumption that the second-order part of the Doppler spectrum has (approximately) a particular shape. Equations 5.5 and 5.6 do not rely on any such assumption as the shape of the Doppler spectrum is estimated from the observed Doppler spectrum itself.

In practice, significant waveheight is estimated by combining the measurements from two radars which most closely match. If only one of these matching measurements is from formula 5.4 then that is chosen as the estimate, otherwise the mean is taken. Figure 5.10 shows a plot of significant waveheight with its 90% confidence interval as a function of time.

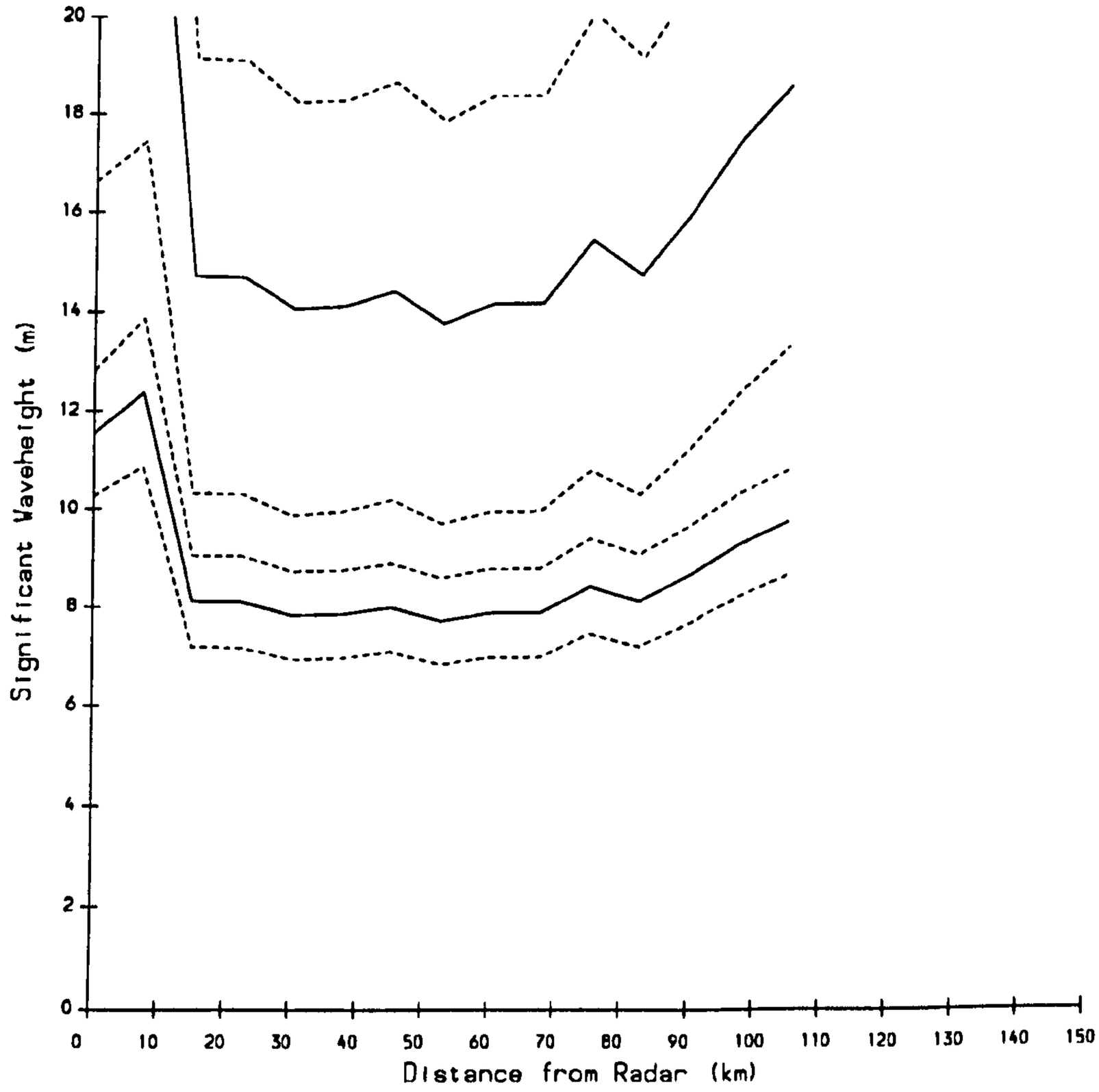

Figure 5.9: A plot of significant waveheight with 90% confidence intervals, as a function of distance from the radar site (with the higher and lower lines representing formula 5.3 and 5.4, respectively).

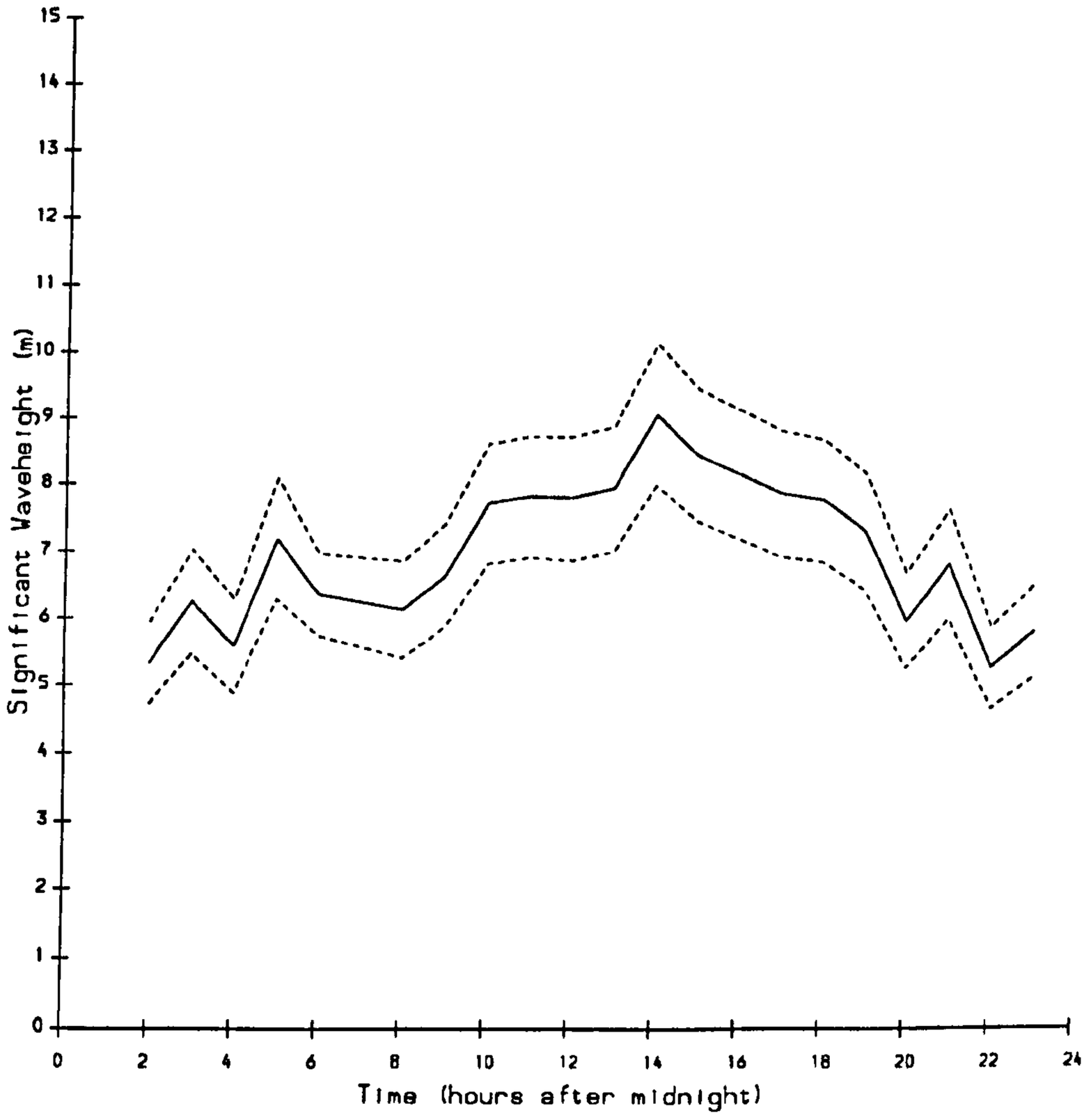

Figure 5.10: A plot of significant waveheight with its 90% confidence interval during March 27^{th} 1987.

5.4.3 Mean Wave Period

The following formula describes the relationship between mean wave period and the Doppler spectrum (see Wyatt *et al.* (1986)) :

$$T_m = \frac{\left(\frac{\sum_{H_{L'}} \sigma_2(\eta)}{\sum_{H_{L'}} \sigma_2(\eta)||\eta|-1|} f_B + \frac{\sum_{H_{U'}} \sigma_2(\eta)}{\sum_{H_{U'}} \sigma(\eta)_2||\eta|-1|} f_B \right)}{2} - \xi}{\phi f_B} \tag{5.7}$$

where
- η is the normalised Doppler frequency
- $\sigma_2(\eta)$ is the Doppler spectrum divided by the first order Bragg power
- $H_{U'}, H_{L'}$ define the upper and lower side lobes of the second order continuum
- f_B is the Bragg frequency
- ξ, ϕ are known engineering parameters

$H_{L'}$ and $H_{U'}$ are the sets of frequency bins corresponding to $\eta \in (0, \eta_P]$ and $\eta \in [\eta_P, 2\eta_P]$ respectively, excluding those bins which contain first order energy (η_P is the normalised frequency of the Bragg peak with most energy, and hence $|\eta_P| = 1$).

Formula 5.7 involves ratios of weighted sums of Doppler spectral energy. The variances and covariances of these weighted sums may be estimated from formulae 3.24 and 3.27. This information allows us to estimate the variance of $\hat{T_m}$ (the estimate of T_m) using a Taylor series expansion. Let

$$\begin{aligned}
A_1 &= \sum_{H_{L'}} \sigma_2(\eta) \\
B_1 &= \sum_{H_{L'}} \sigma_2(\eta)||\eta| - 1| \\
A_2 &= \sum_{H_{U'}} \sigma_2(\eta) \\
B_2 &= \sum_{H_{U'}} \sigma_2(\eta)||\eta| - 1| \\
Y_L &= \frac{A_1}{B_1} \\
Y_U &= \frac{A_2}{B_2}
\end{aligned}$$

i.e.

$$\hat{T}_m = \frac{\left(\frac{Y_L f_B + Y_U f_B}{2} - \xi\right)}{\phi f_B}$$

then,

$$\mathrm{Var}(Y_L) = \frac{\mathrm{Var}(A_1)}{\mathrm{E}^2(B_1)} - \frac{2\mathrm{E}(A_1)\mathrm{Cov}(A_1, B_1)}{\mathrm{E}^3(B_1)} + \frac{\mathrm{E}^2(A_1)\mathrm{Var}(B_1)}{\mathrm{E}^4(B_1)} \quad \text{to first order}$$

and similarly,

$$\mathrm{Var}(Y_U) = \frac{\mathrm{Var}(A_2)}{\mathrm{E}^2(B_2)} - \frac{2\mathrm{E}(A_2)\mathrm{Cov}(A_2, B_2)}{\mathrm{E}^3(B_2)} + \frac{\mathrm{E}^2(A_2)\mathrm{Var}(B_2)}{\mathrm{E}^4(B_2)} \quad \text{to first order}$$

Hence, we may estimate $\mathrm{Var}(\hat{T}_m)$ by substituting $\hat{\sigma}_2(\eta)$ for $\sigma_2(\eta)$:

$$\mathrm{Var}(\hat{T}_m) = \frac{\mathrm{Var}(Y_L) + \mathrm{Var}(Y_U)}{4\phi^2} \tag{5.8}$$

Using a Normal approximation, formula 5.8 may be used to construct an approximate confidence interval for mean wave period. Figure 5.11 shows a plot of mean wave period with its 90% confidence intervals.

Although mean wave period can be measured by a single radar, in practice measurements from two radar are combined. If significant waveheight was derived from only one radar site, then the mean period measurement is taken from the same site. If the significant waveheight measurement is derived from both sites, then the mean period measurement is taken as the average of the mean period measurements from each site. (We recall that although significant waveheight is, under certain conditions, calculated using the *measurement* from only one radar site, it requires *information* from both sites, as described in section 5.4.2). Figure 5.12 shows a plot of mean wave period with its 90% confidence interval as a function of time.

5.4.4 Wind Speed

Dexter and Theodoridis (1982) give the following formula to describe the relationship between wind speed, significant waveheight and peak wave period (based on a wind-wave model which assumes that all waves have been

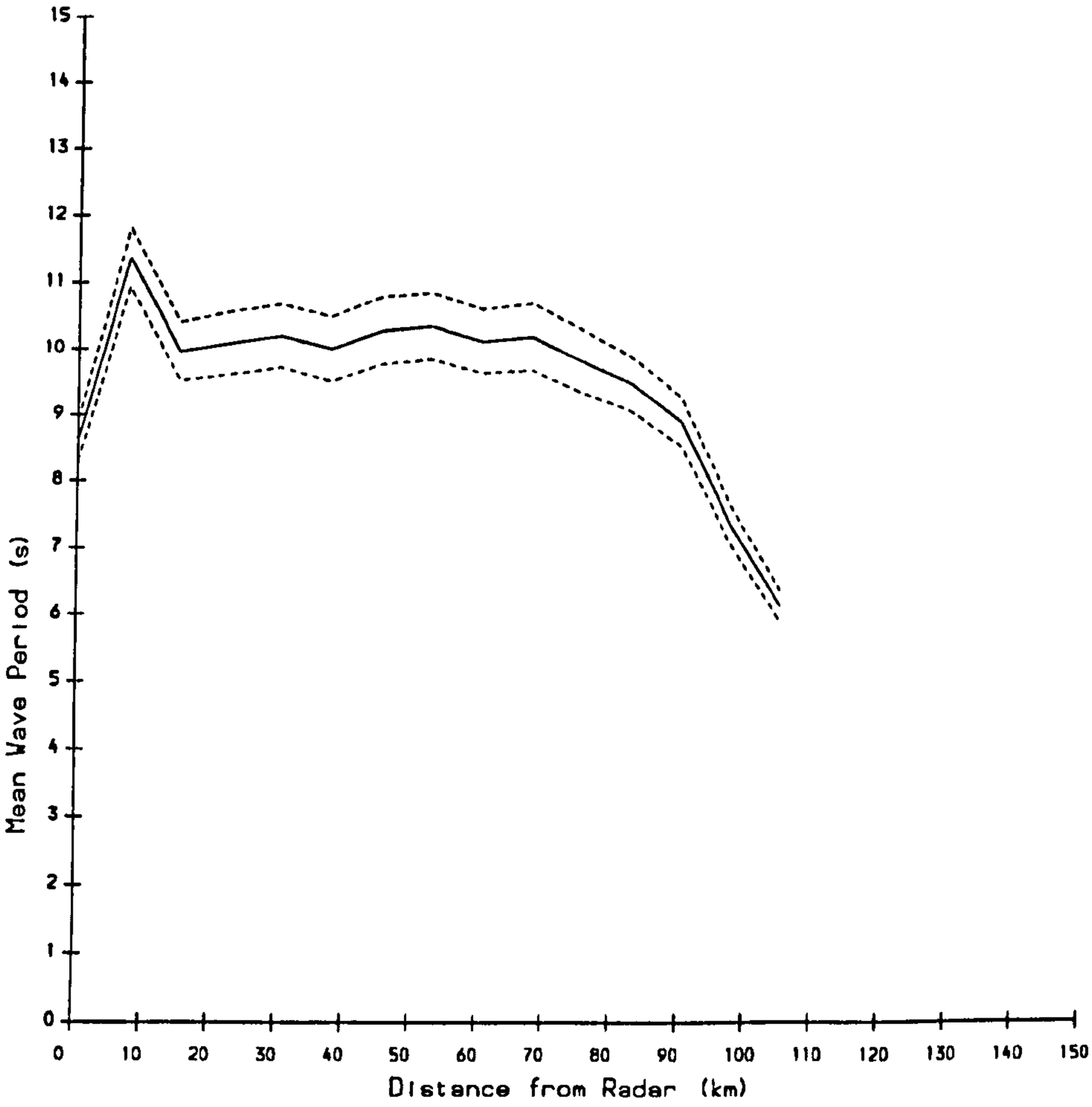

Figure 5.11: A plot of mean wave period with its 90% confidence interval, as a function of distance from the radar site, taken on March 27^{th} 1987.

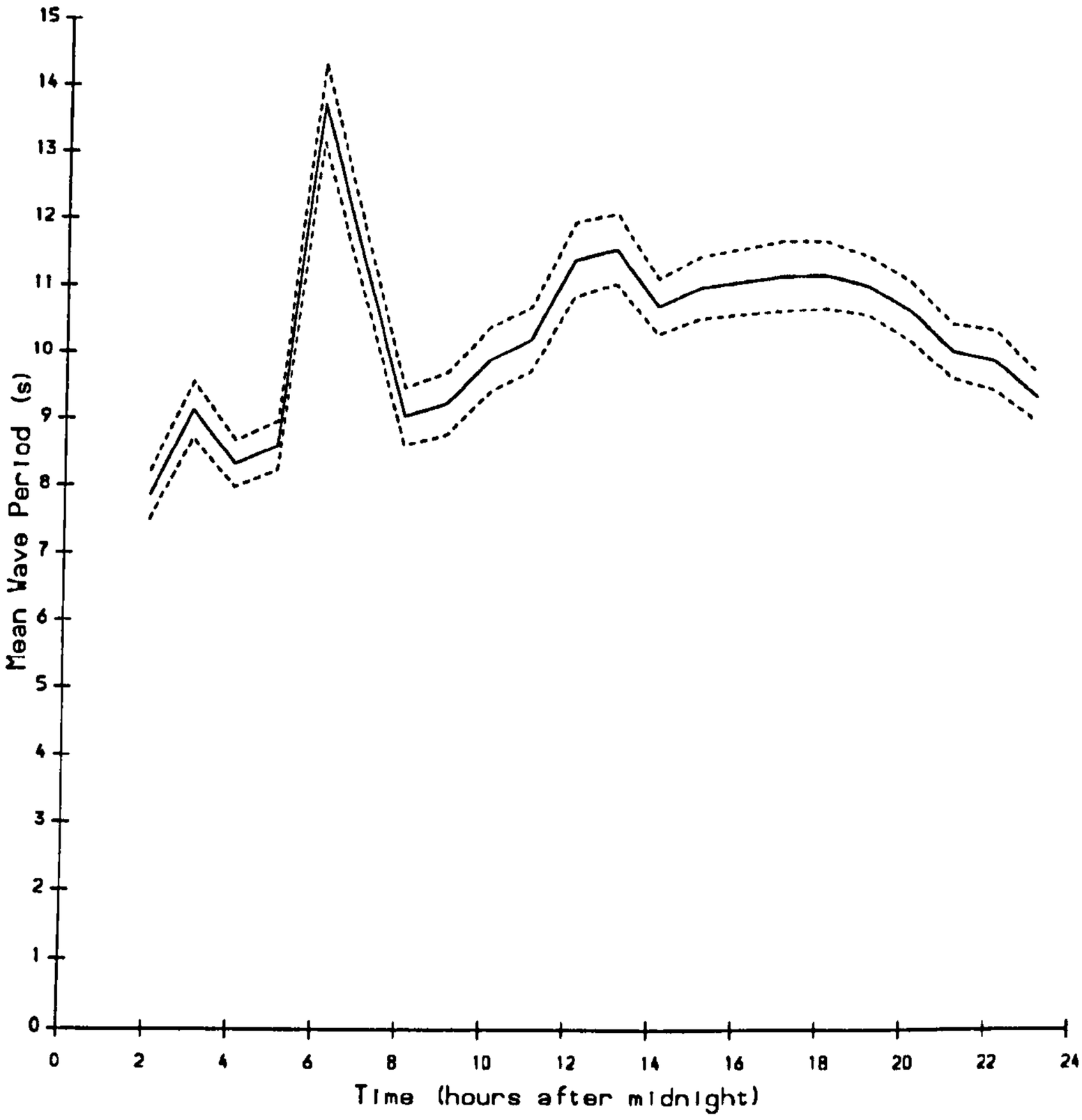

Figure 5.12: A plot of mean wave period with its 90% confidence interval during March 27^{th} 1987.

generated by the *local* wind) :

$$\frac{gH_s}{U^2} = 0.26 \tanh\left(\left(\frac{T_p}{U}\right)^{\frac{3}{2}} \times \frac{(3.5g)^{\frac{3}{2}}}{100}\right)$$

where U is wind speed, H_s is significant waveheight, T_p is peak wave period (which may be estimated by $1.25T_m$) and g is the acceleration due to gravity. Because of the structure of this formula, wind speed is in practice derived using the following iterative scheme :

$$U_j = \sqrt{\frac{gH_s}{0.26 \tanh\left(\left(\frac{T_p}{U_{j-1}}\right)^{\frac{3}{2}} \times \frac{(3.5g)^{\frac{3}{2}}}{100}\right)}}$$

where U_j is the is the wind speed estimate after the j-th iteration. With an initial guess of $U_0 = 10m/s$, this process typically converges after between 2 and 6 iterations.

Consider each iteration as producing the triple (U_j, H_s, T_p) from (U_{j-1}, H_s, T_p) and let

$$p_j = \frac{\partial U_j}{\partial U_{j-1}}$$

$$q_j = \frac{\partial U_j}{\partial H_s}$$

$$p_j = \frac{\partial U_j}{\partial T_p}$$

$$\mathbf{D}_j = \begin{pmatrix} p_j & q_j & r_j \\ 0 & 1 & 0 \\ 0 & 0 & 1 \end{pmatrix}$$

Then, using a Taylor expansion

$$\mathbf{V}_j = \mathbf{D}_j \mathbf{V}_{j-1} \mathbf{D}_j^T \text{ to first order}$$

$$\text{where } \mathbf{V}_j = \begin{pmatrix} \text{Var}(\hat{U}_j) & \text{Cov}(\hat{U}_j, \hat{H}_s) & \text{Cov}(\hat{U}_j, \hat{T}_p) \\ \text{Cov}(\hat{U}_j, \hat{H}_s) & \text{Var}(\hat{H}_s) & \text{Cov}(\hat{H}_s, \hat{T}_p) \\ \text{Cov}(\hat{U}_j, \hat{T}_p) & \text{Cov}(\hat{H}_s, \hat{T}_p) & \text{Var}(\hat{T}_p) \end{pmatrix}$$

Hence,

$$\begin{aligned} \text{Var}(\hat{U}_j) \;=\; & p_j^2 \text{Var}(\hat{U}_{j-1}) + q_j^2 \text{Var}(\hat{H}_s) + r_j^2 \text{Var}(\hat{T}_p) \\ & + 2p_j q_j \text{Cov}(\hat{U}_{j-1}, \hat{H}_s) + 2p_j r_j \text{Cov}(\hat{U}_{j-1}, \hat{T}_p) \end{aligned}$$

$$
\begin{aligned}
& & & +2q_j r_j \mathrm{Cov}(\hat{H}_s, \hat{T}_p) \\
\mathrm{Cov}(\hat{U}_j, \hat{H}_s) &= & & p_j \mathrm{Cov}(\hat{U}_j, \hat{H}_s) + q_j \mathrm{Var}(\hat{H}_s) + r_j \mathrm{Cov}(\hat{H}_s, \hat{T}_p) \\
\mathrm{Cov}(\hat{U}_j, \hat{T}_p) &= & & p_j \mathrm{Cov}(\hat{U}_j, \hat{T}_p) + q_j \mathrm{Cov}(\hat{H}_s, \hat{T}_p) + r_j \mathrm{Var}(\hat{T}_p)
\end{aligned}
$$

to first order, where since $\hat{T}_p = 1.25\hat{T}_m$:

$$
\begin{aligned}
\mathrm{Var}(\hat{T}_p) &= 1.25^2 \mathrm{Var}(\hat{T}_m) \\
\mathrm{Cov}(\hat{H}_s, \hat{T}_p) &= 1.25 \mathrm{Cov}(\hat{H}_s, \hat{T}_m)
\end{aligned}
$$

With this information, it is possible to produce a *first order* estimate of the variance of the wind speed measurement. However, wind speed variances estimated from simulated significant waveheight and mean wave period data were observed to be in the range of $0.2 - 2.0 m^2/s^2$, and quite different from their theoretical first order estimates. This suggests that such first order approximations are not accurate estimates of the variance of the observed wind speed. Fortunately, this is not a serious problem since the purpose of calculating wind speed is the production of a Pierson-Moskovitz model spectrum estimate (see section 5.4.5). This model estimate is used as a "first guess" in the estimation of the full directional frequency spectrum of wave power (see section 5.5.2). It is only left unaltered for wave frequencies over $200mHz$ (approx.) over which range the model shows little variation, even for large differences in wind speed. Figure 5.13 shows a plot of wind speed.

5.4.5 The Wind-Driven Spectrum

The Pierson-Moskovitz model wave spectrum has the following formula (see Tucker (1991)) :

$$S(f) = \alpha_{PM} g^2 (2\pi)^{-4} f^{-5} e^{-\beta \left(\frac{g}{2\pi U f}\right)^4}$$

$$
\text{where} \begin{cases}
\alpha_{PM} = 0.0081 \\
\beta = 0.74 \\
f \text{ is frequency} \\
U \text{ is wind speed} \\
S \text{ is the ocean wave power spectrum}
\end{cases}
$$

This model is based on the assumption that all waves present have been generated by the local wind, and is used as an initial guess in the estimation

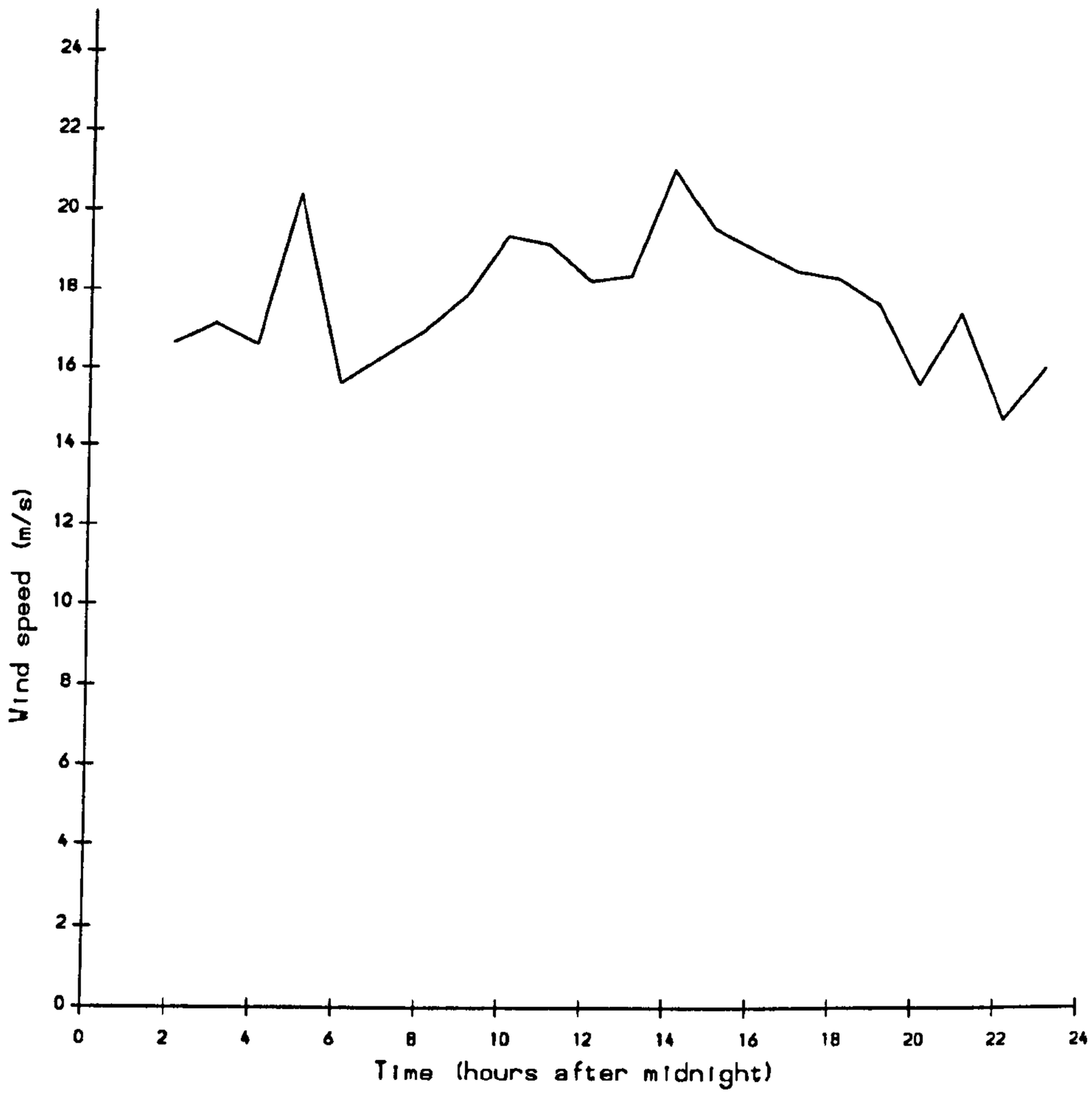

Figure 5.13: A plot of wind speed during March 27^{th} 1987, as a function of time.

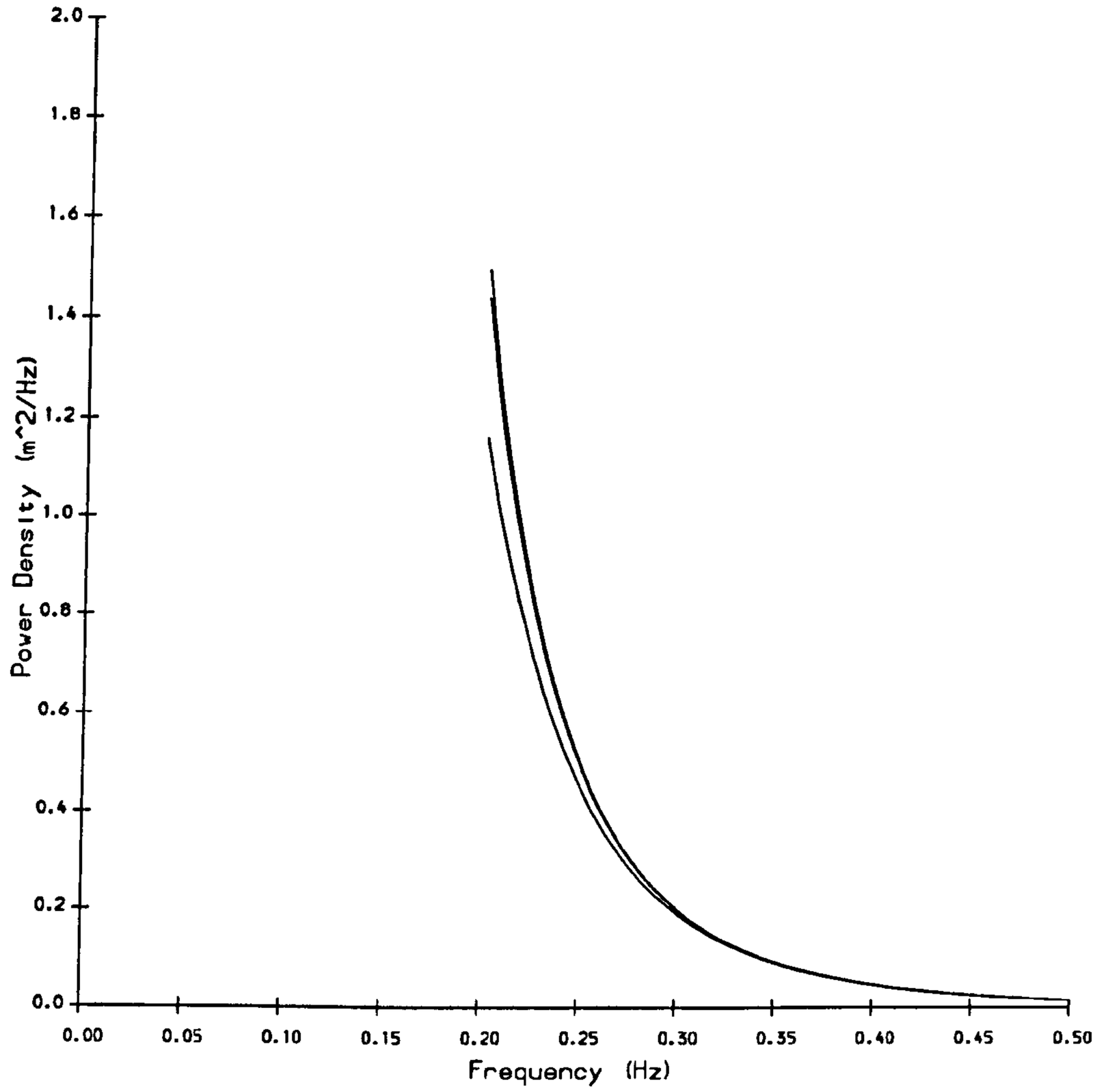

Figure 5.14: The high frequency parts of 3 Pierson-Moskovitz spectra. The top, middle and bottom lines correspond to wind speeds of 20, 15 and $10 m/s$, respectively.

of the full directional ocean wave spectrum (see section 5.5.2). Only the high frequency part (above about $200 mHz$) of this spectrum is unchanged during the radar analysis procedure. Figure 5.14 shows how for 3 quite different wind speeds this part of the spectrum is fairly similar.

5.5 The Inversion Problem

5.5.1 Introduction

In section 5.4 we examined the statistical properties of the ocean wave parameters which may be *directly* derived from the Doppler spectra. Extraction of further information requires the inversion of a non-linear equation which describes the relationship between a Doppler spectrum and the ocean wave spectrum :

$$\sigma(\eta) = \int K(\theta, \eta) S(k(\eta, \theta), \theta) S(k'(\eta, \theta), \theta'(\eta, \theta)) d\theta \qquad (5.9)$$

where K is a kernel containing electromagnetic and hydrodynamic coupling coefficients, σ is a Doppler spectrum, η is the normalised Doppler frequency and S is the ocean wave spectrum (here as a function of wavenumber and direction). K, k, k' and θ' are known functions which depend on the direction and frequency of the radar signal.

Equation 5.9 is known as Barrick's equation.

5.5.2 Analysis Overview and the Inversion Procedure

Figure 5.15 summarises the analysis procedure for obtaining ocean wave measurements from the Doppler spectra produced by an HF radar (spectra from two radars are required in order to resolve a directional ambiguity) as used for the NURWEC2 experiment. Wyatt (1990b) has developed an iterative procedure for the inversion of Barrick's equation (5.9) to obtain an estimate of the ocean wave spectrum. This involves using a modified form of Barrick's equation (5.9) :

$$\sigma_j(\eta) = \int K_j(\theta, \eta) S(k_j(\eta, \theta), \theta) S'(k'_j(\eta, \theta), \theta'_j(\eta, \theta)) d\theta, j = 1 \ldots 4 \qquad (5.10)$$

Here S' refers to the local wind-driven part of the ocean wave spectrum which is estimated by the Pierson-Moskovitz wind-wave model spectrum (see section 5.4.5), adjusted to include a directional term. The subscript j refers to the four versions we have of equation 5.10 — one for each Doppler spectrum side-lobe (the two side-lobes from each side of the main first order Bragg lines are used from each radar). It is worth noting that these modified formulae

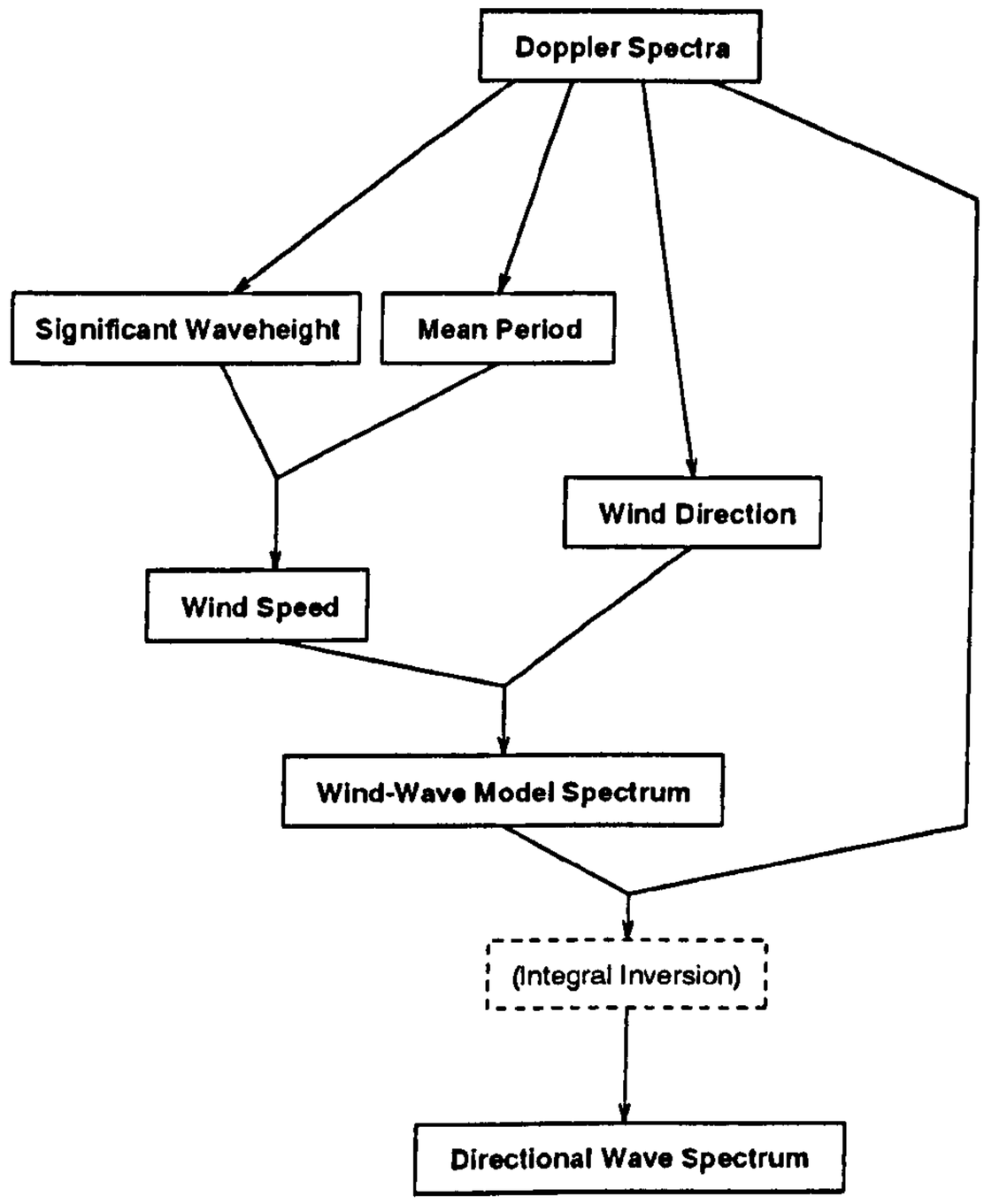

Figure 5.15: Overview of the analysis procedure for obtaining ocean wave measurements using HF radar — the arrows show which parameter estimates are required to produce other parameter estimates (*e.g.* estimates of both significant waveheight and mean period are used in the estimation of wind speed).

are only valid over the limited range of η-values which involve interactions between short waves (described by S') and long waves (described by S). This limitation defines the upper wave frequency bound for the inversion (typically about $200mHz$), the lower wave frequency bound being defined by the points of separation of the first and second order parts of the Doppler spectra.

The iterative inversion procedure derived by Wyatt (1990b) is as follows ($\hat{S}_{j,l}$ refers to the *l-th* estimate of S associated with side-lobe j) :

1. Set initial guess for S :

$$\text{let} \quad \hat{S}_{j,0}(k,\theta) = S_{PM}(k)\frac{1}{v}\cos^4\left(\frac{\theta - \hat{\theta}_W}{2}\right)$$

   where $\hat{\theta}_W$ is the estimated wind direction, and $v = \int_{-\pi}^{\pi}\cos^4\left(\frac{\theta}{2}\right)d\theta$ is a normalising constant. This initial guess is the same as S'.

2. Set iteration counter : $l = 0$

3. Integrate :

$$\hat{\sigma}_{j,l}(\eta) = \int K_j(\theta,\eta)\hat{S}_{j,l}(k_j(\eta,\theta),\theta)S'(k'_j(\eta,\theta),\theta'_j(\eta,\theta))d\theta, j = 1\ldots4$$

   Note that the K_j contain singularities, so the usual Simpson's rule or trapezium rule integration methods need to be modified to be able to cope with this.

4. Estimate the "relative errors" in $\hat{\sigma}_{j,l}$

$$\text{let} \quad \hat{r}_{j,l}(\eta) = \frac{\hat{\sigma}_j(\eta) - \hat{\sigma}_{j,l}(\eta)}{\hat{\sigma}_{j,l}(\eta)}, j = 1\ldots4$$

5. Increment l and start to calculate next iteration :

$$\hat{S}_{j,l}(k(\eta,\theta),\theta) = \hat{S}_{j,l-1}(k(\eta,\theta),\theta)\prod_{m=1}^{4}\left(1 + \frac{K_m(\eta,\theta)}{\max_\theta(K_m(\eta,\theta))}\hat{r}_{m,l-1}(\eta)\right),$$
$$j = 1\ldots4$$

   Note that the values of η for which we have an $\hat{r}$ will not necessarily be the same for each j, and in such cases the nearest point (in $\eta - space$) to the desired value of η is taken and a weighting applied.

6. "Within-spectrum" smoothing :
   A "nearest point weighted average" is performed on $\hat{S}_{j,l}(k,\theta), j = 1\ldots4$

7. "Between-spectrum" smoothing :
   Smoothing is performed on $\hat{S}_{j,l}(k,\theta), j = 1 \ldots 4$ with $\hat{S}_{m,l}(k,\theta), m \neq j$ at the closest points in (k,θ)-space.

8. Repeat from step 3 until convergence.

This inversion procedure produces an estimate of the ocean wave directional spectrum on a grid which is non-uniform in both wavenumber space and directional frequency space. It is transformed onto a uniform directional frequency grid by taking the mean estimated power of those points closest to a particular set of frequencies and directions (typically $0.005Hz$ and 15° apart). The precise frequency limits of this transformed grid depend on the radar configuration (*i.e.* beam direction and frequency), but are typically approximately $30mHz$ and $200mHz$, and close to the upper limit the distribution of points on the original grid is relatively sparse.

5.5.3 Estimating the Statistical Properties of the Parameters Derived from the Inversion

Because of the nature and structure of equations 5.10, it is unlikely that an analytic solution for the variance of $\hat{S}$ exists. It was therefore decided to use Monte-Carlo methods to simulate observed ocean wave spectra and then to examine the resulting simulations in an attempt to quantify the behaviour of various estimated parameters. The following parameters were chosen for examination :

- (non-directional) ocean wave power spectrum
- mean direction spectrum
- directional spread spectrum

These spectra are functions of the directional ocean wave spectrum and are defined in sections 4.2 and 4.3.2. There are two main reasons behind the choice of these parameters — firstly they tend to summarise the directional spectrum reasonably well, and secondly they are measured by directional wave buoys without the need to make any assumptions about the shape of the underlying directional ocean wave spectrum. The simulation procedure used was as follows :

1. Generate an underlying directional ocean wave spectrum.

2. Choose radar frequencies and beam directions.

3. Calculate the underlying Doppler spectra.

4. Use the underlying Doppler spectra to generate a simulated radar signal in the frequency domain (by convolving the square root of the underlying Doppler spectra with Normally distributed white noise), and mimic the effect in the frequency domain of applying a taper to sequential time series with 75% time overlap. This step introduces the appropriate *sampling variability* into the simulated Doppler spectra — no attempt has been made to simulate the effects of background radio noise.

5. Estimate the directional ocean wave spectrum by inverting the integral equations 5.10 as described in section 5.5.2.

6. Repeat from step 4 until there is a set of 5000 simulations from a particular underlying directional ocean wave spectrum and radar configuration. Having 5000 simulations in each set allows a reasonably accurate estimation of the second order moments (*i.e.* the variances) of the parameters in the sets. Ideally a larger number (such as 20000) would have been produced, but this was prevented by time constraints (each set of 5000 simulations typically took in the order of 10 days to complete on the available equipment).

7. Calculate and store the wave parameters to be examined.

8. Repeat from step 1 using different sea conditions.

In all, 28 sets of 5000 simulations were produced. The radar configurations were chosen to reflect those used in the NURWEC2 trial when the radar footprints included the wave buoy site. The radar frequencies chosen were :

- $9.25MHz$, $9.39MHz$
- $6.815MHz$, $9.39MHz$
- $12.058MHz$, $9.39MHz$
- $16.425MHz$, $6.908MHz$

where the first frequency refers to the south Dyfed site (245.5° beam bearing) and the second refers to the north Devon site (315.0° beam bearing). These frequency configurations are close to those used throughout virtually the entire 5-day period of the NURWEC2 storm. Most of the underlying ocean wave spectra were created using a piece of software developed at the University of Sheffield by Holden and Atanga (1994). This program models wave components generated by the local wind and allows the option of including swell components (other features of the program are described by Holden and Atanga (1994)). Most of the spectra used in this study are described in the following table, which includes all the parameters required by the program (where "amplitude" refers to the relative amplitude of the swell mode, when present, to the wind mode, whose peak frequency and amplitude are derived from the wind speed) :

Spectrum	Modes	Wind	Frequency	Amplitude	Direction	Spread
A	1	$15m/s$			90°	48°
B	1	$6m/s$			90°	48°
C	1	$10m/s$			90°	48°
D	2	$12m/s$	$80mHz$	0.7	30° 350°	48° 27°
F	2	$10m/s$	$90mHz$	1.3	220° 350°	45° 30°
G	2	$10m/s$	$80mHz$	1.3	30° 350°	48° 27°
H	2	$10m/s$	$80mHz$	0.5	30° 350°	48° 27°
I	2	$8m/s$	$80mHz$	1.0	30° 350°	48° 27°

Additionally, four spectra were created with a previous version of the same software which used slightly different parameters. These are tabulated below (here, "amplitude" refers to the absolute peak amplitude of the appropriate mode) :

Spectrum	Modes	Frequency	Direction	Amplitude	Spread
E	3	$140mHz$	80°	$5m^2/Hz$	48°
		$95mHz$	50°	$3m^2/Hz$	27°
		$105mHz$	62°	$4m^2/Hz$	24°
J	2	$140mHz$	150°	$5m^2/Hz$	48°
		$80mHz$	340°	$5m^2/Hz$	27°
K	2	$150mHz$	90°	$5m^2/Hz$	45°
		$70mHz$	180°	$6m^2/Hz$	30°
L	3	$140mHz$	230°	$4m^2/Hz$	48°
		$90mHz$	70°	$5m^2/Hz$	27°
		$60mHz$	20°	$3m^2/Hz$	18°

Figure 5.16 includes a polar contour plot of the underlying ocean spectrum F. The two modes (wind and swell) are clearly distinguished, with the wind mode having a higher peak frequency (*i.e.* it is further away from the origin) and a larger directional spread. This figure also includes the underlying Doppler spectrum for the Dyfed radar operating at $9.25MHz$. Figure 5.17 shows a sampled Doppler spectrum for this radar configuration corresponding to ocean spectrum F. The shape is similar to that of the underlying Doppler spectrum, but the deviation is most obvious where the underlying Doppler spectrum is relatively flat.

As mentioned in step 6, time constraints limited the size of each simulated data set. For the same reason, the *number* of data sets (and hence of underlying ocean spectra) was also constrained. This limited number of spectra does not represent a comprehensive set of underlying ocean conditions, and a study involving a larger such set might yield further relationships than have been uncovered here (see section 5.5.4).

5.5.4 Results from the Simulation Study

The intention behind the simulations described in section 5.5.3 was to examine the behaviour of the variances of the estimated spectral wave parameters and hopefully to identify some pattern which could be used to estimate these variances directly from the observations. The simulated observations were examined using the graphical and statistical capabilities of the Minitab-9 software package. The basic procedure involved first graphically comparing the variances (or functions thereof) with the available parameters (see for ex-

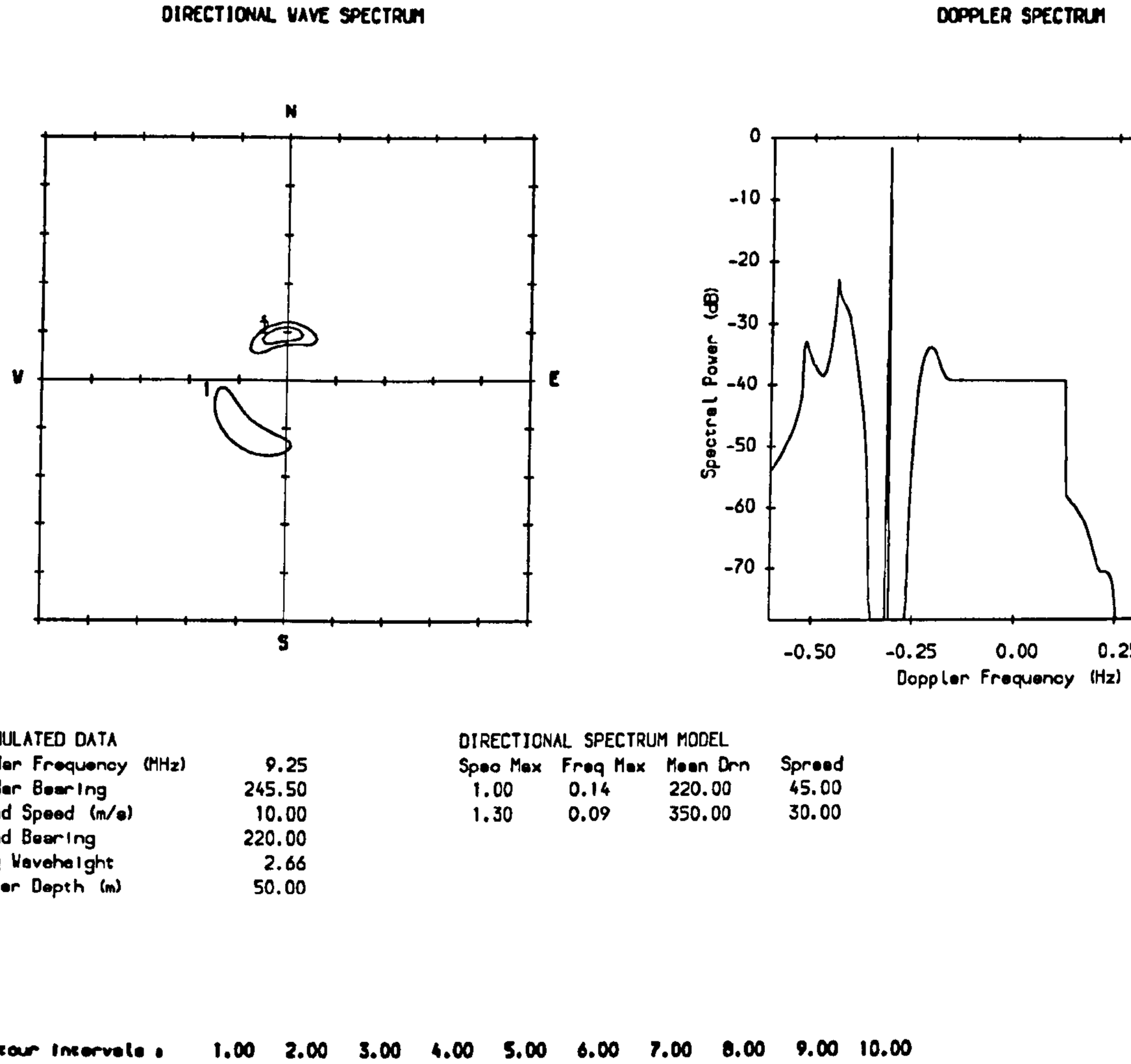

Figure 5.16: A plot created by the ocean spectrum generation program. The graph on the left is a polar contour plot of spectrum F, with wave frequency being proportional to distance from the origin and direction indicating the direction towards which the waves are propagating (the contour units are $m^2/Hz/radian$). The bimodality of this spectrum is clearly illustrated. The graph on the right is the associated mean Doppler spectrum corresponding to the Dyfed radar site transmitting at $9.25MHz$.

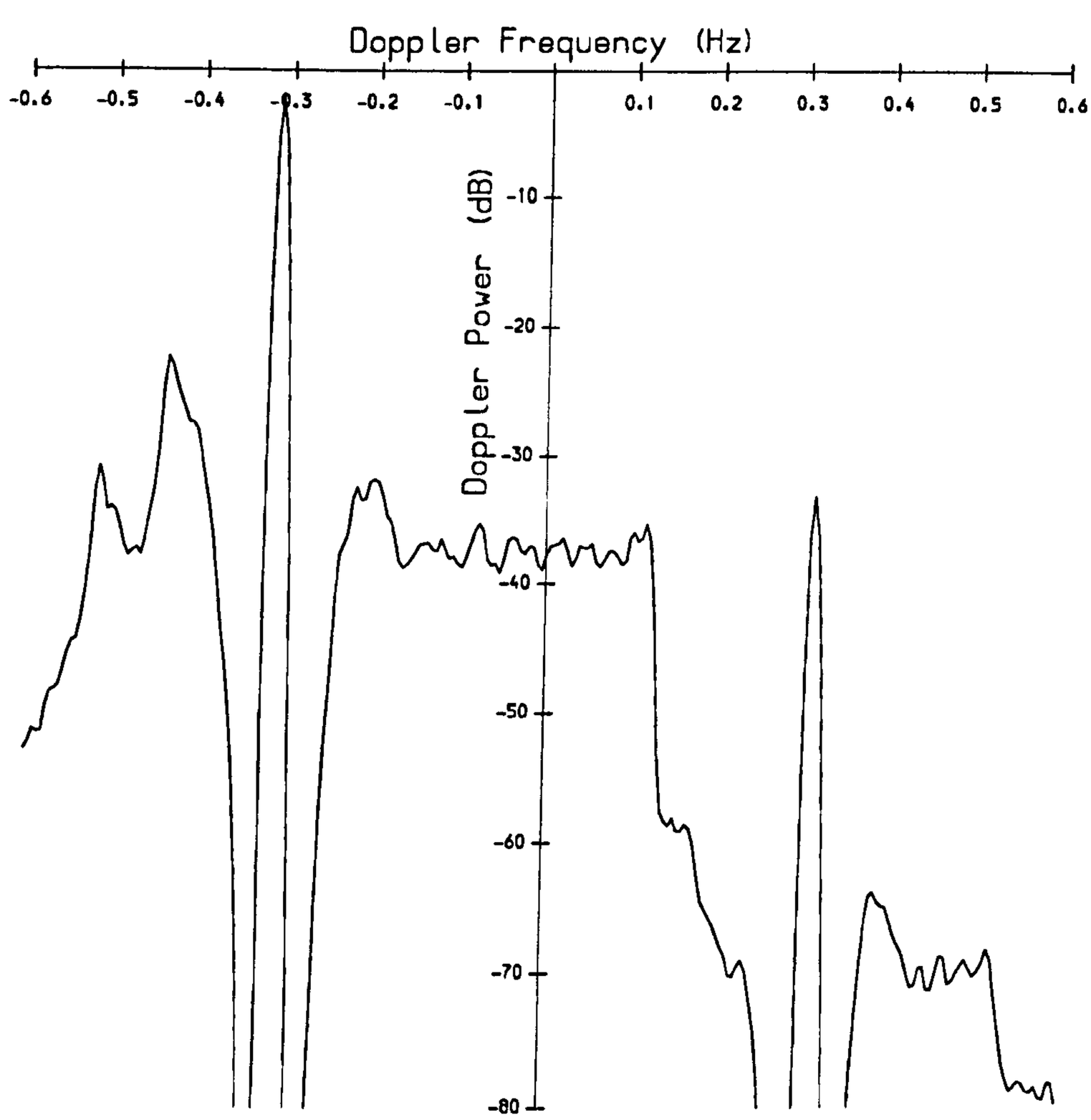

Figure 5.17: A sampled Doppler spectrum corresponding to the Dyfed radar site transmitting at $9.25MHz$ under the ocean wave conditions described by spectrum F.

ample figure 5.18, which suggests a linear relationship at $105mHz$ between directional spread and the variance of mean direction), and then attempting to fit a numerical model to any patterns thus uncovered. The available spectral parameters were :

- power
- mean direction (see section 4.3.2)
- directional spread (see section 4.3.2)
- directional skewness (see Kuik and van Vledder (1984))
- directional kurtosis (see Kuik and van Vledder (1984))

The following relationships became apparent :

- The variances of the parameters are functions of spectral frequency.
- The variances of the parameters vary with radar frequency configuration.
- The variance of spectral power depends on spectral power (allowing us to think in terms of degrees of freedom, for example see figure 5.19).
- The variances of spectral mean direction and of spectral directional spread *both* depend on spectral directional spread, (for example see figure 5.18).

Model fitting techniques were chosen appropriate for the above relationships. These were one-way analysis of variance (see Pearce (1982b)) in the case of spectral power, and analysis of covariance (see Pearce (1982a)) in the case of mean direction and directional spread. The results are given in the tables in figures 5.20 to 5.22. However, even taking all of the above into account, there is still some variation in the behaviour of the second moments (*i.e.* the variances) of the simulated observed parameters for which it has not been possible to account (no relationships involving further parameters were found), suggesting that there are further factors involved in the above relationships (which may be identifiable in a larger study). Nevertheless, we are now in a position where we can estimate these variances at least approximately.

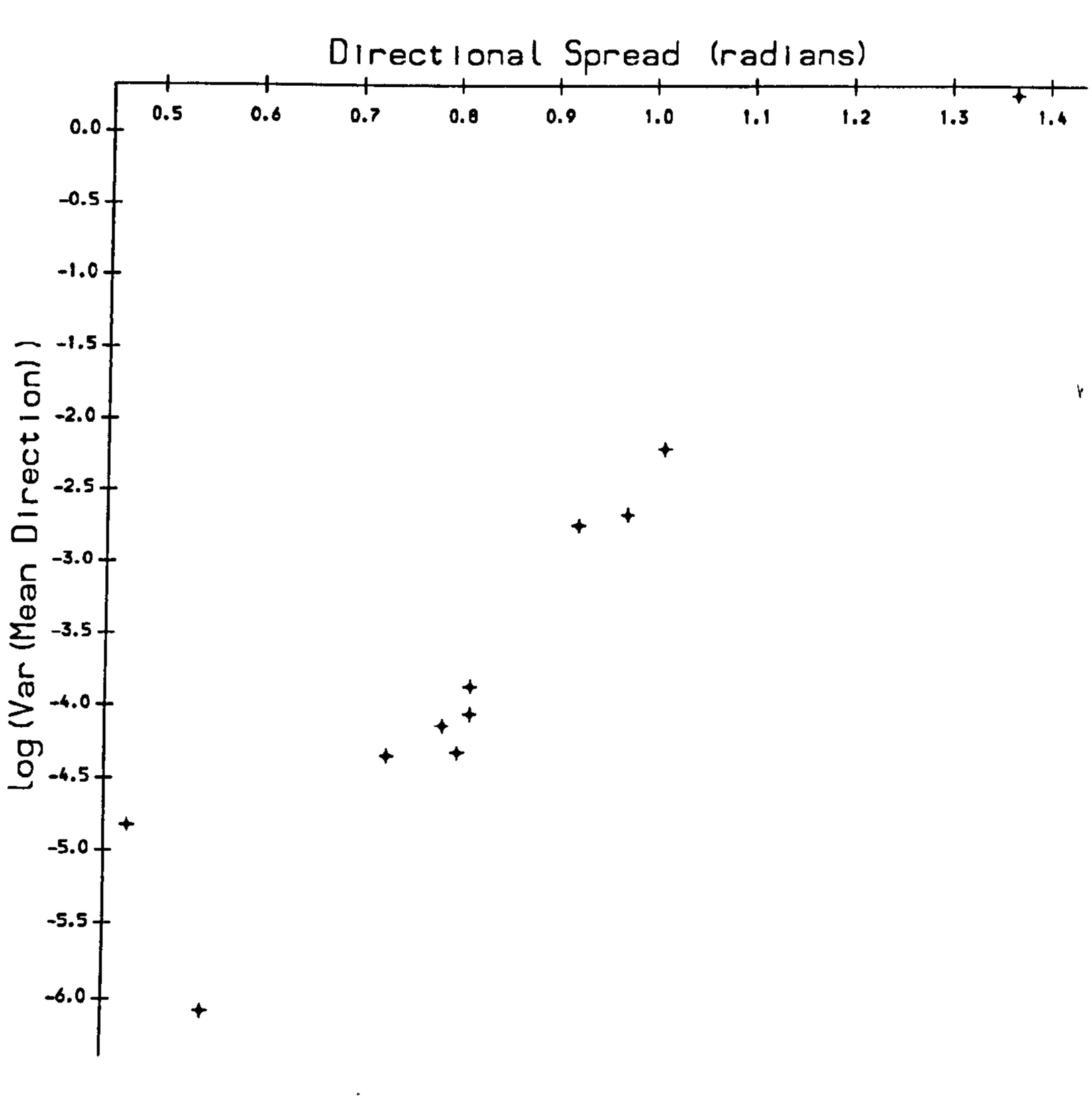

Figure 5.18: A plot of the logarithm of the variance of mean wave direction against directional spread at $105mHz$. The pattern is typical of that observed at other frequencies.

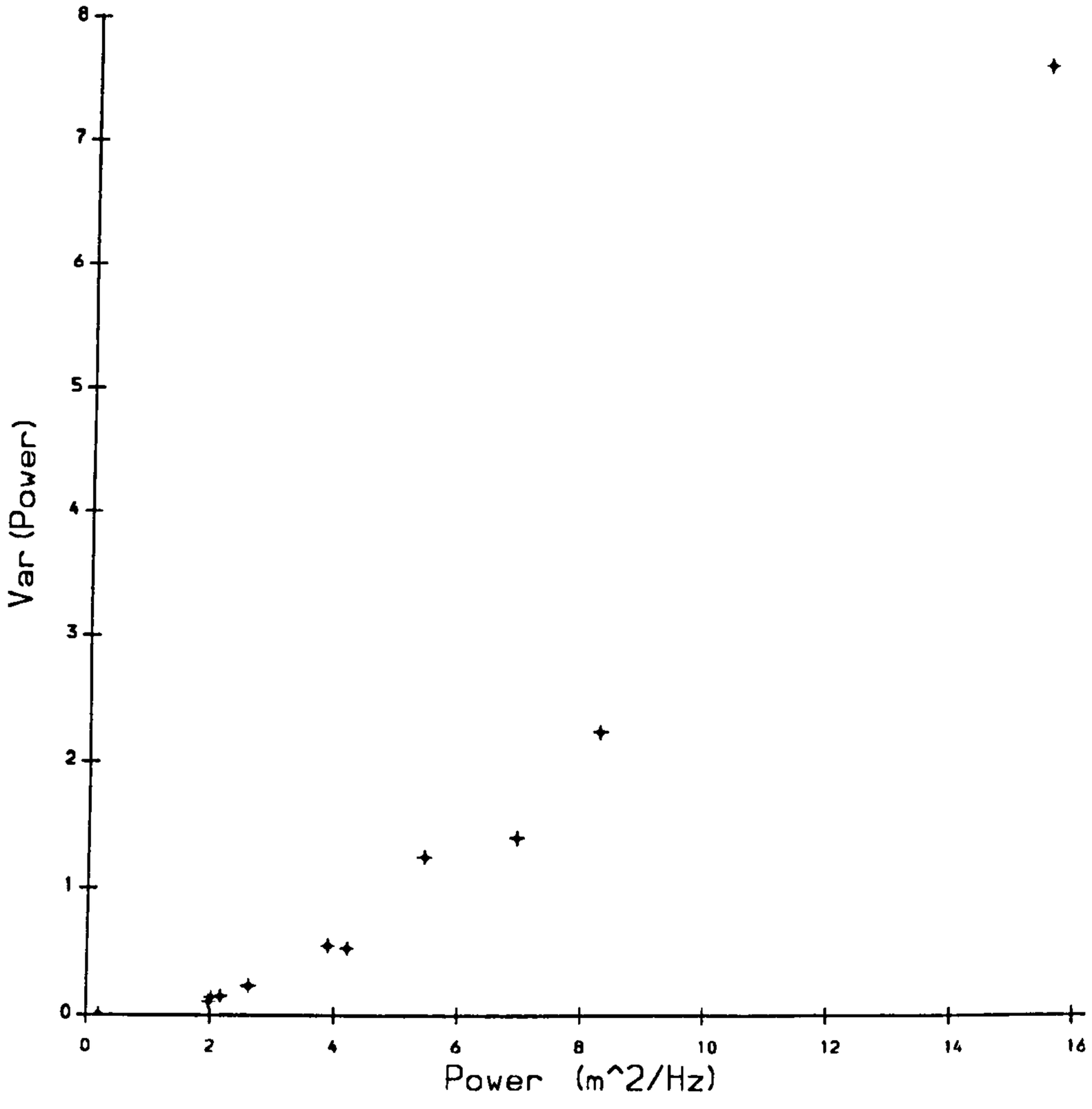

Figure 5.19: A plot of spectral power variance against spectral power at $115mHz$. The pattern is typical of that observed at other frequencies.

The mean numbers of degrees of freedom (defined as twice the variance divided by the square of the expectation) of the simulated spectral power observations are given in the table in figure 5.20 as a function of wave frequency and radar frequency configuration. The missing values refer to where there is not enough information to reliably estimate the properties of the parameter. This is because these wave frequencies are at the extreme ranges of what the inversion process can handle at the given radar frequency configurations.

The mean logarithms of the variances of the simulated spectral mean direction observations are given as a function of wave frequency and radar frequency configuration in the table in figure 5.21, which includes a factor which should be used as shown in equation 5.11.

$$\log(\mathrm{Var}(\textit{mean direction})) = \textit{factor} \times \textit{directional spread} + \textit{table entry} \quad (5.11)$$

i.e. we have a straight line relationship in which the factor acts as the slope and the frequency table entry as intercept.

The mean logarithms of the variances of the simulated spectral directional spread observations are given as a function of wave frequency and radar frequency configuration in the table in figure 5.22, which includes a factor which should be used as shown in equation 5.12.

$$\log(\mathrm{Var}(\textit{directional spread})) = \textit{factor} \times \textit{directional spread} + \textit{table entry} \quad (5.12)$$

We note that for each radar frequency, the measurements with most variability tend to correspond to those frequency bins whose measurements have been calculated by averaging a smaller number of points from the original inversion (see section 5.5.2). Typical numbers of such points are given in the table in figure 5.23.

It is thus now possible to estimate the variances of spectral power, mean wave direction and directional spread as measured by HF radar pairs with configurations as examined above. In chapter 7 we will use this information to compare radar and wave buoy performances using NURWEC2 data.

Wave Frequency (mHz)	Radar Frequencies (MHz)			
	9.25,9.39	6.815,9.39	12.058,9.39	16.425,6.908
40	23.2	—	—	—
45	21.6	16.3	—	—
50	24.3	16.5	—	—
55	34.1	26.9	—	—
60	41.8	41.4	—	—
65	50.3	52.6	—	—
70	48.3	44.7	37.6	43.6
75	48.4	47.1	40.7	45.4
80	47.9	48.5	44.7	48.4
85	49.4	52.0	50.6	51.6
90	50.1	55.1	55.0	55.6
95	52.1	57.0	59.9	60.1
100	53.9	59.3	64.5	64.0
105	55.1	62.0	65.0	65.6
110	56.0	62.3	67.8	67.5
115	59.1	63.9	70.1	68.1
120	53.5	89.7	53.9	73.2
125	55.8	91.0	57.5	74.6
130	57.8	92.5	56.0	72.1
135	59.3	98.6	60.0	73.9
140	62.7	96.8	67.0	57.1
145	61.5	96.8	69.2	50.9
150	63.8	91.9	65.2	51.9
160	70.8	86.8	62.6	55.8
170	43.4	61.2	52.1	33.2
180	37.8	48.6	59.4	38.7
190	43.2	—	53.9	—
200	42.1	—	57.2	—
210	35.8	—	42.4	—

Figure 5.20: A table showing the mean numbers of degrees of freedom of the simulated spectral power observations as a function of wave frequency and radar frequency configuration. The missing values refer to where there is not enough information to reliably estimate the properties of the parameter.

Wave Frequency (mHz)	Radar Frequencies (MHz)			
	9.25,9.39	6.815,9.39	12.058,9.39	16.425,6.908
40	-0.38	—	—	—
45	0.18	-0.64	—	—
50	-0.24	-0.91	—	—
55	-1.11	-1.11	—	—
60	-2.16	-2.19	—	—
65	-2.87	-3.15	—	—
70	-2.97	-2.64	-1.92	-1.89
75	-3.08	-2.69	-1.89	-2.03
80	-3.06	-2.85	-2.08	-2.08
85	-3.14	-3.19	-2.61	-2.55
90	-3.31	-3.58	-3.06	-3.10
95	-3.75	-3.76	-3.49	-3.59
100	-4.14	-4.02	-3.92	-3.97
105	-4.47	-4.13	-4.14	-4.15
110	-4.71	-4.34	-4.37	-4.36
115	-4.73	-4.43	-4.46	-4.43
120	-4.71	-4.26	-3.98	-4.67
125	-4.80	-4.36	-4.23	-4.54
130	-4.82	-4.39	-4.35	-4.75
135	-4.79	-4.30	-4.27	-4.65
140	-4.87	-4.32	-4.57	-5.07
145	-4.85	-4.27	-4.68	-4.88
150	-4.95	-4.03	-4.77	-4.99
160	-4.98	-4.15	-4.95	-5.12
170	-4.80	-3.78	-5.24	-5.37
180	-4.62	-2.95	-5.29	-5.46
190	-3.87	—	-5.12	—
200	-3.22	—	-4.18	—
210	-4.21	—	-2.61	—
factor	7.03	3.03	6.60	7.68

Figure 5.21: A table showing the mean logarithms of the variances of the simulated spectral mean direction observations as a function of wave frequency and radar frequency configuration. The missing values refer to where there is not enough information to reliably estimate the properties of the parameter.

Wave Frequency (mHz)	Radar Frequencies (MHz)			
	9.25,9.39	6.815,9.39	12.058,9.39	16.425,6.908
40	-3.70	—	—	—
45	-3.85	-4.03	—	—
50	-3.86	-4.10	—	—
55	-3.94	-4.33	—	—
60	-4.13	-4.57	—	—
65	-4.40	-4.90	—	—
70	-4.57	-4.82	-4.19	-4.23
75	-4.78	-5.10	-4.44	-4.52
80	-4.96	-5.83	-4.76	-4.92
85	-4.97	-5.55	-4.98	-5.02
90	-5.01	-5.65	-5.17	-4.97
95	-5.13	-5.75	-5.25	-4.94
100	-5.24	-5.84	-5.37	-4.98
105	-5.47	-5.94	-5.46	-5.06
110	-5.56	-5.98	-5.62	-5.12
115	-5.72	-6.09	-5.66	-5.23
120	-5.53	-6.18	-5.07	-5.31
125	-5.73	-6.18	-5.39	-5.50
130	-5.79	-6.33	-5.20	-5.45
135	-5.90	-6.44	-5.51	-5.49
140	-5.97	-6.38	-5.43	-6.47
145	-5.91	-6.52	-5.48	-6.96
150	-6.05	-6.05	-5.74	-7.07
160	-6.12	-6.19	-5.75	-7.16
170	-6.60	-5.18	-6.20	-7.16
180	-6.26	-5.06	-6.70	-6.55
190	-5.95	—	-6.92	—
200	-5.77	—	-6.53	—
210	-6.13	—	-6.12	—
factor	0.63	-1.18	0.59	1.26

Figure 5.22: A table showing the mean logarithms of the variances of the simulated spectral directional spread observations as a function of wave frequency and radar frequency configuration. The missing values refer to where there is not enough information to reliably estimate the properties of the parameter.

Wave Frequency (mHz)	Radar Frequencies (MHz)			
	9.25,9.39	6.815,9.39	12.058,9.39	16.425,6.908
40	104	—	—	—
45	101	96	—	—
50	102	105	—	—
55	97	100	—	—
60	101	108	—	—
65	103	103	—	—
70	104	94	103	104
75	111	109	111	104
80	94	103	104	106
85	105	100	100	101
90	100	100	97	105
95	104	98	100	93
100	98	100	104	102
105	104	103	102	101
110	97	98	96	102
115	99	100	104	99
120	94	102	95	105
125	108	104	103	97
130	105	96	101	103
135	93	72	93	84
140	112	81	113	58
145	98	54	98	62
150	92	48	109	58
160	108	70	167	91
170	66	48	116	82
180	49	41	89	71
190	37	—	54	—
200	27	—	44	—
210	22	—	27	—

Figure 5.23: A table showing typical quantities of inverted points as a function of wave frequency and radar frequency configuration.

Chapter 6

System Intercomparisons

6.1 Introduction

The use of HF radar to measure ocean wave parameters is a relatively recent development (see Wyatt (1990a) for further details). It would therefore be useful to have information on the performance of this system. Sections 5.4 and 5.5.4 describe how we may produce approximate confidence intervals for the means of various parameters, but it would also be desirable to evaluate the relationship between these means and the corresponding underlying values for the true ocean spectrum ("sea truth"). Unfortunately, there is currently no wave measurement system which is known to give unbiased estimates of sea truth parameters, however, wave buoys are often used as yardsticks. One example of such use was NORCSEX '88 (*Nor*wegian *C*ontinental *S*helf *Ex*periment) in which measurements from wave buoys were compared with those from an airborne SAR (*S*ynthetic *A*perture *R*adar) and from the GEOSAT radar altimeter (see Olsen and Barstow (1988)). Also noteworthy is the WADIC project (see section 6.3). This chapter presents a maximum likelihood approach for deriving the relationship between the mean ocean wave parameters as measured by HF radar and by directional wave buoys.

6.2 Required Assumptions

For a meaningful system intercomparison, the following assumptions are required :

1. that there is temporal stationarity over the period of measurement,
2. that there is spatial stationarity over the area of measurement,
3. that the different systems measure independently.

If the systems are not operating simultaneously, then assumption 1 must hold over the *combined* measurement period. Likewise, assumption 2 must also hold over the area *between* measurement sites. If either of these is broken then the intercomparison is invalid as like is not being compared with like. Šova and Wyatt (1994) have used data from the WADIC experiment (see section 6.3) to examine such scales of stationarity in the ocean wave field. Their temporal examination suggests that the breaking of stationarity is wind-related. At "high" wind speeds (greater then $8.1m/s$) this seems to take between 40 and 60 minutes with a fluctuating wind, and between 60 and 120 minutes with a stable wind. At lower wind speeds, stationarity assumptions are broken within 180 minutes. Due to data problems, their spatial examination has not produced any strong conclusions. The intercomparisons presented in chapter 7 are based on near-simultaneous measurements over periods lasting approximately 30 minutes. It is therefore unlikely that the assumption of (approximate) temporal stationarity does not hold. However, the NURWEC2 radars each measure over a $7.5-15km$ long ring segment with a width of 12°, and these segments do not perfectly overlap. It has thus been necessary to assume spatial stationarity without there being strong evidence to justify this.

6.3 Existing Approaches to System Intercomparison

The most comprehensive field intercomparison of commercially available ocean wave measurement systems was probably the WADIC (*Wa*ve *Di*rection

Calibration) project (see Allender *et al.* (1989)). The devices examined included 7 models of wave buoy, as well as other types of system. For a particular parameter (such as mean period) least squares and principal axis (see Krogstad *et al.* (1988)) regressions (between pairs of instruments) were performed both on the entire data set and on various subsets (defined according to ranges of significant waveheight), the standard deviations of the measurements being approximated using a (not necessarily linear) function of the measurements themselves. For spectral power, relative bias was estimated taking ratios of measurements from a pair of systems (at each frequency) and deriving confidence intervals from the resulting (F-) distribution.

The relative bias of spectral power between the Wavec buoy and HF radars of the NURWEC2 field trial (see section 1.4) has been estimated by a symmetrical regression through the origin (separately for each frequency) and confidence intervals derived therefrom (see Wyatt (1991)). However, to date the bulk of intercomparisons using NURWEC2 data have been restricted to the graphical methods (*e.g.* scatterplots) and linear regression.

The approach adopted in this study makes use of the fact that we have estimates of the variances of each parameter which are not simple functions of that particular parameter (and hence relies on less approximation than the WADIC approach described above). Using this information we wish to model the relationship between the means of the parameter as measured by the radars and their Wavec equivalents. This is referred to as a *functional relationship* (see Kendall and Stuart (1973)). We now introduce the concept of maximum likelihood estimation.

6.4 The Basic Principles of Maximum Likelihood Estimation

Maximum likelihood estimation consists of assuming a statistical model for a given data set and then finding the values of the model parameters with the highest probability density of producing that data set. These values are known as the *maximum likelihood estimates* of the true parameters.

Consider a set of independent observations $x_j, j = 1 \ldots n$ from a distribution where the probability density of an x_j taking the value y is $f(y|\Theta)$ *i.e.* a function of y, given Θ, where Θ is a set of parameters which we wish to

estimate. The likelihood function is defined as the probability density of the observations :

$$\text{lik}(\Theta|\mathbf{x}) = \prod_{j=1}^{n} f(x_j|\Theta) \tag{6.1}$$

At its maximum (with respect to Θ), the likelihood function (if it is well-behaved, and provided that the maximum is not achieved on the boundary of the parameter space) has a derivative (with respect to Θ) of zero. Because equation 6.1 involves a product, it is usually more convenient to work with its natural logarithm (since the logarithm is a monotonic increasing function, the maximum will be at the same place in Θ-space). Thus :

$$\frac{\partial \text{loglik}(\Theta|\mathbf{x})}{\partial \theta_m} = \frac{\partial \sum_{j=1}^{n} \log(f(x_j|\Theta))}{\partial \theta_m}$$

where θ_m is the m-th element of Θ. The maximum likelihood estimate of θ_m ($\hat{\theta}_m$) then satisfies the equation :

$$\left. \frac{\partial \sum_{j=1}^{n} \log(f(x_j|\theta))}{\partial \theta_m} \right|_{\Theta=\hat{\Theta}} = 0$$

The variance-covariance matrix of the estimated parameters $\hat{\Theta}$ is (asymptotically) the inverse of the information matrix $\mathbf{I}_\Theta$, whose (l,m)-th element is defined as follows :

$$\mathbf{I}_\Theta(l,m) = -\left. \frac{\partial^2 \text{loglik}(\Theta|\mathbf{x})}{\partial \theta_l \partial \theta_m} \right|_{\Theta=\hat{\Theta}}$$

6.5 Application to Wave Measurement System Intercomparison

6.5.1 Linear Relationship Case

Consider a set of paired observations (x_j, y_j) of variables X_j and Y_j respectively ($j = 1 \ldots n$) where :

$$\begin{aligned} X_j &\sim \text{N}(\mu_j, \sigma^2_{x_j}) \\ Y_j &\sim \text{N}(a + b\mu_j, \sigma^2_{y_j}) \end{aligned}$$

where each σ^2 is known, each μ is unknown and all the Xs and Ys are mutually independent. The likelihood equation is :

$$\text{lik}(a, b, \mu | \mathbf{x}, \mathbf{y}, \sigma^2_{\mathbf{x}}, \sigma^2_{\mathbf{y}}) = \prod_{j=1}^{n} \frac{1}{2\pi\sqrt{\sigma^2_{x_j}\sigma^2_{y_j}}} e^{-\frac{1}{2}\frac{(x_j-\mu_j)^2}{\sigma^2_{x_j}} - \frac{1}{2}\frac{(y_j-b\mu_j-a)^2}{\sigma^2_{y_j}}}$$

Hence,

$$\begin{aligned}
&\text{loglik}(a, b, \mu | \mathbf{x}, \mathbf{y}, \sigma^2_{\mathbf{x}}, \sigma^2_{\mathbf{y}}) \\
&= \sum_{j=1}^{n} \left(-\log(2\pi) - \frac{1}{2}\log(\sigma^2_{x_j}\sigma^2_{y_j}) - \frac{1}{2}\frac{(x_j-\mu_j)^2}{\sigma^2_{x_j}} - \frac{1}{2}\frac{(y_j-b\mu_j-a)^2}{\sigma^2_{y_j}} \right)
\end{aligned}$$

Differentiating the log-likelihood with respect to the parameters we get :

$$\begin{aligned}
\frac{\partial \text{loglik}(a, b, \mu | \mathbf{x}, \mathbf{y}, \sigma^2_{\mathbf{x}}, \sigma^2_{\mathbf{y}})}{\partial a} &\propto b\sum_{j=1}^{n}\frac{\mu_j}{\sigma^2_{y_j}} + a\sum_{j=1}^{n}\frac{1}{\sigma^2_{y_j}} - \sum_{j=1}^{n}\frac{y_j}{\sigma^2_{y_j}} \\
\frac{\partial \text{loglik}(a, b, \mu | \mathbf{x}, \mathbf{y}, \sigma^2_{\mathbf{x}}, \sigma^2_{\mathbf{y}})}{\partial b} &\propto b\sum_{j=1}^{n}\frac{\mu_j^2}{\sigma^2_{y_j}} + a\sum_{j=1}^{n}\frac{\mu_j}{\sigma^2_{y_j}} - \sum_{j=1}^{n}\frac{\mu_j y_j}{\sigma^2_{y_j}} \\
\frac{\partial \text{loglik}(a, b, \mu | \mathbf{x}, \mathbf{y}, \sigma^2_{\mathbf{x}}, \sigma^2_{\mathbf{y}})}{\partial \mu_j} &\propto \left(\frac{1}{\sigma^2_{x_j}} + \frac{b^2}{\sigma^2_{y_j}}\right)\mu_j + \frac{b(a-y_j)}{\sigma^2_{y_j}} - \frac{x_j}{\sigma^2_{x_j}}
\end{aligned}$$

and hence the maximum likelihood estimates of the parameters satisfy the following equations :

$$\begin{aligned}
\hat{a} &= \frac{\sum_{j=1}^{n}\frac{y_j-\hat{b}\hat{\mu}_j}{\sigma^2_{y_j}}}{\sum_{j=1}^{n}\frac{1}{\sigma^2_{y_j}}} \\
\hat{b} &= \frac{\sum_{j=1}^{n}\frac{\hat{\mu}_j(y_j-\hat{a})}{\sigma^2_{y_j}}}{\sum_{j=1}^{n}\frac{\hat{\mu}_j^2}{\sigma^2_{y_j}}} \\
\hat{\mu}_j &= \frac{\frac{x_j}{\sigma^2_{x_j}} - \frac{\hat{b}(\hat{a}-y_j)}{\sigma^2_{y_j}}}{\frac{1}{\sigma^2_{x_j}} + \frac{\hat{b}^2}{\sigma^2_{y_j}}}
\end{aligned} \tag{6.2}$$

Equations 6.2 may be solved iteratively given some suitable "initial guesses" of $\hat{a}$ and $\hat{b}$.

If we now suppose that the Xs refer to a particular parameter as measured by one system and that the Ys refer to the same parameter as measured by another *and* that the relationship between the expectations of the Xs and the Ys is linear, we may then use equations 6.2 to produce the maximum likelihood estimates of the slope and intercept of this relationship. (We

note that since both the Xs and the Ys are estimates of the same ocean wave parameter, unity and zero would be logical initial guesses of $\hat{b}$ and $\hat{a}$ respectively). As an example, figure 6.1 shows a scatter plot of mean wave period measurements taken during WADIC as measured (simultaneously) by two different wave buoys (a Wavec and a Waverider), with the maximum likelihood linear relationship superimposed. The equation of the line is :

$$T_m{}_{Waverider} = 0.928 \times T_m{}_{Wavec} + 0.505 secs$$

This line appears to fit the data quite well, and hence a linear relationship seems appropriate in this case. Unfortunately, each iteration produces only a fairly small change in $\hat{a}$ and $\hat{b}$. Therefore, the convergence criteria need to be quite strict (*e.g.* stopping the iteration when both $\hat{a}$ and $\hat{b}$ change by no more than 0.0001% gives an accuracy of about 3 decimal places). It should be noted that interchanging X and Y produces a line giving the same relationship (*i.e.* reflected about $y = x$). In this example, the convergence criteria were satisfied after 592 iterations (or after 816 iterations with the axes reversed).

As a comparison, the linear relationship estimated using standard regression techniques (see Krogstad *et al.* (1988)) is:

$$T_m{}_{Waverider} = 0.947 \times T_m{}_{Wavec} + 0.439 secs$$

This is clearly similar to what we have derived above.

Figure 6.2 shows the estimated relative mean bias of the Wavec mean period with respect to the Waverider mean period with its 95% (pointwise) confidence interval (as calculated from the inverse of the information matrix). The choice of 95% is because of the duality of confidence intervals and hypothesis tests. For instance, suppose we wish to test for zero Wavec bias for some value of the Waverider mean — *if* zero bias lies outside the 95% confidence interval at that value of the Waverider mean, *then* the data show some evidence to suggest *non-zero* bias at that point. However, in fitting a linear relationship we are implying that zero bias can only occur at a single point. Of more use would be an estimate of some set of parameter values over which the relative bias is within certain limits ($\pm\alpha$% for example). This may be achieved by asking the question :
"For what values is there no evidence to suggest a relative Wavec bias greater than α% in magnitude?"

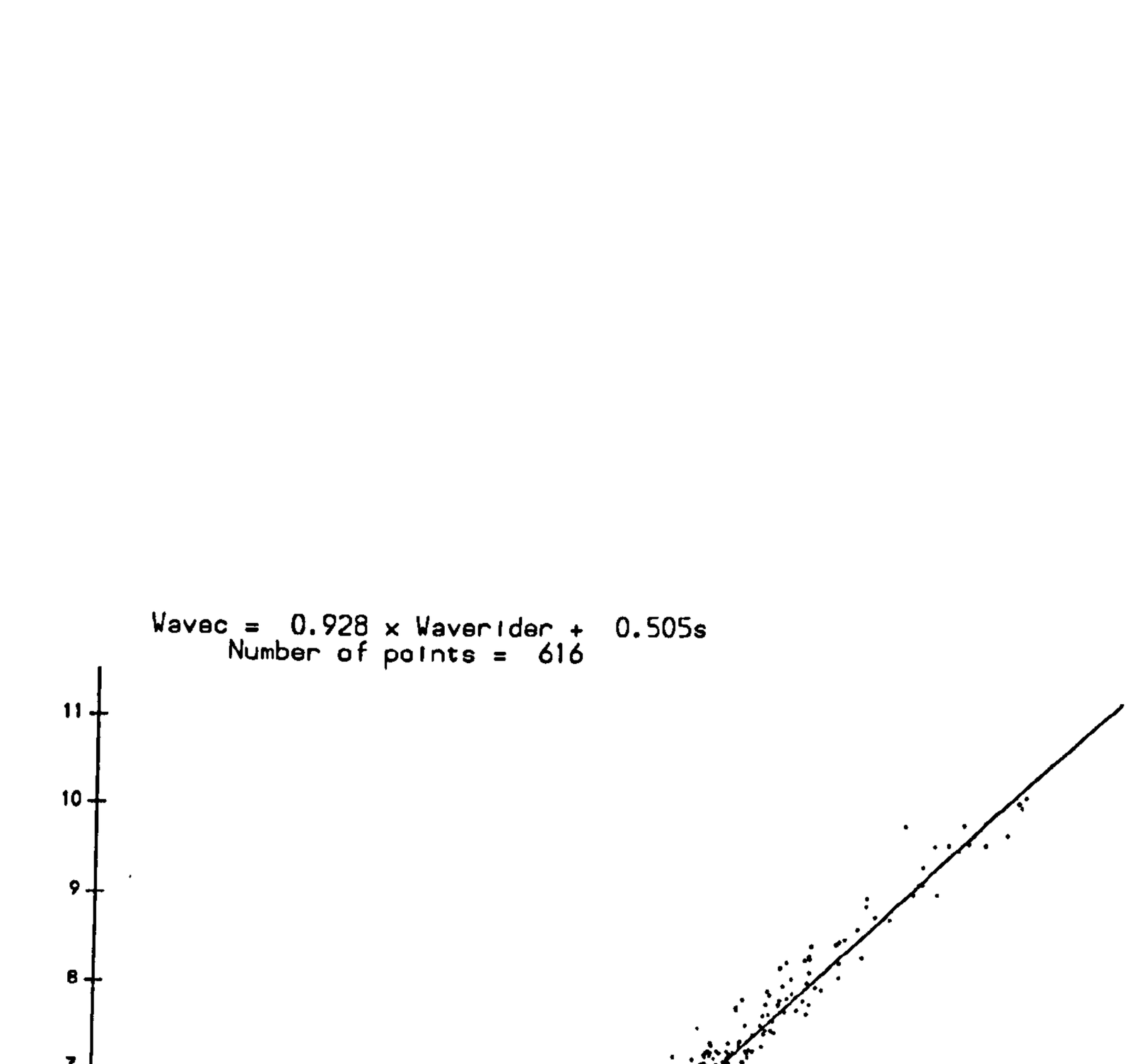

Figure 6.1: A scatter plot of Wavec mean period against Waverider mean period during WADIC with the maximum likelihood linear relationship superimposed.

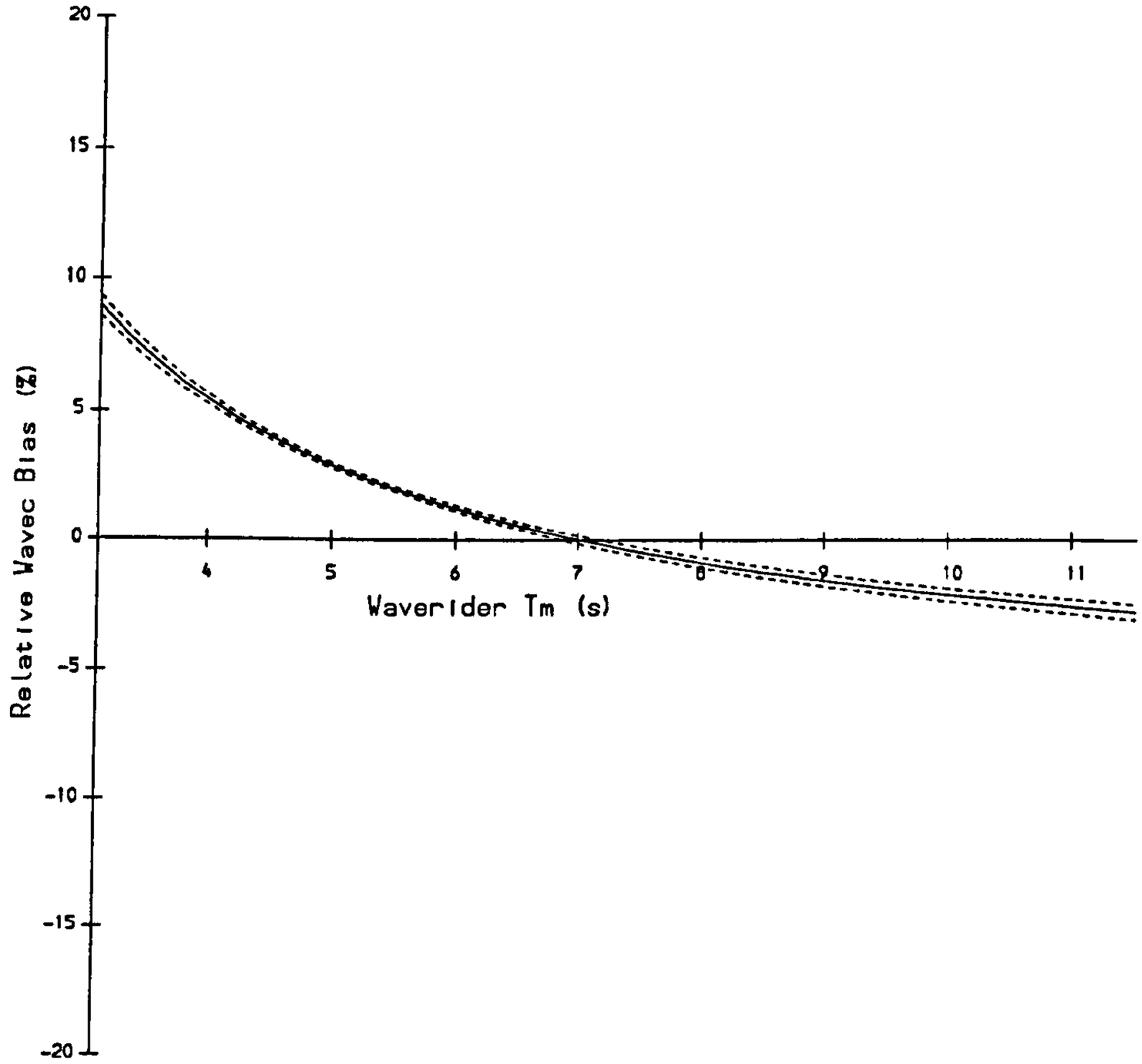

Figure 6.2: A plot of estimated Wavec mean period relative mean bias against Waverider mean period with its 95% confidence interval.

The answer is those values for which the 95% confidence interval does not exclude all relative biases within $\pm\alpha\%$.

From figure 6.2, the data show no evidence to suggest a Wavec bias outside $\pm 2\%$ for mean Waverider mean periods within $(5.5s, 10.3s)$, and no evidence to suggest a Wavec bias outside $\pm 5\%$ for mean Waverider mean periods greater than $4.1s$ (over the range of the data). Below $4.1s$ there is evidence to suggest that the Wavec overestimates mean wave period with respect to the Waverider.

6.5.2 Linear Relationship of Logarithms Case

For a comparison of spectral power, a linear relationship between the mean logarithm of spectral energy (at the same frequency for each measurement

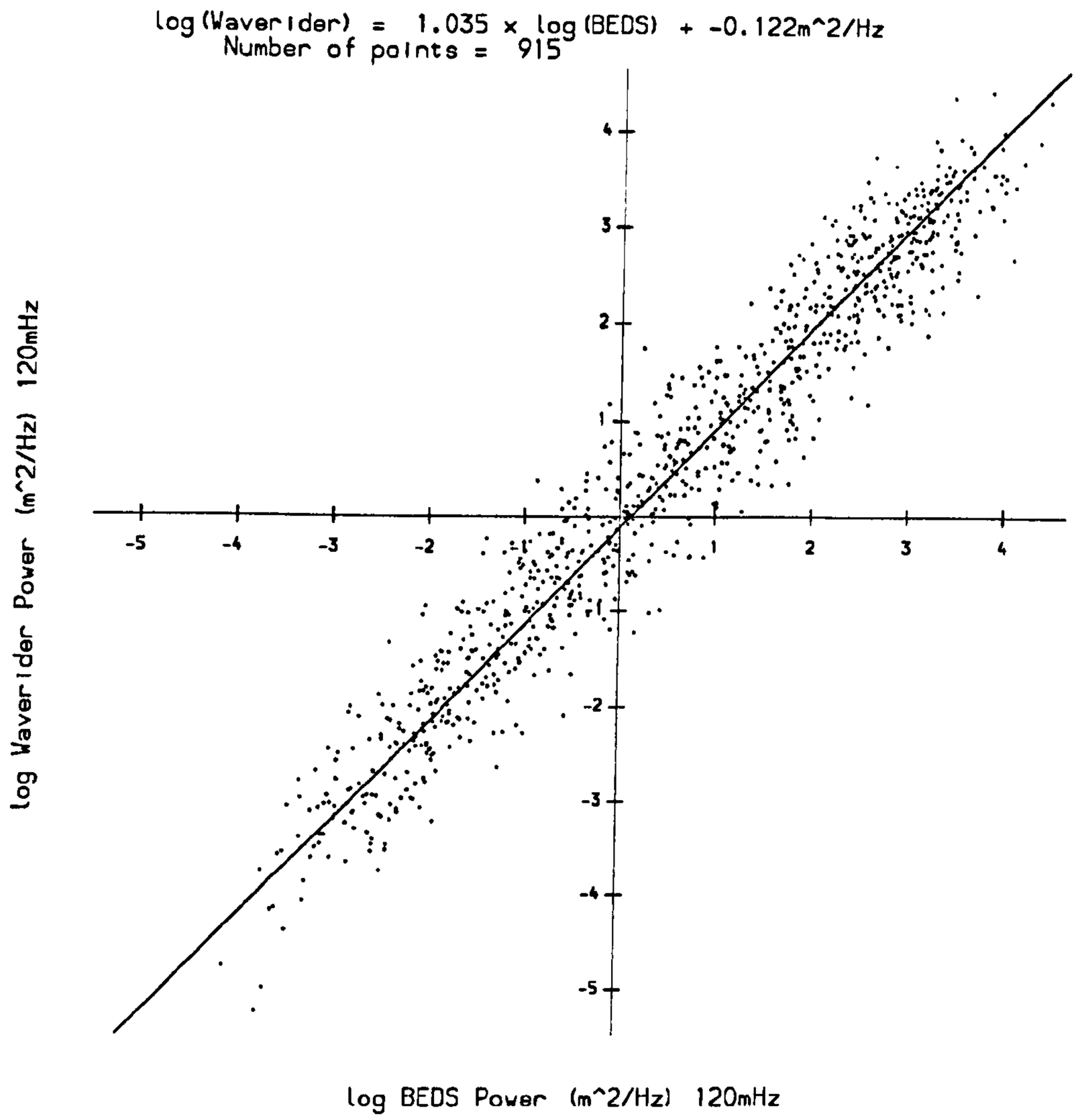

Figure 6.3: A scatter plot of the logarithm of Waverider spectral power against the logarithm of BEDS spectral power (both at $0.12Hz$) during WADIC with the maximum likelihood linear relationship superimposed.

system) appears to be appropriate, as demonstrated by figure 6.3 which shows a scatter plot of the logarithm of spectral power at $0.12Hz$ during WADIC as measured (simultaneously) by a Waverider buoy and an array of lasers (forming part of BEDS, the "*B*est *E*stimate *D*ata *S*et") with the maximum likelihood linear relationship (calculated as described in section 6.5.1) superimposed. The equation of the line is :

$$\log(S(0.12Hz)_{Waverider}) = 1.035 \times \log(S(0.12Hz)_{BEDS}) - 0.122$$

Figure 6.4 shows the estimated relative mean bias of the Waverider spectral power at $0.12Hz$ to the BEDS equivalent with its 95% (pointwise) confidence interval (as calculated from the inverse of the information matrix). From this figure, the data show no evidence to suggest a Waverider bias outside $\pm 2\%$ for mean BEDS power (at $0.12Hz$) above $7.1m^2/Hz$, and no evidence to

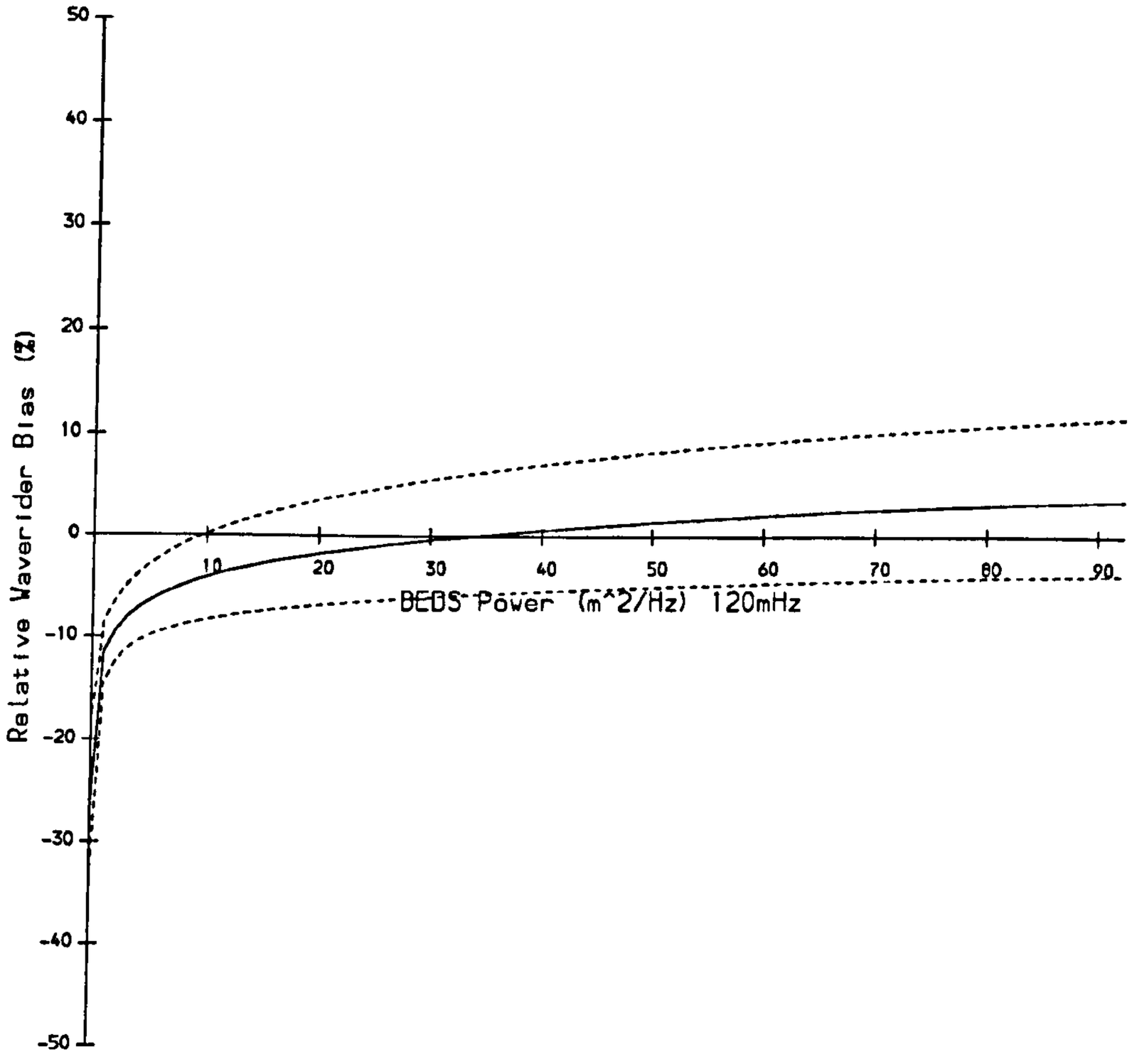

Figure 6.4: A plot of estimated Waverider spectral power relative mean bias against BEDS spectral energy (both at $0.12Hz$) with its 95% confidence interval.

suggest a Waverider bias outside $\pm 5\%$ for mean BEDS power (at $0.12Hz$) greater than $3.0m^2/Hz$ (over the range of the data). Below $3.0m^2/Hz$ there is evidence to suggest that the Waverider underestimates mean spectral power at $0.12Hz$ with respect to BEDS.

6.5.3 Directional Difference Case

Since any measurement of mean direction can only be relative (*e.g.* to magnetic north) and not absolute, and 0° is the same direction as 360°, it makes little sense to think in terms of proportionality between measurements, but rather of the difference between them. Consider a set of observed directional differences ψ_j of paired measurements from two systems taken independently

from variables $\Psi_j (j = 1 \ldots n)$ where :

$$\Psi_j \sim \mathrm{N}(\mu, \sigma_j^2)$$

where each σ_j^2 is known. The likelihood equation is :

$$\mathrm{lik}(\mu|\psi, \sigma^2) = \prod_{j=1}^{n} \frac{1}{\sqrt{2\pi\sigma_j^2}} e^{-\frac{1}{2}\left(\frac{\psi-\mu}{\sigma_j}\right)^2}$$

Hence,

$$\mathrm{loglik}(\mu|\psi, \sigma^2) = -\frac{n}{2}\log(2\pi) - \frac{1}{2}\sum_{j=1}^{n}\log(\sigma_j^2) - \frac{1}{2}\sum_{j=1}^{n}\left(\frac{\psi_j - \mu}{\sigma_j^2}\right)^2$$

and differentiating with respect to μ we get :

$$\frac{\partial \mathrm{loglik}(\mu|\psi, \sigma^2)}{\partial \mu} = -\mu\sum_{j=1}^{n}\frac{1}{\sigma_j^2} + \sum_{j=1}^{n}\frac{\psi_j}{\sigma_j^2} \tag{6.3}$$

and hence (by setting equation 6.3 to zero) the maximum likelihood estimate of μ (the mean directional difference) is a weighted mean :

$$\hat{\mu} = \frac{\sum_{j=1}^{n}\frac{\psi_j}{\sigma_j^2}}{\sum_{j=1}^{n}\frac{1}{\sigma_j^2}}$$

and from this we may calculate the variance of $\hat{\mu}$ directly :

$$\mathrm{Var}(\hat{\mu}) = \frac{1}{\sum_{j=1}^{n}\frac{1}{\sigma_j^2}}$$

As an example, figure 6.5 shows a scatter plot of Norwave buoy mean wave direction measurements at $0.12Hz$ from WADIC against their BEDS counterparts, with the maximum likelihood relationship superimposed. The equation of the line is :

$$\theta_0{}_{Norwave} = \theta_0{}_{BEDS} - 8.178^\circ$$

The 95% confidence interval of the bias is $(-9.357^\circ, -6.999^\circ)$, and hence the data show evidence to suggest a bias of greater than $\pm 5^\circ$ but no evidence to suggest a bias of greater than $\pm 10^\circ$. Allender *et al.* (1989) do not go into

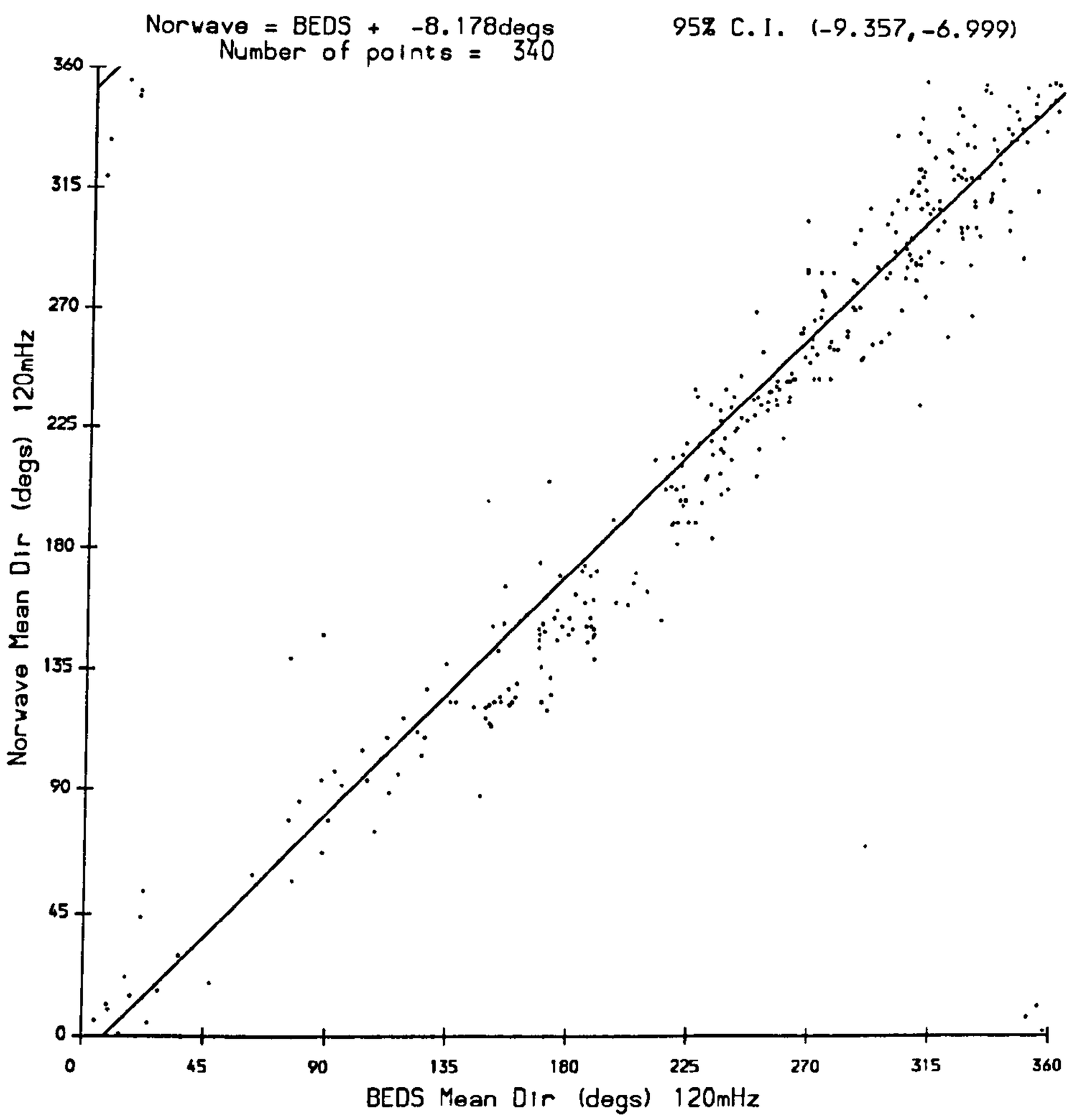

Figure 6.5: A scatter plot of Norwave mean wave direction against BEDS mean wave direction (both at $0.12Hz$) during WADIC with the maximum likelihood relationship superimposed.

detail regarding mean direction comparisons, but state that the Norwave wave direction is biased 9° on average relative to BEDS and that the "reliable frequency range for mean direction" (as measured by the Norwave buoy) is $[0.08Hz, 0.37Hz]$. We note, however, that the data in figure 6.5 appear to deviate slightly from a linear relationship, indicating that a single value for bias (as opposed to a function of direction) may be inappropriate in this case.

Chapter 7

Results from NURWEC2

7.1 Introduction

In chapter 6 we derived the maximum likelihood estimates for various relationships between ocean wave parameters as measured by two independent wave measuring systems. In this chapter we estimate such relationships between HF radar and wave buoy performances using data from the NURWEC2 (*N*etherlands *UK* *R*adar *W*ave buoy *E*xperimental *C*omparison, see section 1.4) field trial. Unfortunately, complete wave buoy data is not available at each frequency, but only for integrals over the following frequencies :

- $30 - 45mHz$
- $45 - 60mHz$
- $60 - 85mHz$
- $85 - 100mHz$
- $100 - 125mHz$
- $125 - 155mHz$
- $160 - 200mHz$

Hence, the intercomparison of frequency domain data has been based on the above frequency ranges. The results presented use the techniques described

in section 6.5 and use data recorded during the NURWEC2 storm. We will now examine each wave parameter in turn.

7.2 Significant Waveheight

Figure 7.1 shows a scatter plot of HF radar significant waveheight measurements from NURWEC2 against their wave buoy counterparts, with the maximum likelihood linear relationship superimposed. The equation of the line is :

$$H_{s_{Radar}} = 0.986 \times H_{s_{Wavec}} + 0.111m$$

A linear relationship appears appropriate in this case. From figure 7.2 the data show no evidence to suggest a radar bias outside $\pm 2\%$ for mean Wavec significant waveheight over the whole range of the data.

7.3 Mean Wave Period

Figure 7.3 shows a scatter plot of HF radar mean period measurements from NURWEC2 against their wave buoy counterparts, with the maximum likelihood linear relationship superimposed. The equation of the line is :

$$T_{m_{Radar}} = 1.284 \times T_{m_{Wavec}} - 2.348secs$$

A linear relationship appears appropriate in this case, although there are three outliers (each with a relatively large variance, and hence little influence on the relationship). From figure 7.4 the data show no evidence to suggest a radar bias outside $\pm 2\%$ for mean Wavec mean periods within $(7.6s, 9.4s)$, and no evidence to suggest a radar bias outside $\pm 5\%$ for mean Wavec mean periods within $(6.8s, 11.0s)$. Below and above these ranges there is evidence to suggest that the radars respectively underestimate and overestimate with respect to the mean Wavec mean period.

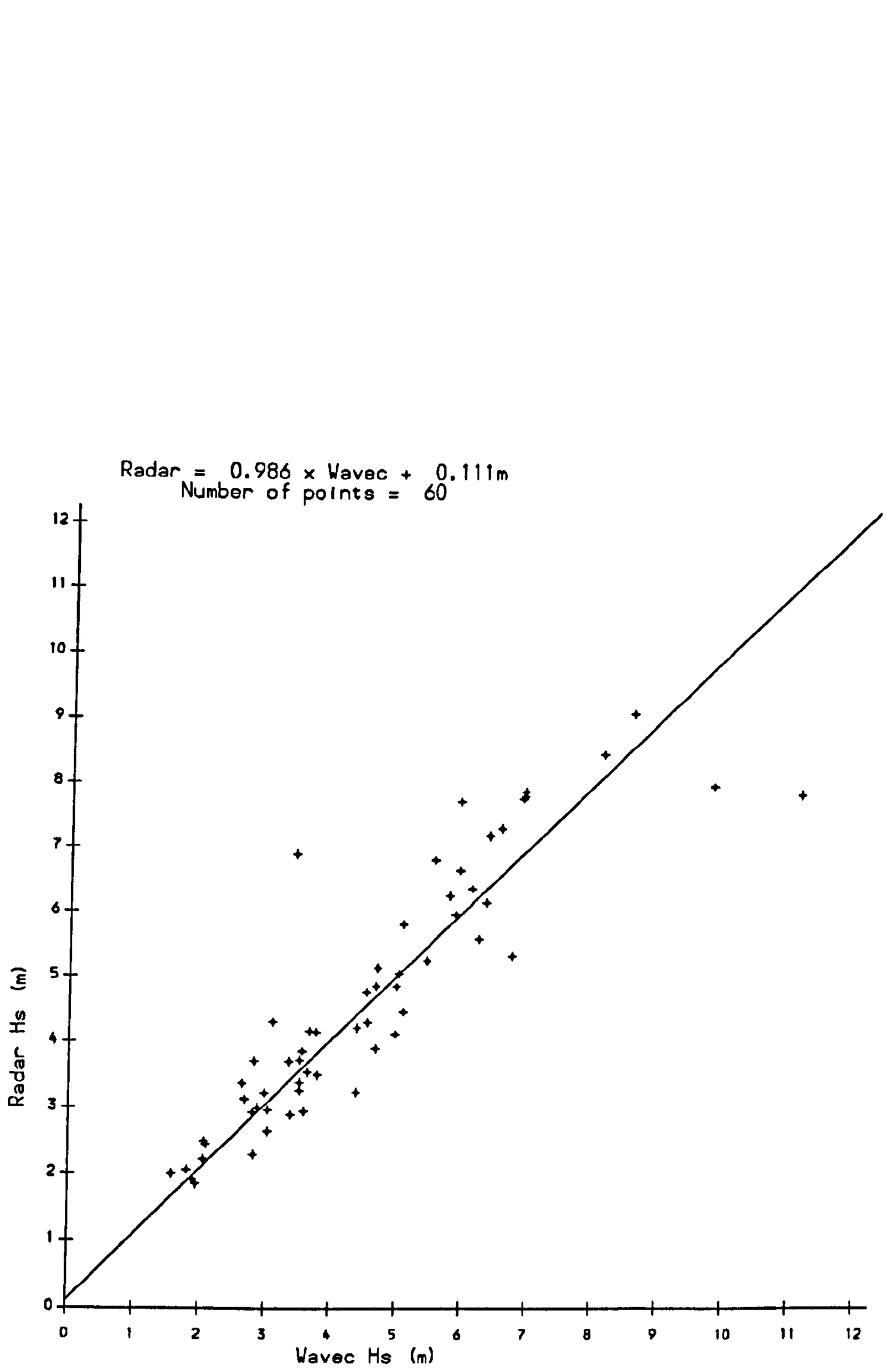

Figure 7.1: A scatter plot of HF radar significant waveheight against wave buoy significant waveheight during the NURWEC2 storm with the maximum likelihood linear relationship superimposed. The estimated relationship and the number of points are displayed at the top of the figure.

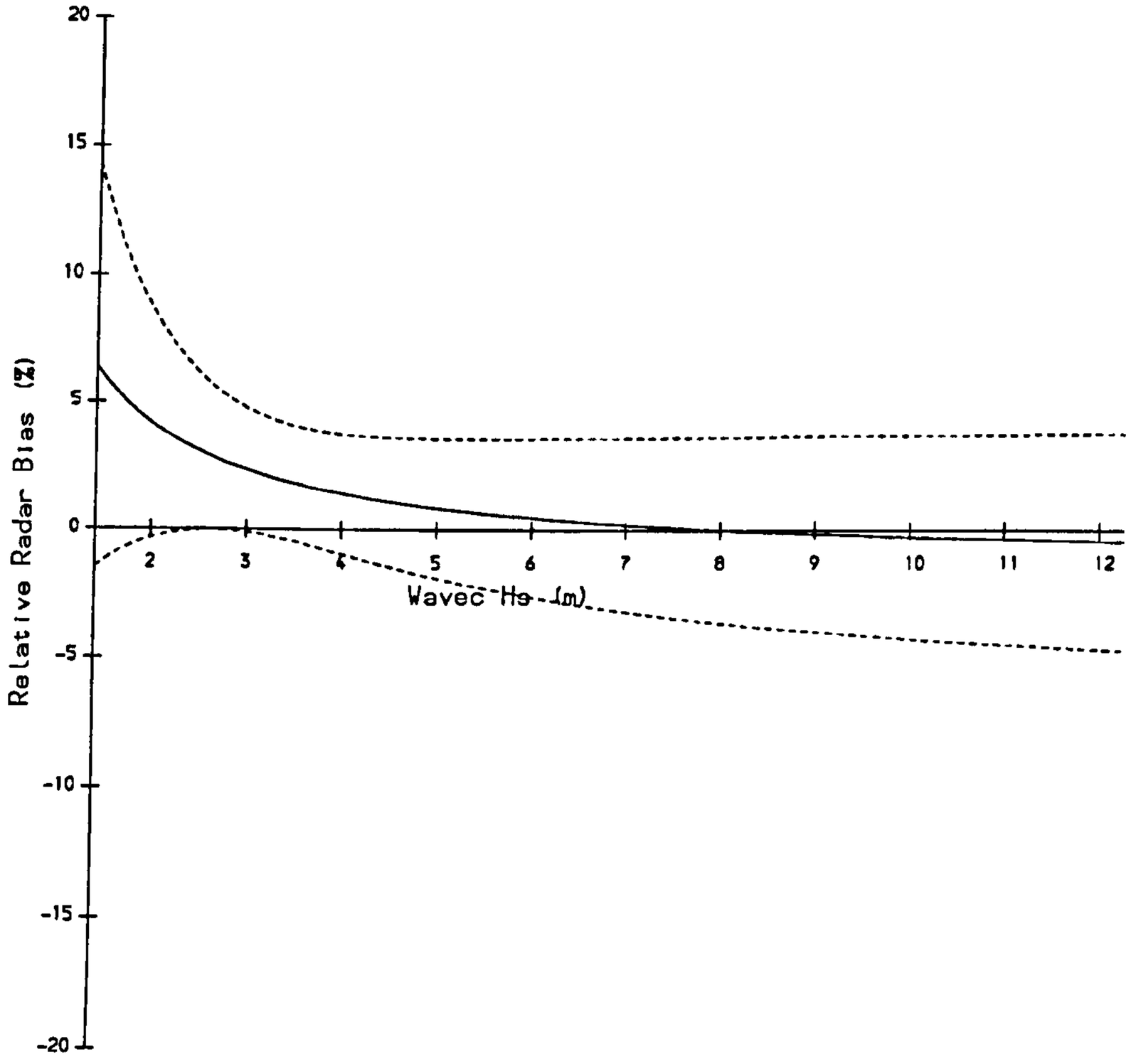

Figure 7.2: A plot of estimated HF radar significant waveheight relative mean bias against wave buoy significant waveheight with its 95% confidence interval.

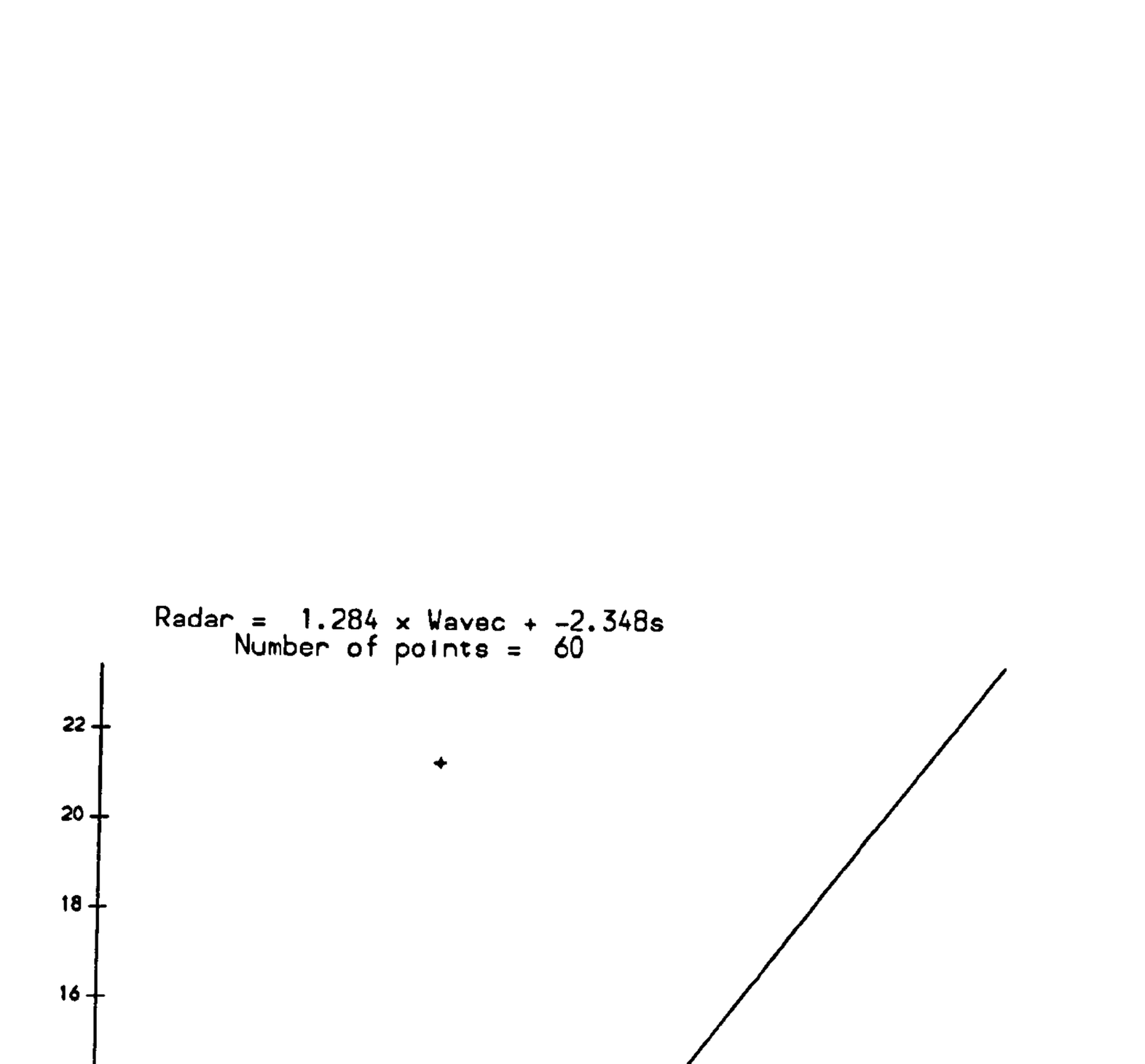

Figure 7.3: A scatter plot of HF radar mean wave period against wave buoy mean wave period during the NURWEC2 storm with the maximum likelihood linear relationship superimposed. The estimated relationship and the number of points are displayed at the top of the figure.

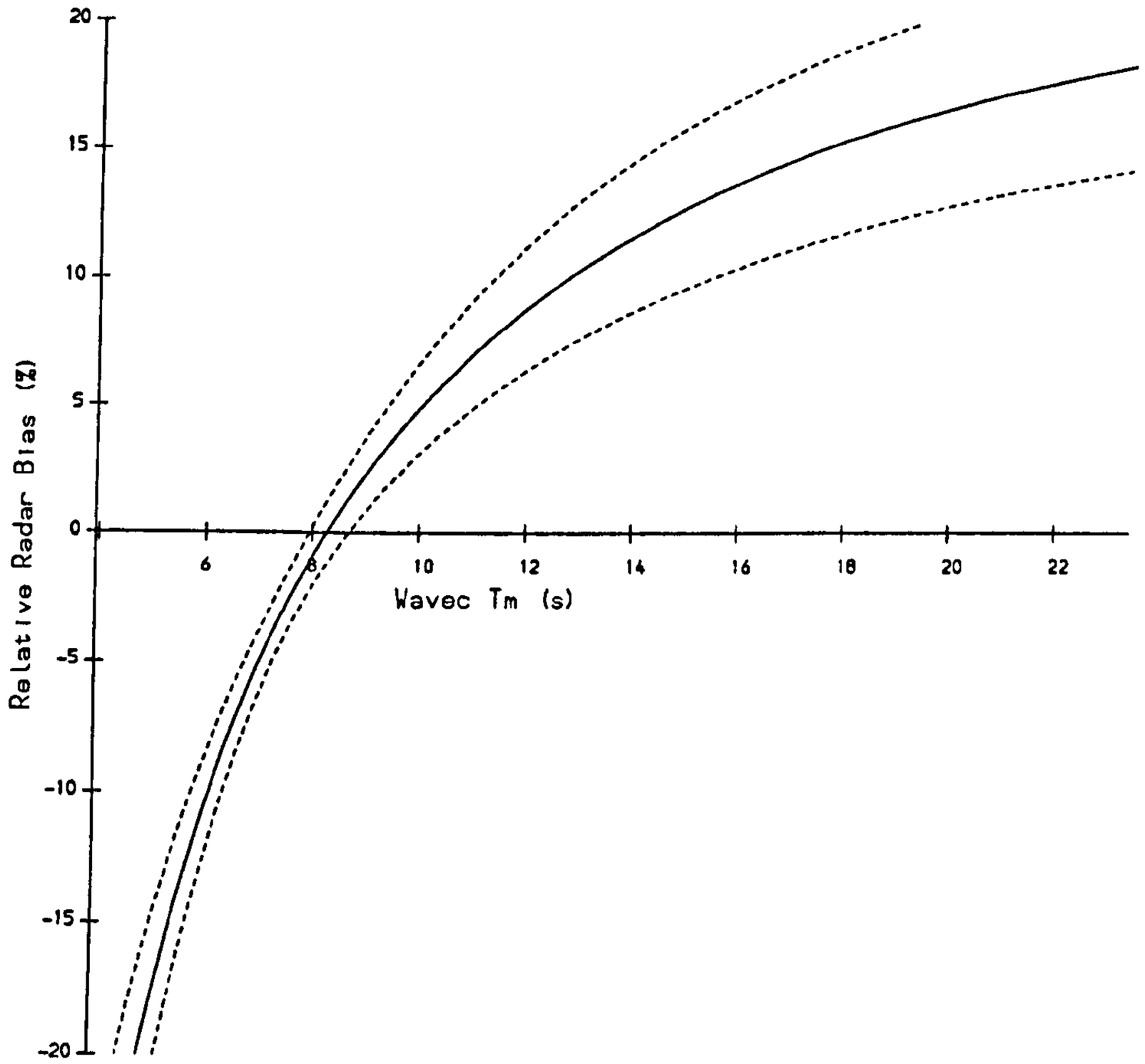

Figure 7.4: A plot of estimated HF radar mean wave period relative mean bias against wave buoy mean wave period with its 95% confidence interval.

7.4 Spectral Power

As described in section 6.5.2, (natural) logarithms of the spectral power estimates of both the radar and buoy have been taken before fitting the maximum likelihood estimates of the linear (on a logarithmic scale) relationship. We now examine these relationships separately for each frequency range. Each relationship is displayed at the top of the appropriate figure, together with the number of points (*e.g.* see figure 7.6).

7.4.1 Spectral Power at 30-45mHz

Figure 7.5 shows a scatter plot of the natural logarithms of HF radar spectral power measurements in the $30-45mHz$ range taken during NURWEC2, against their wave buoy counterparts. The maximum likelihood algorithm failed to converge for this data set. Because of the outliers in the upper left-hand portion of the plot, it is unlikely that any intuitively sensible (*i.e.* monotonically strictly increasing) function could satisfactorily be fitted to these data, and it would therefore be unwise to attempt to draw any conclusions about the relationship therefrom.

7.4.2 Spectral Power at 45-60mHz

Figure 7.6 shows a scatter plot of the natural logarithms of HF radar spectral power measurements in the $45-60mHz$ range taken during NURWEC2, against their wave buoy counterparts, with the maximum likelihood linear relationship superimposed. The equation of the line is :

$$\log(S(45-60mHz)_{Radar}) = 1.136 \times \log(S(45-60mHz)_{Wavec}) + 1.954m^2$$

The line does not appear to fit the data particularly well, suggesting that either a curved relationship would be more appropriate or that there is a problem with the outliers in the lower left-hand portion of the plot. Again, attempts to draw any conclusions about the relationship would therefore be unwise.

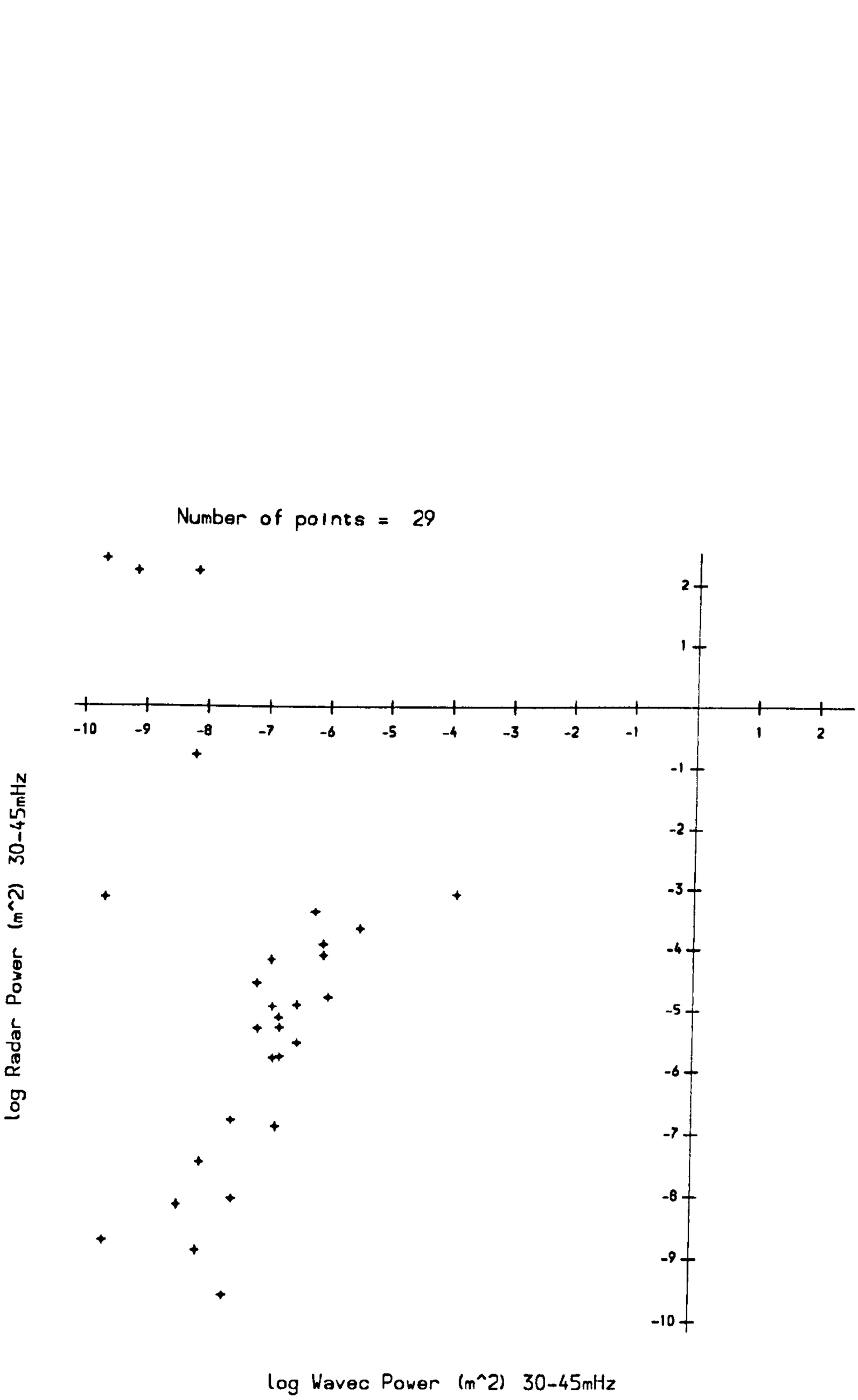

Figure 7.5: A scatter plot of the natural logarithms of HF radar spectral power over $30 - 45mHz$ against their wave buoy equivalents during the NURWEC2 storm.

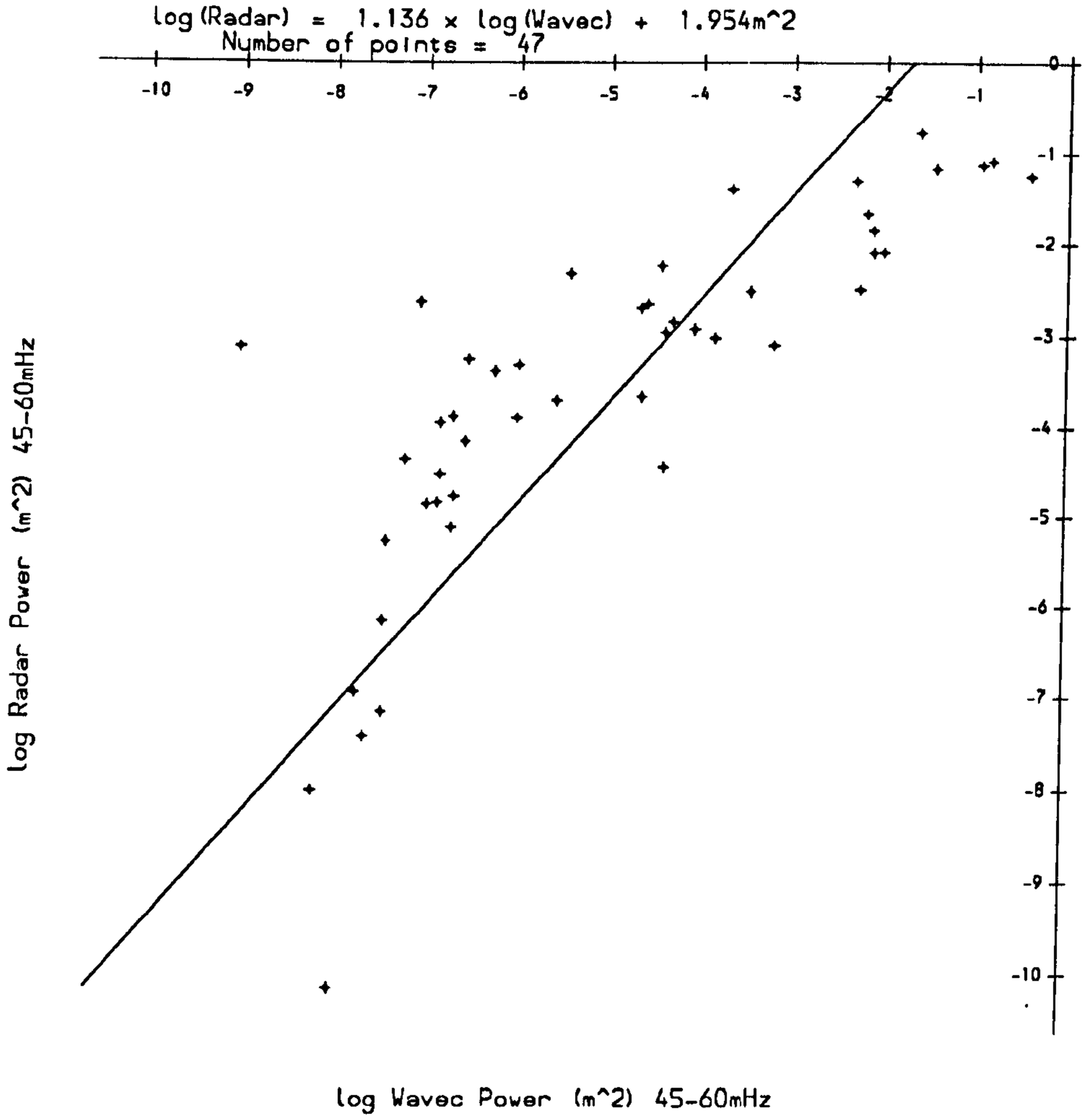

Figure 7.6: A scatter plot of the natural logarithms of HF radar spectral power over $45 - 60mHz$ against their wave buoy equivalents during the NURWEC2 storm, with the maximum likelihood linear relationship superimposed.

7.4.3 Spectral Power at 60-85mHz

Figure 7.7 shows a scatter plot of the natural logarithms of HF radar spectral power measurements in the $60-85mHz$ range taken during NURWEC2, against their wave buoy counterparts, with the maximum likelihood linear relationship superimposed. The equation of the line is :

$$\log(S(60-85mHz)_{Radar}) = 0.776 \times \log(S(60-85mHz)_{Wavec}) - 0.351m^2$$

A linear relationship appears appropriate in this case. From figure 7.8 the data show no evidence to suggest a radar bias outside $\pm 2\%$ for mean Wavec spectral powers within $(0.17m^2, 0.29m^2)$, and no evidence to suggest a radar bias outside $\pm 5\%$ for mean Wavec spectral power within $(0.17m^2, 0.34m^2)$. Below and above these ranges there is evidence to suggest that the radars respectively overestimate and underestimate with respect to the mean Wavec spectral power.

7.4.4 Spectral Power at 85-100mHz

Figure 7.9 shows a scatter plot of the natural logarithms of HF radar spectral power measurements in the $85-100mHz$ range taken during NURWEC2, against their wave buoy counterparts, with the maximum likelihood linear relationship superimposed. The equation of the line is :

$$\log(S(85-100mHz)_{Radar}) = 0.958 \times \log(S(85-100mHz)_{Wavec}) - 0.008m^2$$

A linear relationship appears appropriate in this case. From figure 7.10 the data show no evidence to suggest a radar bias outside $\pm 2\%$ over the entire range of the data.

7.4.5 Spectral Power at 100-125mHz

Figure 7.11 shows a scatter plot of the natural logarithms of HF radar spectral power measurements in the $100-125mHz$ range taken during NURWEC2, against their wave buoy counterparts, with the maximum likelihood linear

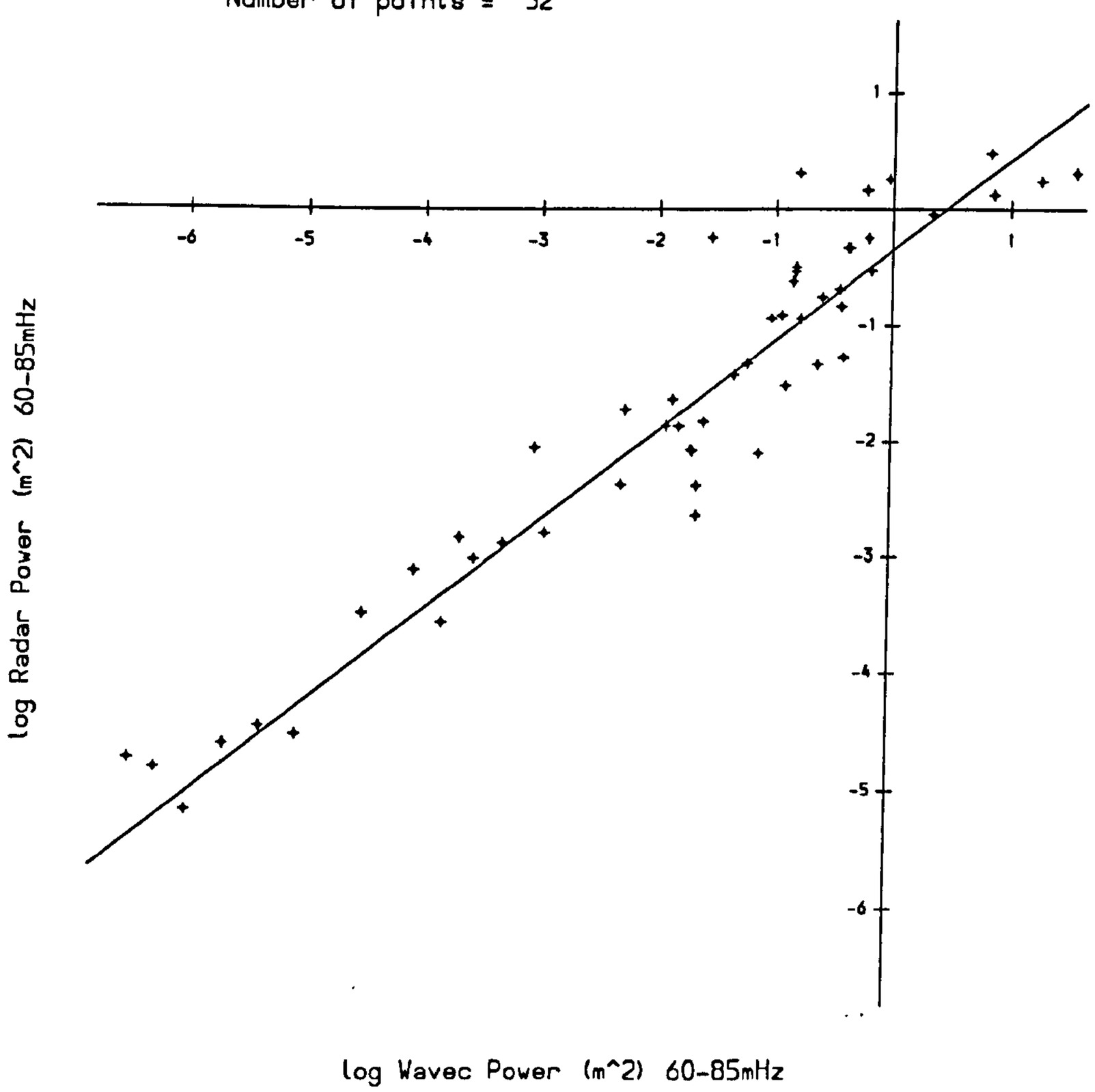

Figure 7.7: A scatter plot of the natural logarithms of HF radar spectral power over $60 - 85mHz$ against their wave buoy equivalents during the NURWEC2 storm, with the maximum likelihood linear relationship superimposed.

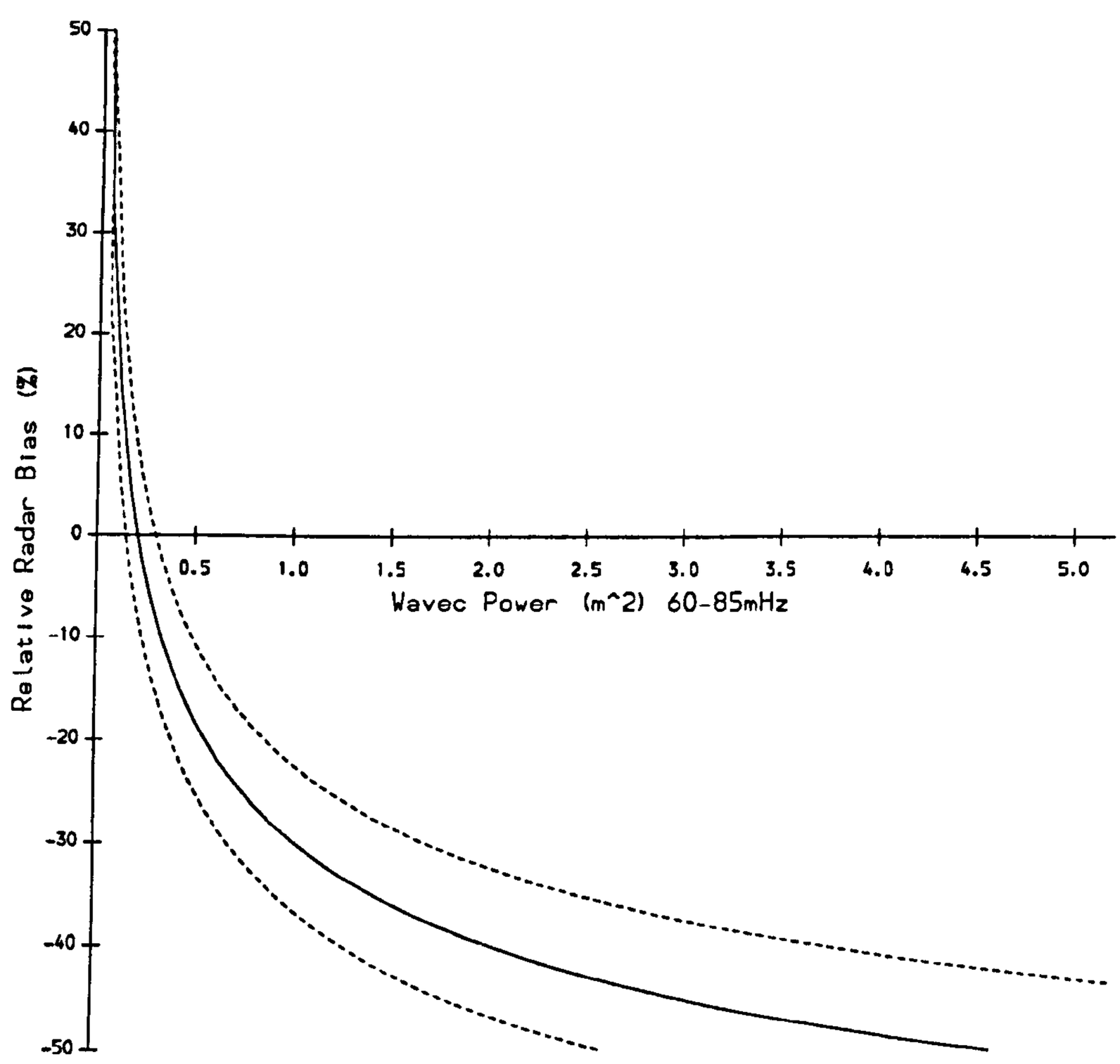

Figure 7.8: A plot of estimated HF radar spectral power relative mean bias against wave buoy mean spectral power (both over $60 - 85mHz$) with its 95% confidence interval.

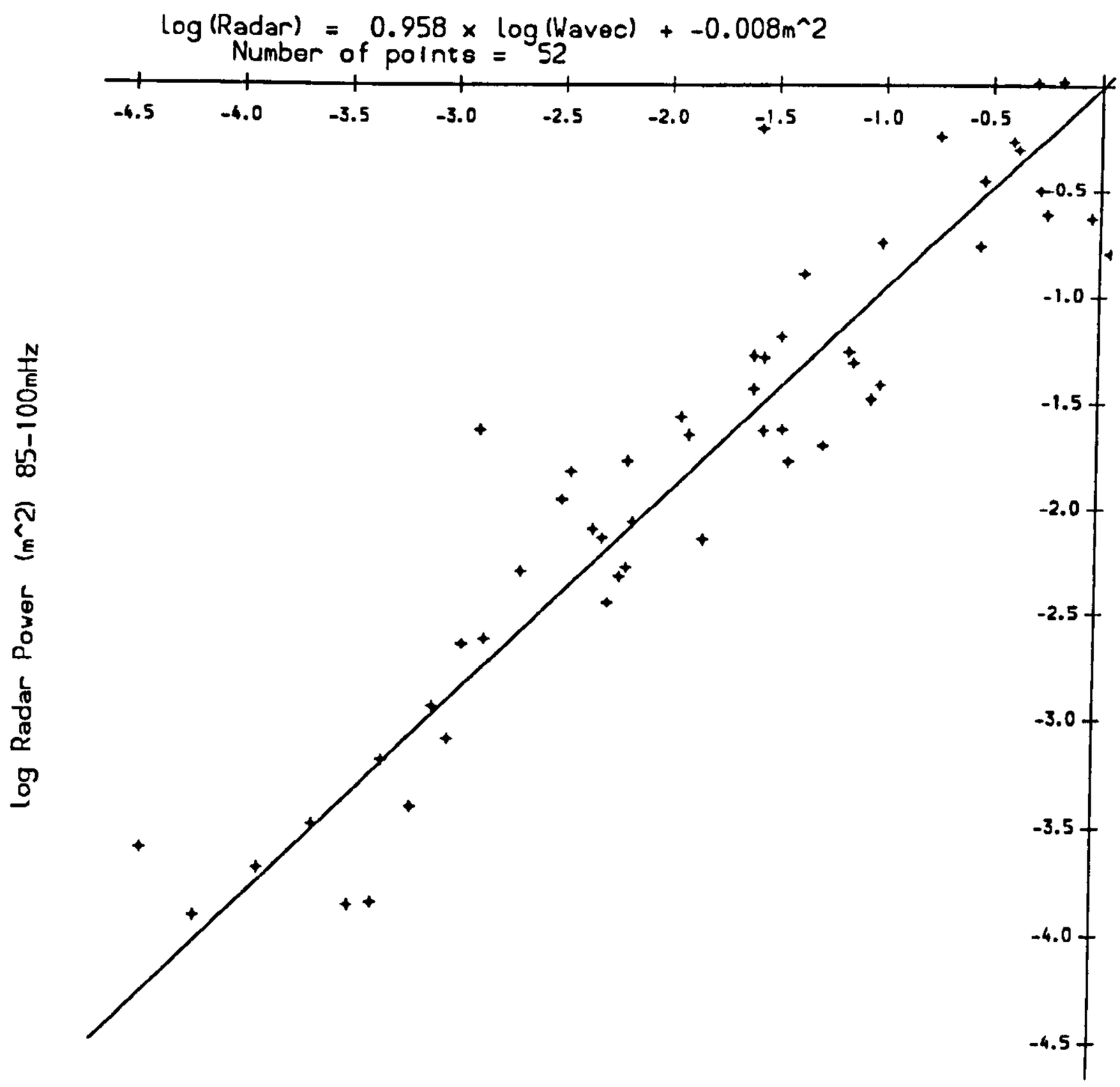

Figure 7.9: A scatter plot of the natural logarithms of HF radar spectral power over $85 - 100mHz$ against their wave buoy equivalents during the NURWEC2 storm, with the maximum likelihood linear relationship superimposed.

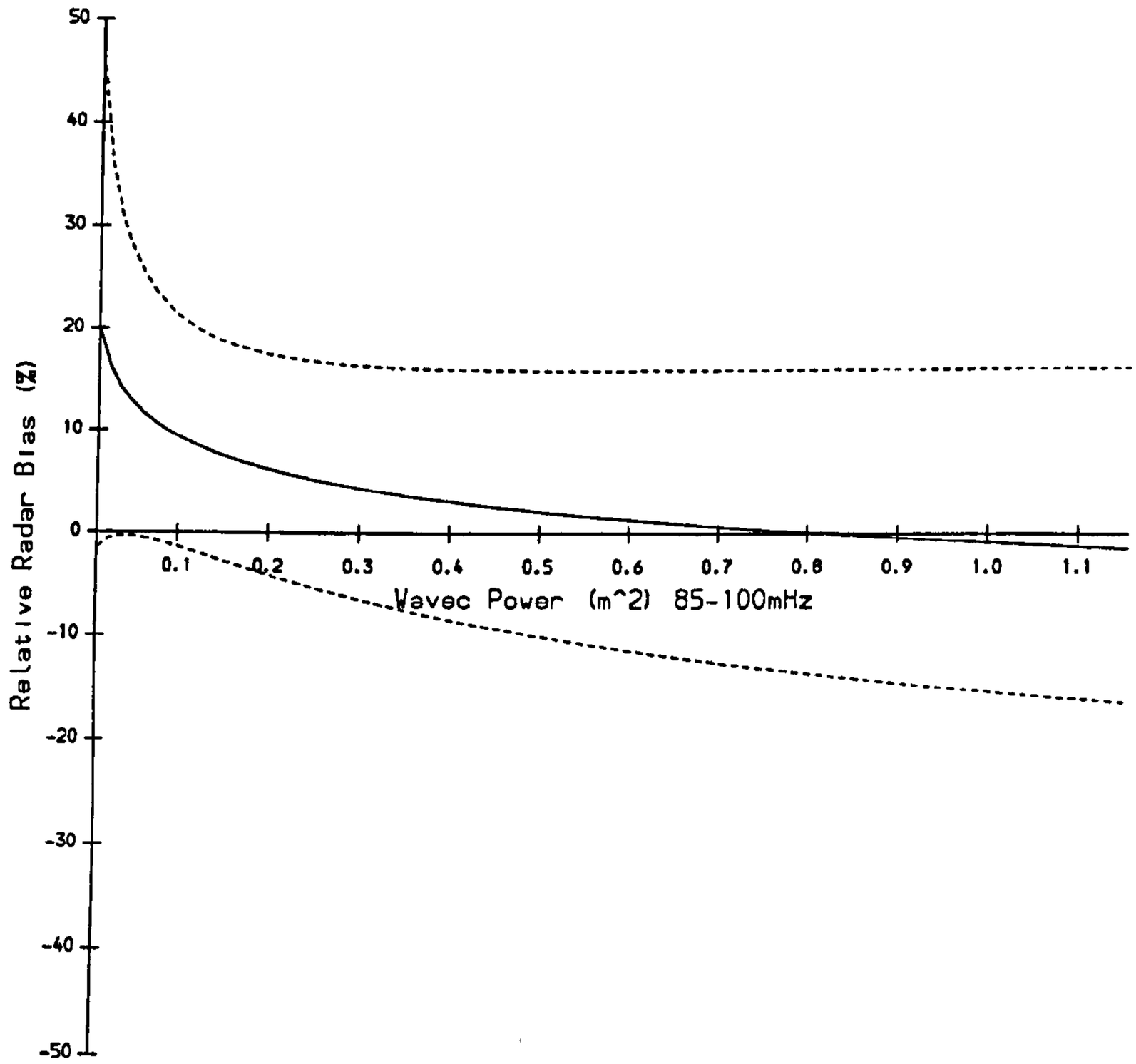

Figure 7.10: A plot of estimated HF radar spectral power relative mean bias against wave buoy mean spectral power (both over $85 - 100mHz$) with its 95% confidence interval.

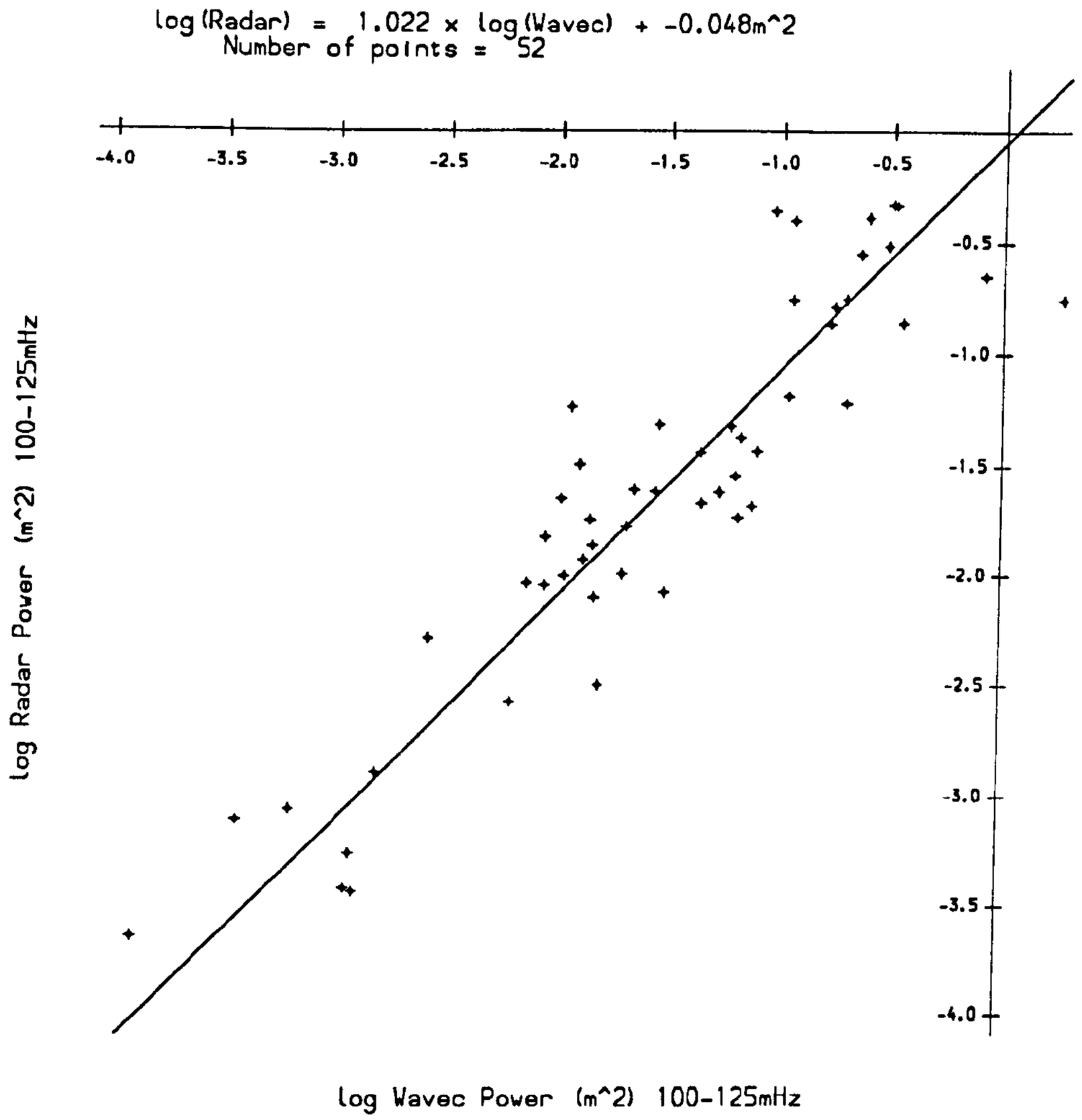

Figure 7.11: A scatter plot of the natural logarithms of HF radar spectral power over $100 - 125mHz$ against their wave buoy equivalents during the NURWEC2 storm, with the maximum likelihood linear relationship superimposed.

relationship superimposed. The equation of the line is :

$$\log(S(100-125mHz)_{Radar}) = 1.022 \times \log(S(100-125mHz)_{Wavec}) - 0.048m^2$$

A linear relationship appears appropriate in this case. From figure 7.12 the data show no evidence to suggest a radar bias outside $\pm 2\%$ over the entire range of the data.

7.4.6 Spectral Power at 125-155mHz

Figure 7.13 shows a scatter plot of the natural logarithms of HF radar spectral power measurements in the $125 - 155mHz$ range taken during NURWEC2,

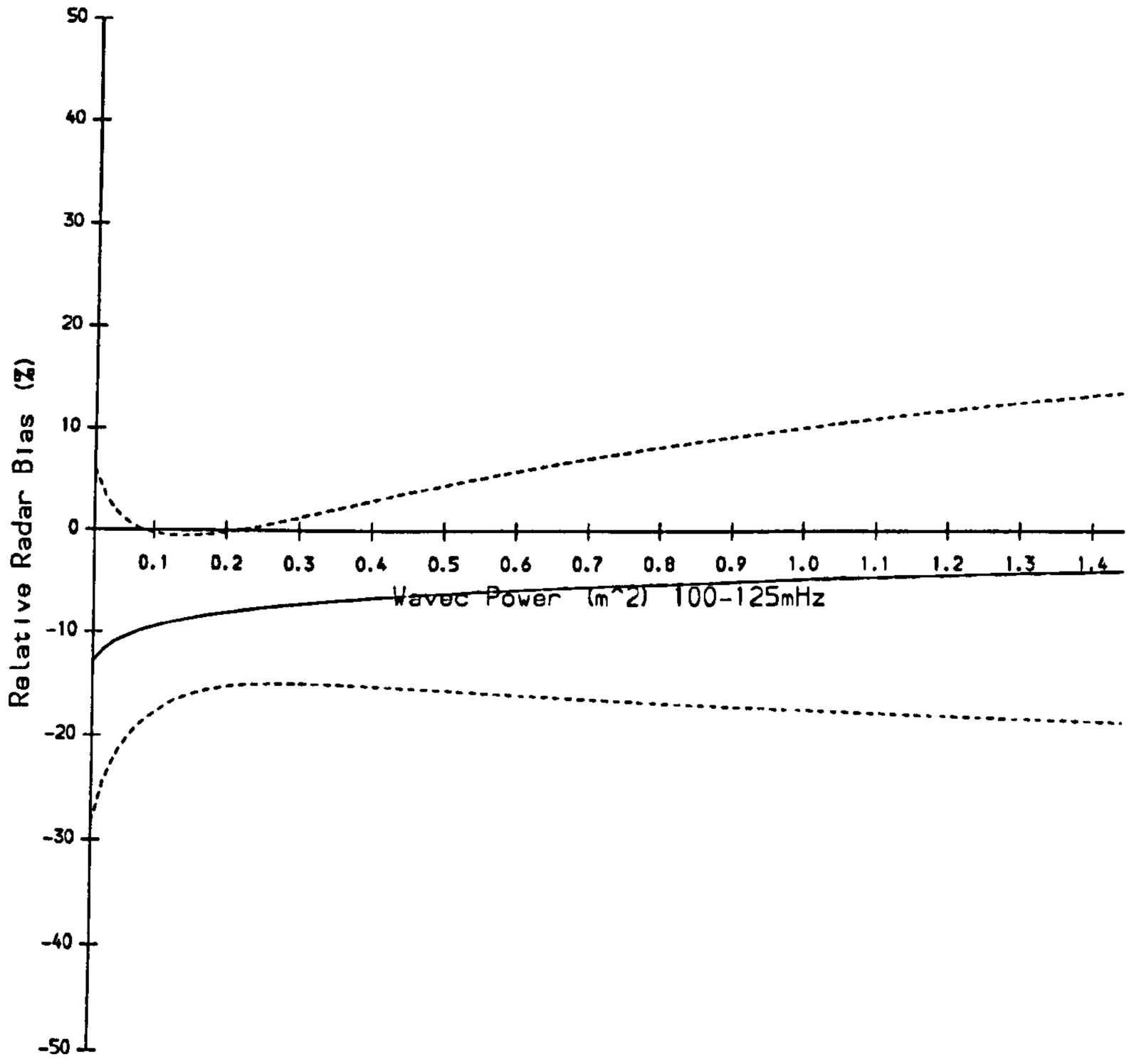

Figure 7.12: A plot of estimated HF radar spectral power relative mean bias against wave buoy mean spectral power (both over $100 - 125mHz$) with its 95% confidence interval.

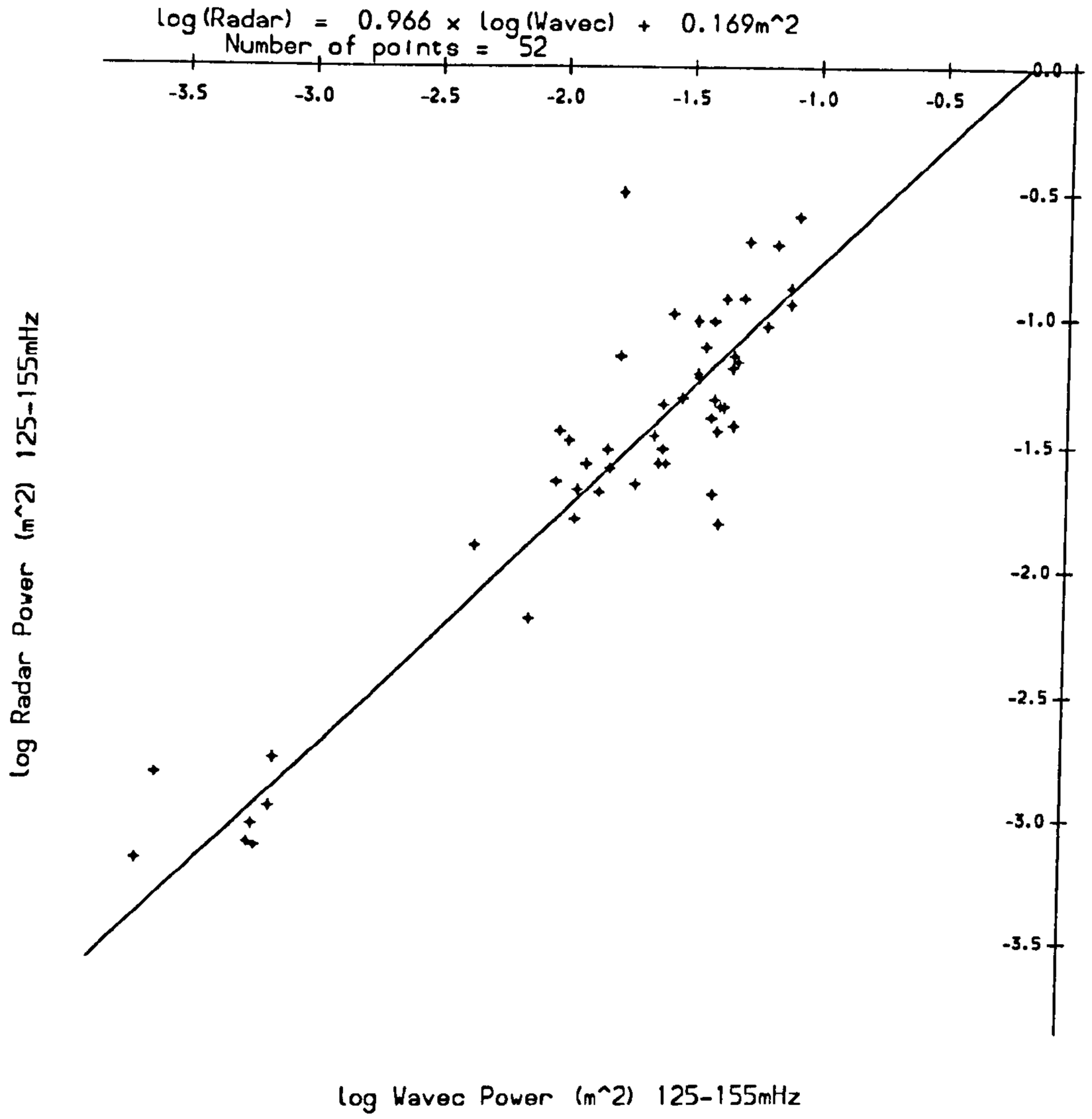

Figure 7.13: A scatter plot of the natural logarithms of HF radar spectral power over $125 - 155mHz$ against their wave buoy equivalents during the NURWEC2 storm, with the maximum likelihood linear relationship superimposed.

against their wave buoy counterparts, with the maximum likelihood linear relationship superimposed. The equation of the line is :

$$\log(S(125{-}155mHz)_{Radar}) = 0.966 \times \log(S(125{-}155mHz)_{Wavec}) + 0.169m^2$$

A linear relationship appears appropriate in this case. From figure 7.14 the data show some evidence to suggest a radar bias greater than +5% over the entire range of the data.

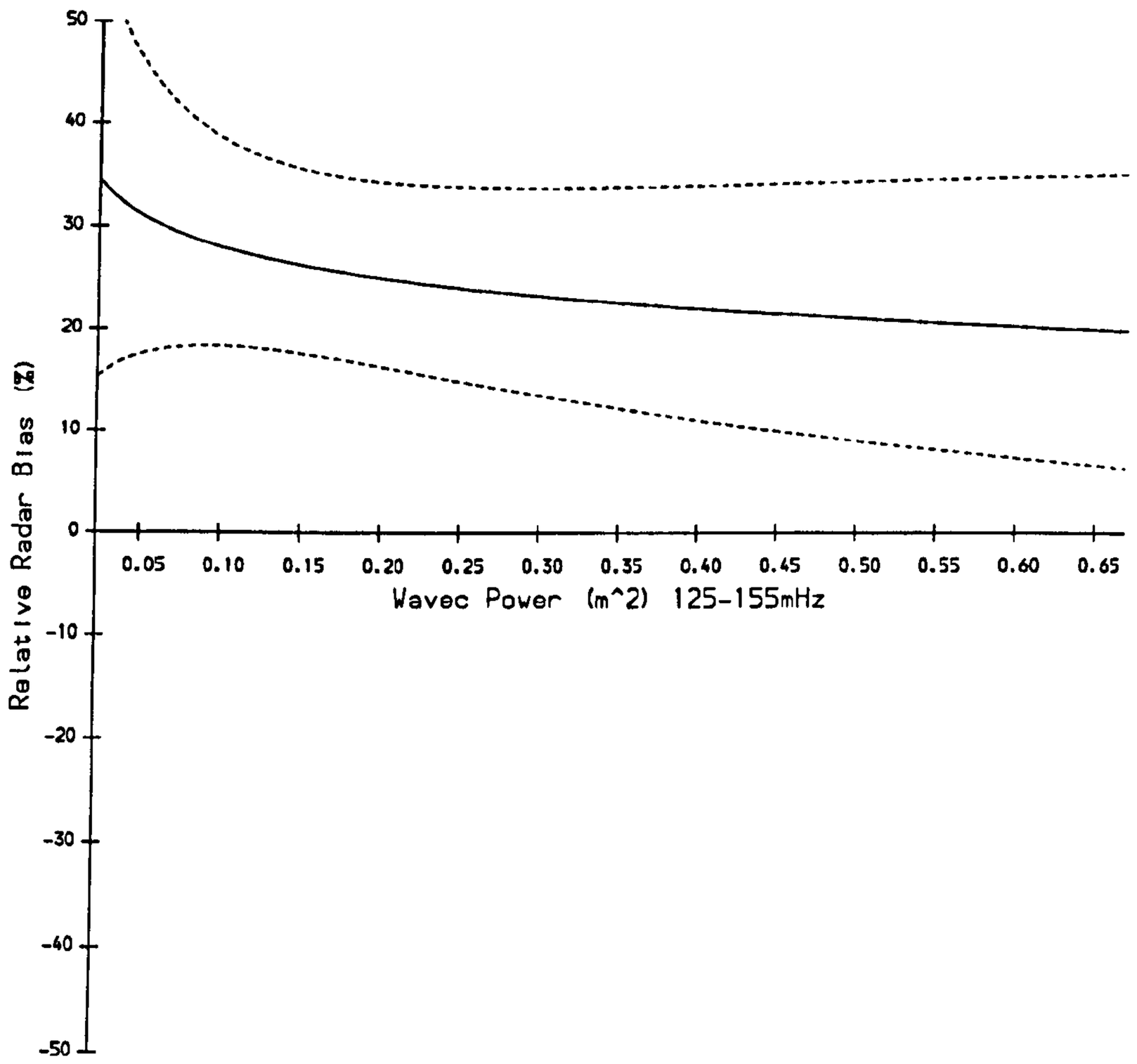

Figure 7.14: A plot of estimated HF radar spectral power relative mean bias against wave buoy mean spectral power (both over $125 - 155mHz$) with its 95% confidence interval.

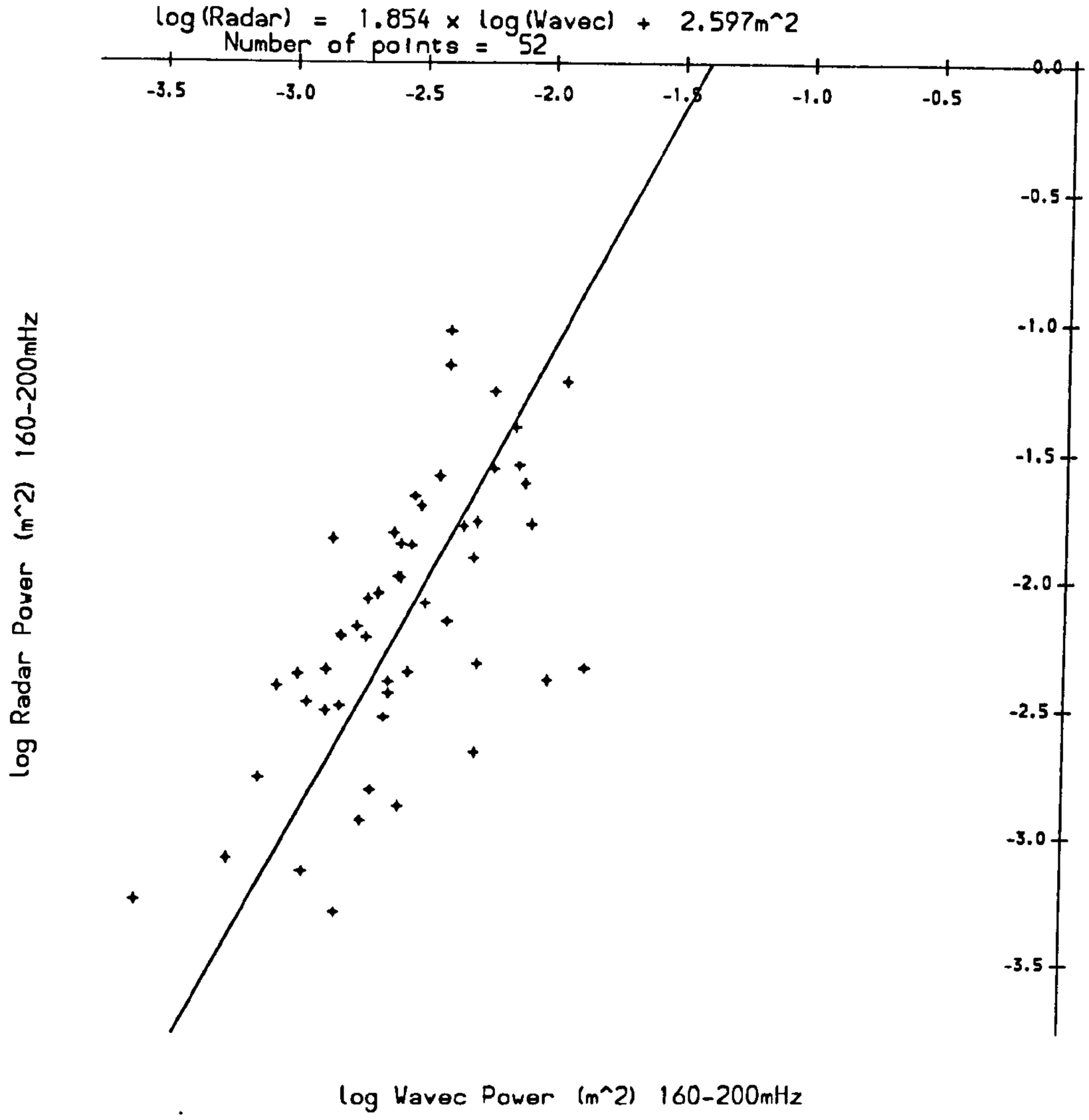

Figure 7.15: A scatter plot of the natural logarithms of HF radar spectral power over $160 - 200mHz$ against their wave buoy equivalents during the NURWEC2 storm, with the maximum likelihood linear relationship superimposed.

7.4.7 Spectral Power at 160-200mHz

Figure 7.15 shows a scatter plot of the natural logarithms of HF radar spectral power measurements in the $160 - 200mHz$ range taken during NURWEC2, against their wave buoy counterparts, with the maximum likelihood linear relationship superimposed. The equation of the line is :

$$\log(S(160-200mHz)_{Radar}) = 1.854 \times \log(S(160-200mHz)_{Wavec}) + 2.597m^2$$

A linear relationship appears reasonable in this case. However, the wide spread of points from the line with respect to the range of the data would make estimation somewhat unreliable, and it would therefore be unwise to attempt to draw any conclusions about such a relationship.

7.4.8 Comment on Radar Performance

The Radar and Wavec perform similarly (in terms of relative mean bias of spectral power estimates) over the frequencies $85-125mHz$ (the bulk of wave power is typically within these frequencies, and hence this is where reliable performance is particularly important). That there should be some discrepancy outside this range is not surprising. At the more extreme frequencies, we approach the frequency limits of the radar inversion routine where, if anywhere, radar reliability is likely to be at its weakest. At lower frequencies (which typically have relatively low power levels) it is generally accepted that wave buoy measurements are highly prone to noise. Finally, because radars and wave buoys measure waves in such fundamentally different ways, comparable behaviour over all frequencies would be unexpected.

7.5 Spectral Mean direction

The (absolute) radar biases with respect to the wave buoy mean direction spectrum have been calculated as described in section 6.5.3. We now examine these biases separately for each frequency range. Each estimated bias (with its 95% confidence interval) is displayed at the top of the appropriate figure, together with the number of points (*e.g.* see figure 7.16).

7.5.1 Spectral Mean Direction at 30-45mHz

Figure 7.16 shows a scatter plot of the HF radar spectral mean direction measurements in the $30-45mHz$ range taken during NURWEC2, against their wave buoy counterparts. The maximum likelihood bias is superimposed, however, the scatter of the data makes it impossible to derive any useful information therefrom.

7.5.2 Spectral Mean Direction at 45-60mHz

Figure 7.17 shows a scatter plot of the HF radar spectral mean direction measurements in the $45-60mHz$ range taken during NURWEC2, against their wave buoy counterparts. The maximum likelihood bias is superimposed,

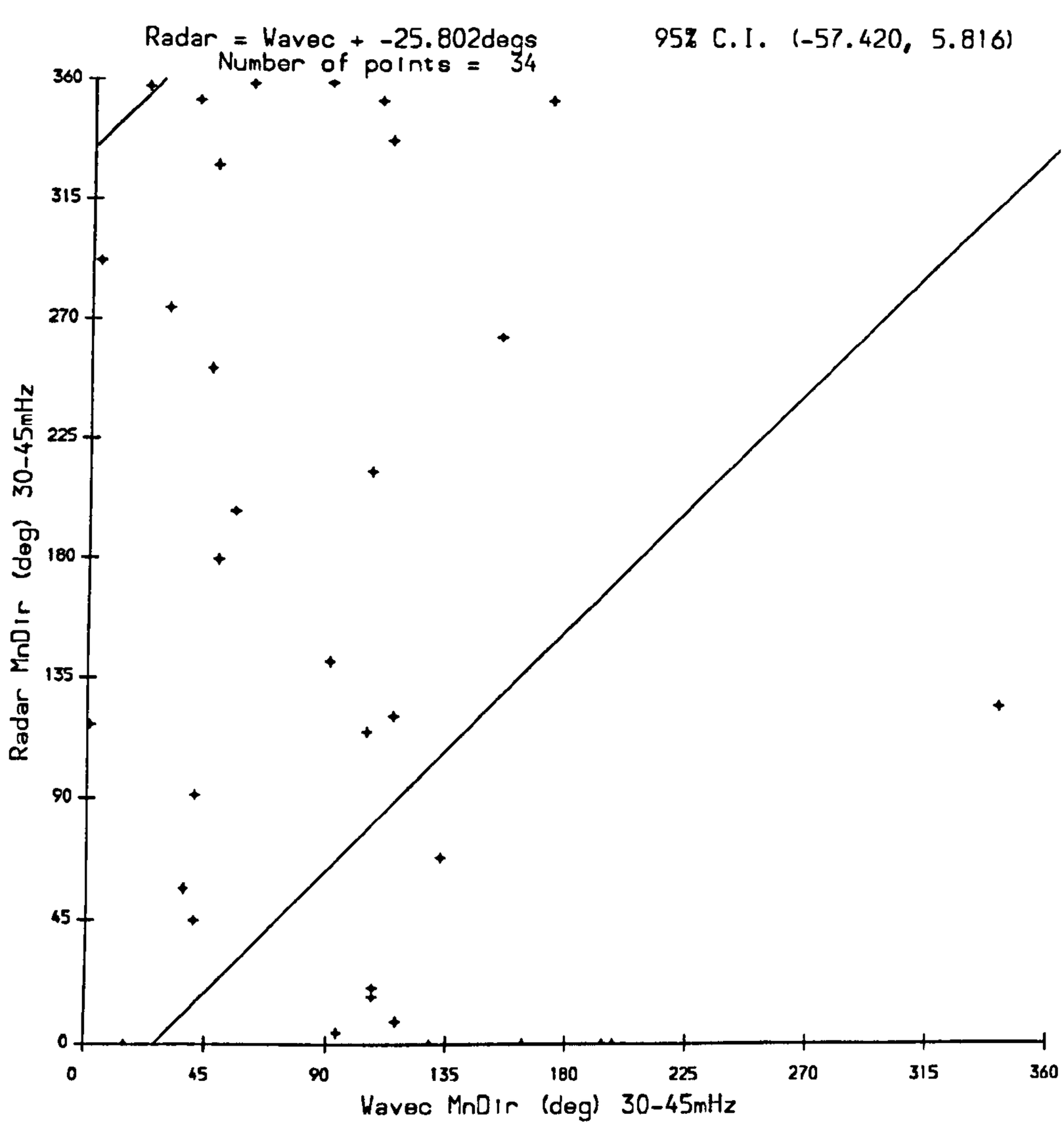

Figure 7.16: A scatter plot of HF radar spectral mean direction over $30 - 45mHz$ against their wave buoy equivalents during the NURWEC2 storm, with the maximum likelihood bias estimate superimposed.

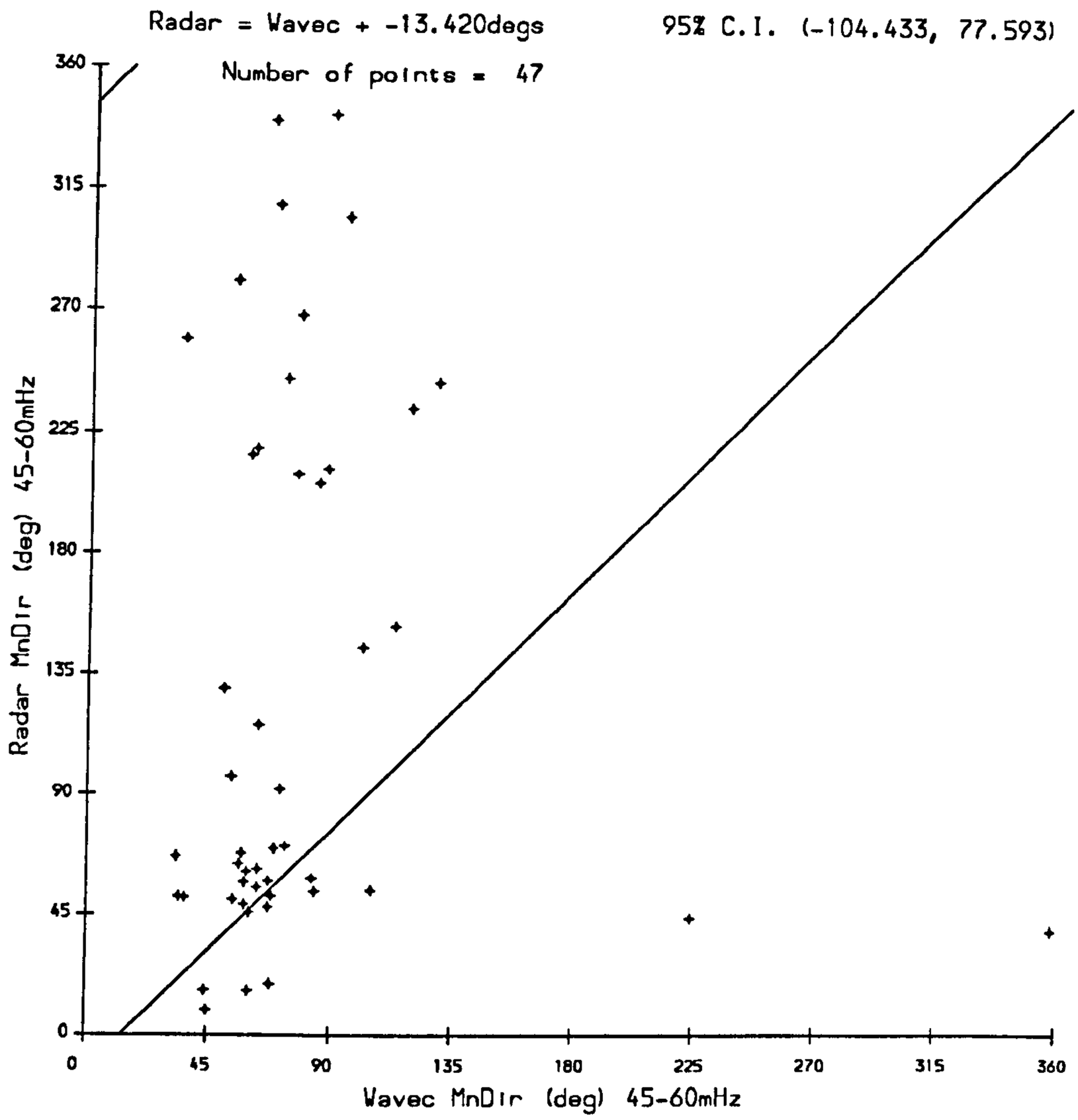

Figure 7.17: A scatter plot of HF radar spectral mean direction over $45 - 60mHz$ against their wave buoy equivalents during the NURWEC2 storm, with the maximum likelihood bias estimate superimposed.

however, as before, the scatter of the data makes it impossible to derive any useful information therefrom.

7.5.3 Spectral Mean Direction at 60-85mHz

Figure 7.18 shows a scatter plot of the HF radar spectral mean direction measurements in the $60 - 85mHz$ range taken during NURWEC2, against their wave buoy counterparts, with the maximum likelihood bias estimate superimposed. The scatter of the data makes it difficult to derive any useful information, however, the bias line does pass through the region where the points are clustered (in the $45° - 90°$ range).

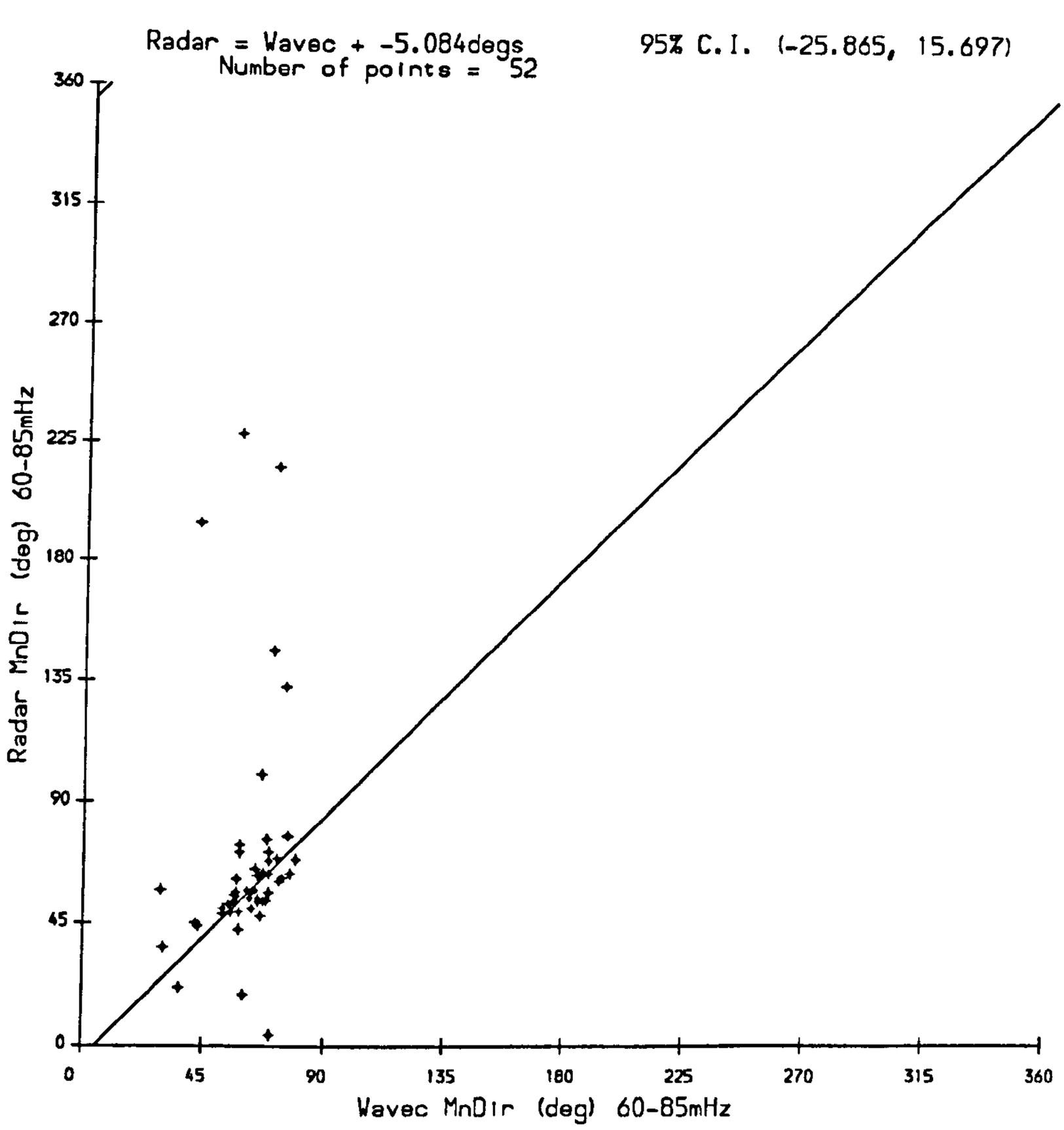

Figure 7.18: A scatter plot of HF radar spectral mean direction over $60 - 85mHz$ against their wave buoy equivalents during the NURWEC2 storm, with the maximum likelihood bias estimate superimposed.

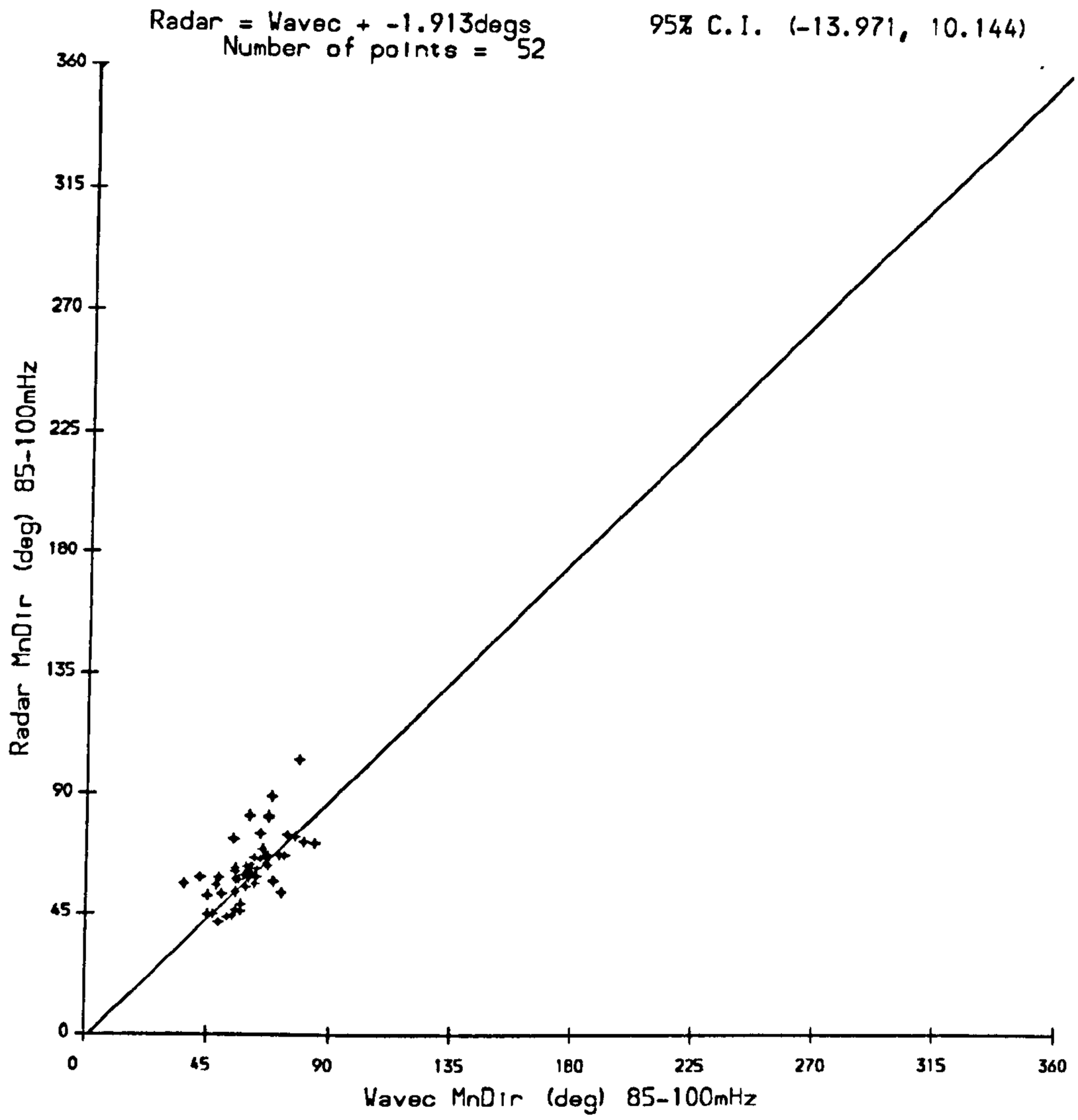

Figure 7.19: A scatter plot of HF radar spectral mean direction over $85 - 100mHz$ against their wave buoy equivalents during the NURWEC2 storm, with the maximum likelihood bias estimate superimposed.

7.5.4 Spectral Mean Direction at 85-100mHz

Figure 7.19 shows a scatter plot of the HF radar spectral mean direction measurements in the $85 - 100mHz$ range taken during NURWEC2, against their wave buoy counterparts, with the maximum likelihood bias estimate superimposed. The data show no evidence to suggest a bias between the Wavec and radar measurements and the model appears to be appropriate, but the limited range of the data make such conclusions rather weak.

7.5.5 Spectral Mean Direction at 100-125mHz

Figure 7.20 shows a scatter plot of the HF radar spectral mean direction measurements in the $100 - 125mHz$ range taken during NURWEC2, against

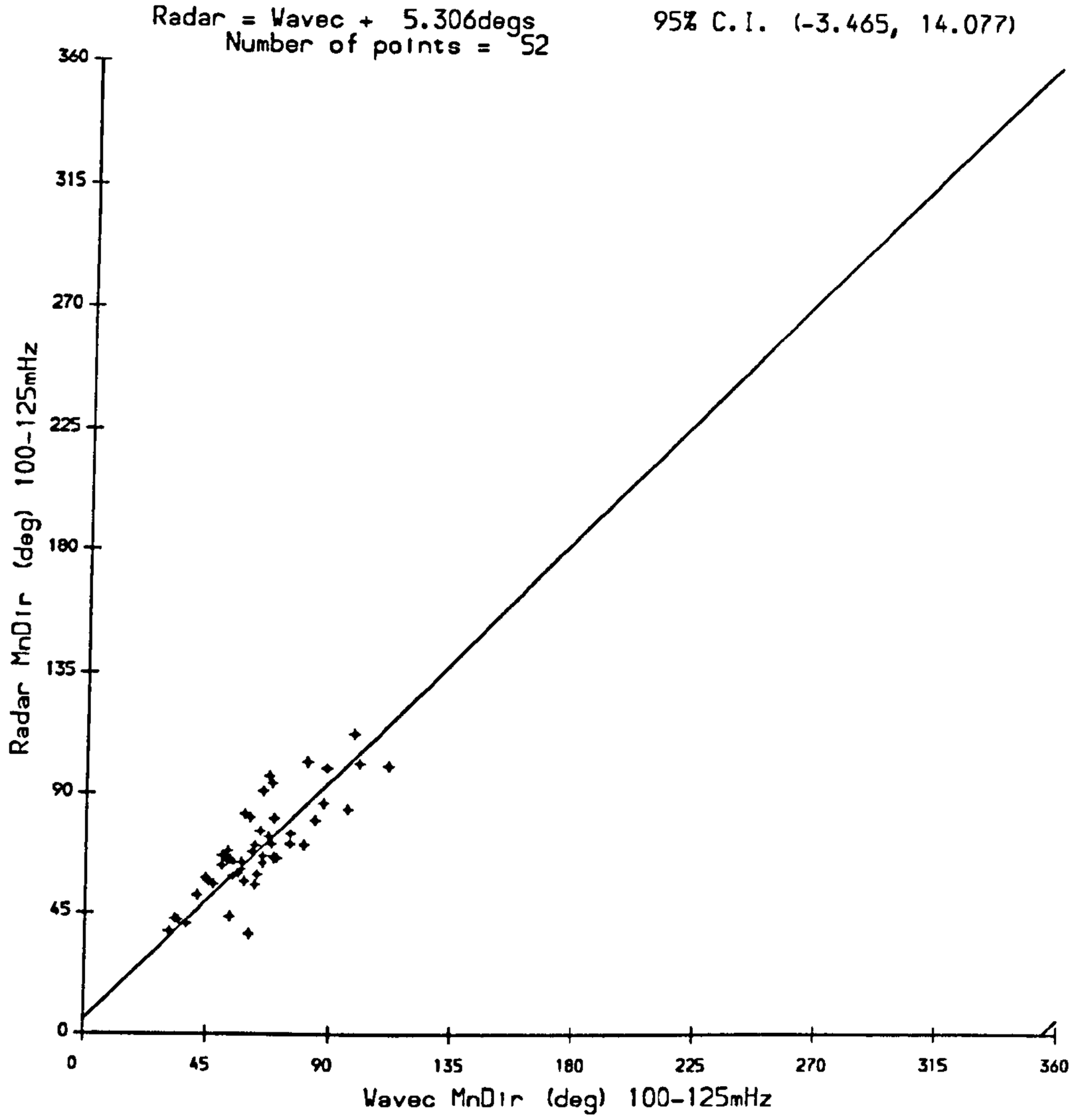

Figure 7.20: A scatter plot of HF radar spectral mean direction over $100-125mHz$ against their wave buoy equivalents during the NURWEC2 storm, with the maximum likelihood bias estimate superimposed.

their wave buoy counterparts, with the maximum likelihood bias estimate superimposed. As before, the data show no evidence to suggest a bias between the Wavec and radar measurements and the model appears to be appropriate, but the limited range of the data make such conclusions rather weak.

7.5.6 Spectral Mean Direction at 125-155mHz

Figure 7.21 shows a scatter plot of the HF radar spectral mean direction measurements in the $125-155mHz$ range taken during NURWEC2, against their wave buoy counterparts, with the maximum likelihood bias estimate superimposed. As before, the data show no evidence to suggest a bias between the Wavec and radar measurements and the model appears to be appropriate, but the limited range of the data make such conclusions rather weak.

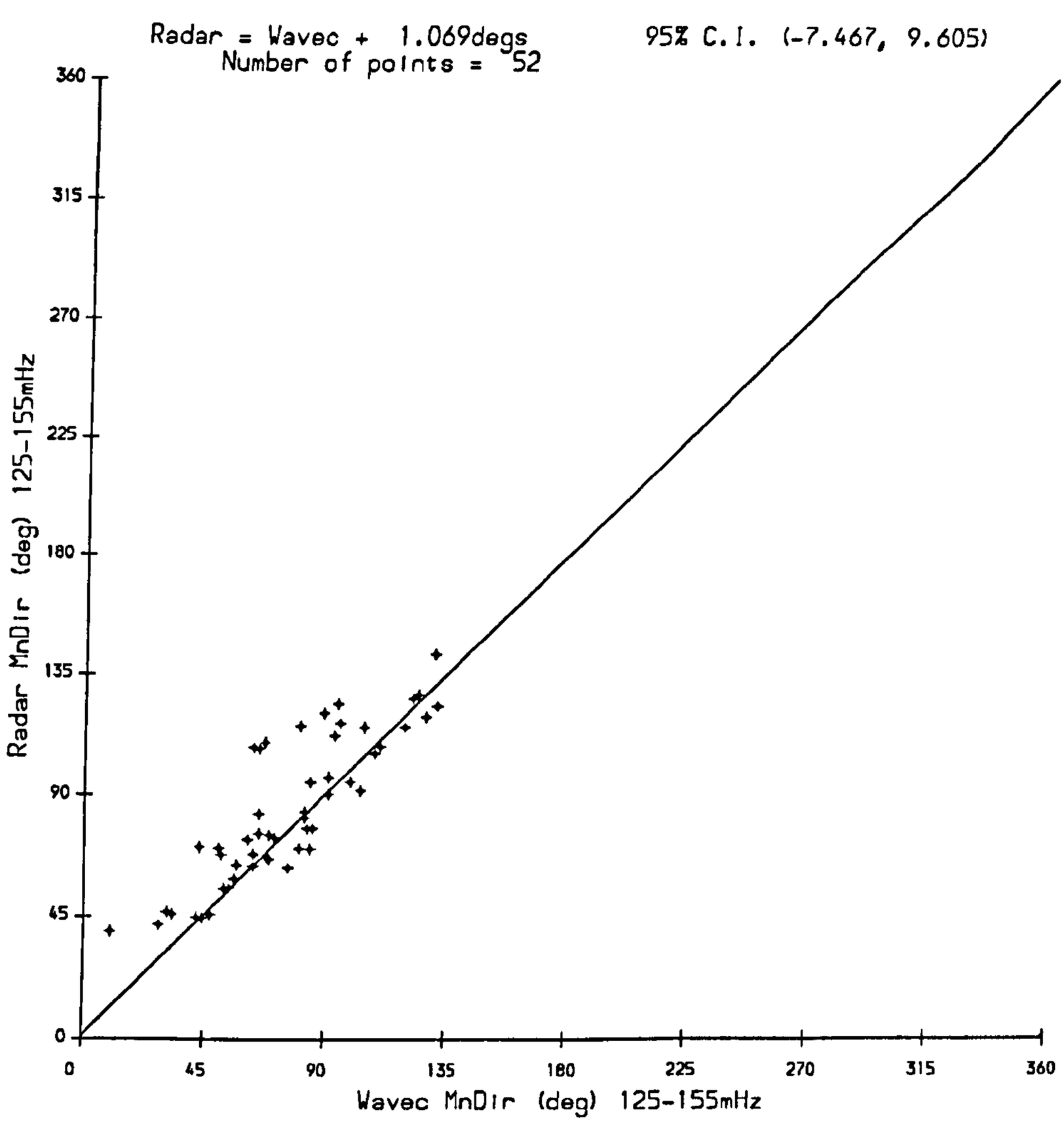

Figure 7.21: A scatter plot of HF radar spectral mean direction over $125 - 155mHz$ against their wave buoy equivalents during the NURWEC2 storm, with the maximum likelihood bias estimate superimposed.

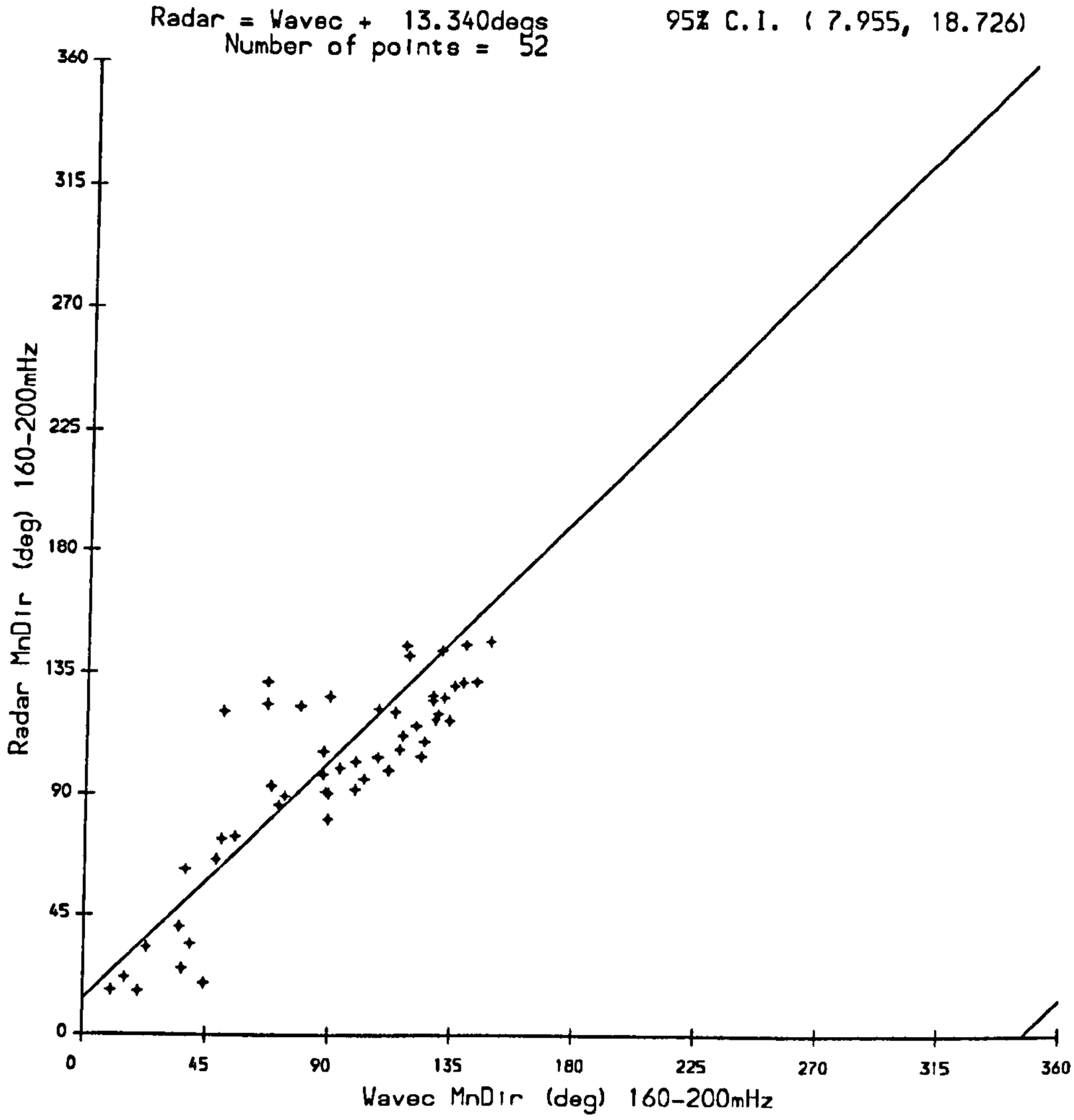

Figure 7.22: A scatter plot of HF radar spectral mean direction over $160-200mHz$ against their wave buoy equivalents during the NURWEC2 storm, with the maximum likelihood bias estimate superimposed.

7.5.7 Spectral Mean Direction at 160-200mHz

Figure 7.22 shows a scatter plot of the HF radar spectral mean direction measurements in the $160-200mHz$ range taken during NURWEC2, against their wave buoy counterparts, with the maximum likelihood bias estimate superimposed. The data show some evidence to suggest a bias (estimated at 13.34°) between the Wavec and radar measurements. There appears to also be some deviation from the model, but once again the limited range of the data make such conclusions rather weak.

7.5.8 Comment on Radar Performance

The Radar and Wavec perform similarly (in terms of bias of spectral mean direction estimates) over the frequencies $85 - 155mHz$ *over the range of the data.* Possible reasons for discrepancy outside this frequency range are discussed in section 7.4. However, the limited ranges of observed spectral mean direction in the data make it impossible to draw any meaningful conclusions about the *general* reliability of the radar measurements.

7.6 Spectral Directional Spread

Figure 7.23 shows a scatter plot of HF radar spectral directional spread measurements in the $85 - 100mHz$ range taken during NURWEC2, against their wave buoy counterparts. The large scatter of the data with respect to their range of values make it impossible to fit any *meaningful* relationship to this data set. Such behaviour is encountered for spectral directional spread measurements at all available frequencies, therefore no further inference has been attempted on the spectral directional spread parameters.

7.7 Intercomparison Summary

The NURWEC2 storm data suggest that the HF radar pair and the Wavec buoy show good correspondence for significant waveheight measurements and spectral power measurements (over $85 - 125mHz$). There is also a fair correspondence for mean period measurements in the range 6.8-11.0*secs.* Spectral mean direction shows good correspondence over $85 - 155mHz$, but the range of available data is somewhat limited. Spectral directional spread estimates show a poor correspondence over all frequencies.

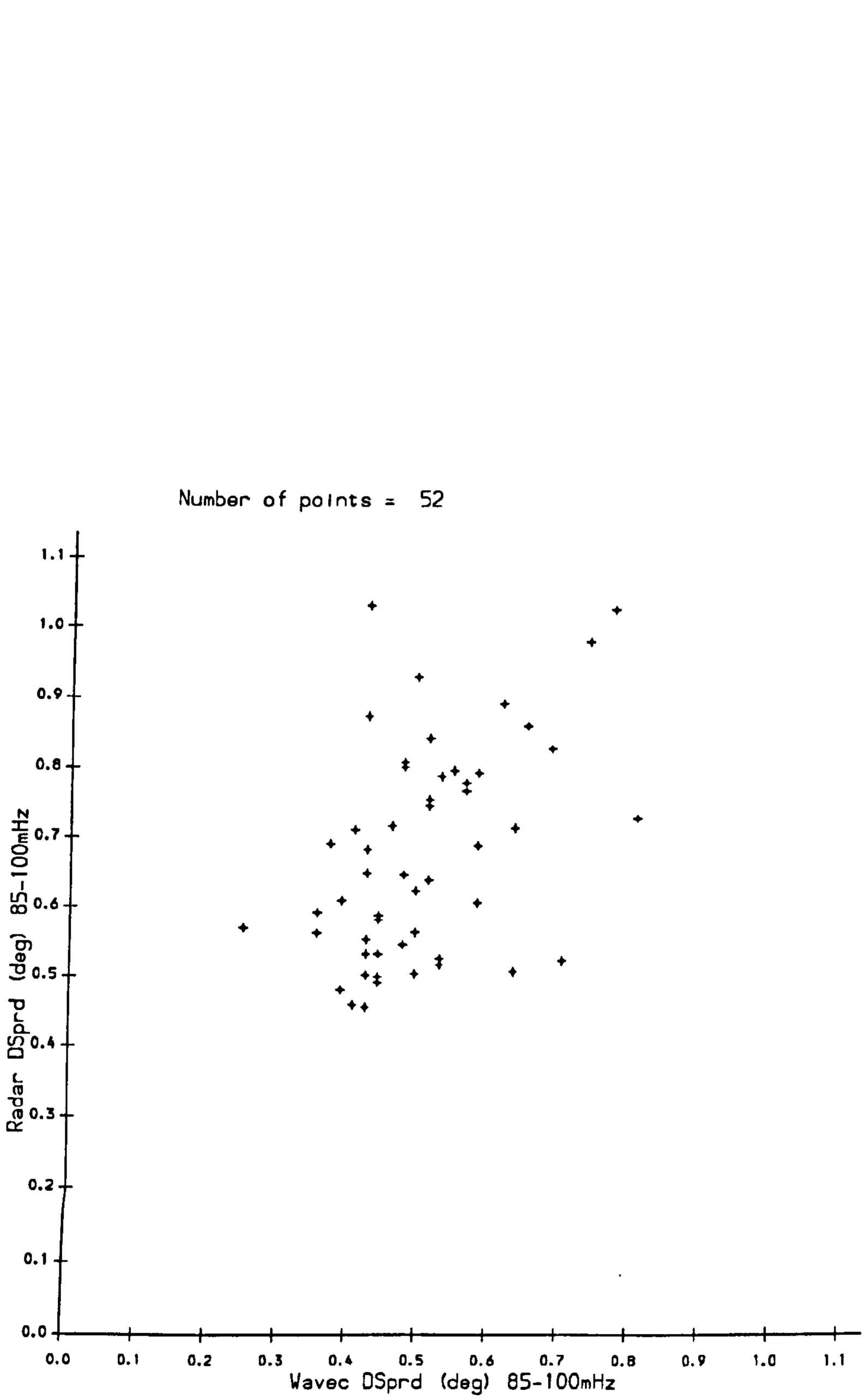

Figure 7.23: A scatter plot of HF radar spectral directional spread over $85 - 100mHz$ against their wave buoy equivalents during the NURWEC2 storm.

Chapter 8

Conclusions

8.1 Theoretical Developments

This study has involved the development of theory in three main categories :

Firstly, expressions have been derived for the estimation of variances of (and covariances between) weighted integrals of power (or energy) spectra calculated from tapered time series.

Secondly, the distributions of a variety of wave measurements as measured by HF radars have been determined (though in the case of spectral parameters, which are derived from the inversion of Barrick's equation, this has only been possible through the use of simulated data). These are :

- wind direction
- significant waveheight
- mean wave period
- spectral power
- spectral mean direction
- spectral directional spread

This information may be used to produce confidence intervals for the underlying parameters. The variances of the spectral parameters depend on

spectral frequency and the radar configuration. Additionally, the variance of spectral power depends on spectral power and the variances of mean direction and directional spread both depend on directional spread.

Thirdly, methods have been developed by which the relationship between observations by two different measuring systems of the same parameter may be estimated, taking into account that there is statistical variability in both measurement systems and also that the variance of each observation is estimable.

8.2 HF Radar Performance during the NURWEC2 Field Trial

Confidence intervals for the radar measurements have been produced which are, in the case of significant waveheight and mean wave period, of comparable width to those obtained from the corresponding NURWEC2 Wavec measurements. For significant waveheight the 90% radar confidence limits vary from ±8.2% to ±13.6% from the observations. For mean wave period they vary from ±3.5% to ±8.2%. In the case of spectral power, the 90% confidence intervals are narrower than those obtained from the corresponding NURWEC2 Wavec measurements, with the limits varying from ±25% to ±33% (approximately, depending on ocean wave frequency and radar operating frequency) except at the frequency limits of the inversion algorithm.

This study has also involved the intercomparison of radar and wave buoy data taken during the NURWEC2 storm, by the application of the above mentioned theoretical developments. The data suggest that the radars and the wave buoy show good correspondence for significant waveheight measurements and spectral power measurements (over $85 - 125mHz$ — the frequencies with most wave power, and hence those of most importance). There is also a fair correspondence for mean period measurements in the range $6.8 - 11.0secs$. Spectral mean direction shows good correspondence over $85 - 155mHz$ over the somewhat limited directional range (*i.e.* as observed during the NURWEC2 storm) of the data. Spectral directional spread estimates show a poor correspondence over all frequencies.

Where the correspondence between the radar and wave buoy measurements is poor, it is not possible to decide with which system (if not both) the prob-

lem lies. Where the correspondence is good, the data are consistent with the assumption that the difference in bias between the two systems (relative to sea truth) is negligible, which combined with the fact that radar and wave buoys measure waves in drastically different ways, tends to lend some credibility to both systems. For such parameters, an oceanographer who would be satisfied with wave buoy measurements is likely to be just as contented with HF radar measurements. There are, of course, other advantages in using an HF radar system, such as wide area coverage.

8.3 Possibilities for Further Research

The variety of simulations of those radar measurements which are obtained by the inversion of Barrick's equation has been by necessity limited (each set of 5000 simulations would typically take of the order of 10 days to complete on the available equipment). With the ever increasing development of computer technology, a much wider range of simulations will become possible, hopefully leading to a better understanding of the statistical behaviour of these estimates than has been achieved in this study. It would also be useful to know what effect the inclusion of background radio noise would have on these measurements. At the same time, research is presently underway on the improvement of the inversion algorithm, with emphasis on the extraction of data from higher wave frequencies (the current upper limit for the PISCES system is about $200mHz$, depending on radar frequency). These improved estimates may have different distributions from the ones available to this study.

Apart from the PISCES HF radar system used during NURWEC2, there is currently in operation another HF radar system called OSCR (*O*cean *S*urface *C*urrent *R*adar). As its name suggests, OSCR was originally designed for surface current measurement, but OSCR data has also been successfully used for wave measurement. OSCR operates at a much higher frequency than PISCES ($27MHz$), and the examination of the statistical properties of data derived from the inversion of Barrick's equation at this frequency would be another possible avenue for further study.

Finally, other intercomparison trials involving HF radar systems are planned. The SCAWVEX (*S*urface *C*urrent *a*nd *W*ave *V*ariability *Ex*periment) series of trials are expected to start in early 1996 and will consist of wave mea-

surements from an OSCR type HF radar, wave buoys and possibly other systems.

References

Allender, J., Audunson, T., Barstow, S. F., Bjerken, S., Krogstad, H. E., Steinbakke, P., Vartdal, L., Borgman, L. E. and Graham, C. (1989) The WADIC Project: A Comprehensive Field Evaluation of Directional Wave Instrumentation, *Ocean Engineering*, **16**(5/6), pp. 505–536.

Barrick, D. E. (1980) Accuracy of Parameter Extraction from Sample-Averaged Sea-Echo Doppler Spectra, *IEEE Transactions on Antennas and Propagation*, **AP-28**(1), pp. 1–11.

Barrick, D. E. and Snider, J. B. (1977) The Statistics of HF Sea-Echo Doppler Spectra, *IEEE Transactions on Antennas and Propagation*, **AP-25**(1), pp. 19–28.

Chatfield, C. (1989) *The Analysis of Time Series : An Introduction (Fourth Edition)*, Chapman and Hall.

Cox, D. R. and Miller, H. D. (1965) *The Theory of Stochastic Processes*, Methuen.

Dexter, P. E. and Theodoridis, S. (1982) Surface Wind Speed Extraction from HF Sky Wave Radar Doppler Spectra, *Radio Science*, **17**(3), pp. 643–652.

Harris, F. J. (1978) On the Use of Windows for Harmonic Analysis with the Discrete Fourier Transform, *Proceedings of the IEEE*, 66(1), pp. 51–83.

Holden, G. J. and Atanga, J. N. (1994) Modelling and Processing HF Radar Doppler Spectra, *Technical Report ACM Internal Report*, Applied Mathematics Section, School of Mathematics and Statistics, University of Sheffield.

Jenkins, G. M. and Watts, D. G. (1968) *Spectral Analysis and its Applications*, Holden-Day.

Kendall, M. G. and Stuart, A. (1973) *The Advanced Theory of Statistics : Volume 2 - Inference and Relationship (Third Edition)*, Griffin.

Kinsman, B. (1965) *Wind waves — Their Generation and Propagation on the Ocean Surface*, Prentice-Hall.

Krogstad, H. E., Barstow, S. F., Vartdal, L., Bjerken, S. and Audunson, T. (1988) *WADIC Phase 3: Intercomparison of Directional Wave Measurement Systems. WADIC Project Final Report Vol II*, Oceanor A/S & IKU Sintef-Gruppen.

Kuik, A. J. and van Vledder, G. P. (1984) Proposed Method for the Routine Analysis of Pitch-Roll Buoy Data, *Symposium : Description and Modelling of Directional Seas, København, 18-20 June 1984.*

Long, R. B. (1980) The Statistical Evaluation of Directional Spectrum Estimates Derived from Pitch/Roll Buoy Data, *Journal of Physical Oceanography*, **10**, pp. 944–952.

Neave, H. R. (1978) *Statistics Tables for Mathematicians, Engineers, Economists and the Behavioural and Management sciences*, Unwin Hyman.

Olsen, R. B. and Barstow, S. F. (1988) *Wave Measurements on Haltenbanken During NORCSEX '88: An Intercomparison of Buoy, Synthetic Aperture Radar and Altimeter Data*, Oceanor A/S.

Pearce, S. C. (1982a) Analysis of Covariance, *Encyclopedia of Statistical Sciences, Volume 1*, Wiley-Interscience.

Pearce, S. C. (1982b) Analysis of Variance, *Encyclopedia of Statistical Sciences, Volume 1*, Wiley-Interscience.

Shearman, E. D. R. (1983) Radio Science and Oceanography, *Radio Science*, **18**, pp. 299–320.

Šova, M. G. and Wyatt, L. R. (1991) The Implications of Statistical Variability on the Intercomparison of Wave Measurement Systems, *1991 International Geoscience and Remote Sensing Symposium, Helsinki University of Technology, 3–6 June 1991.*

Šova, M. G. and Wyatt, L. R. (1994) *Spatial and Temporal Variability in Ocean Wave Measurement*, report presented to HSE on completion of project P2881, to be published by HSE.

Tucker, M. J. (1991) *Waves in Ocean Engineering — Measurement, Analysis, Interpretation*, Ellis Horwood.

Welch, P. D. (1967) The Use of Fast Fourier Transform for the Estimation of Power Spectra: A Method Based on Time Averaging Over Short, Modified Periodograms, *IEEE Transactions on Audio and Electroacoustics*, **AU-15**, pp. 70–73.

Wyatt, L. R. (1983) The Measurement of Oceanographic Parameters Using Dekametric Radar, *Remote Sensing Applications in Marine Science and Technology*, , pp. 183–205.

Wyatt, L. R. (1988a) HF Radar Wave Measurement during NURWEC2, *Proceedings of IGARSS '88 Symposium, Edinburgh, Scotland, 13–16 September 1988.*

Wyatt, L. R. (1988b) HF Radar Wind Measurement during NURWEC2, *Proceedings of IGARSS '88 Symposium, Edinburgh, Scotland, 13–16 September 1988.*

Wyatt, L. R. (1988c) Significant Waveheight Measurement with H.F. Radar, *International Journal of Remote Sensing*, **9**(6), pp. 1087–1095.

Wyatt, L. R. (1990a) Progress in the Interpretation of HF Sea Echo: HF Radar as a Remote Sensing Tool, *IEE Proceedings*, **137**(2), pp. 139–148.

Wyatt, L. R. (1990b) A Relaxation Method for Integral Inversion Applied to HF Radar Measurement of the Ocean Wave Directional Spectrum, *International Journal of Remote Sensing*, **11**(8), pp. 1481–1494.

Wyatt, L. R. (1991) High-Frequency Radar Measurements of the Ocean Wave-Directional Spectrum, *IEEE Journal of Oceanic Engineering*, **16**(1), pp. 163–169.

Wyatt, L. R. and Holden, G. J. (1991) The Remote Sensing of Very Long Ocean Waves using HF Radar, *1991 International Geoscience and Remote Sensing Symposium, Helsinki University of Technology, 3–6 June 1991.*

Wyatt, L. R., Venn, J., Burrows, G. D., Ponsford, A. M., Moorhead, M. D. and van Heteren, J. (1986) HF Radar Measurements of Ocean Wave Parameters during NURWEC, *IEEE Journal of Oceanic Engineering*, **OE-11**(2), pp. 219–234.

Wyatt, L. R., Venn, J., Moorhead, M. D., Burrows, G. D., Ponsford, A. M. and van Heteren, J. (1985) HF Radar Measurements of Significant Wave-height and Mean Period During NURWEC, *Advances in Underwater Technology and Offshore Engineering, Vol 4, Graham & Trotman.*